Title
Dual-Specificity Inhibitors of Lipid and Protein Kinases

Permalink
https://escholarship.org/uc/item/7372d6r8

Author
Apsel, Beth

Publication Date
2008-06-24

Peer reviewed|Thesis/dissertation

Dual-Specificity Inhibitors of Lipid and Protein Kinases

by

Beth Apsel

DISSERTATION

Submitted in partial satisfaction of the requirements for the degree of

DOCTOR OF PHILOSOPHY

in

Chemistry and Chemical Biology

in the

GRADUATE DIVISION

of the

UNIVERSITY OF CALIFORNIA, SAN FRANCISCO

Dual-specificity inhibitors of lipid and protein kinases

Beth Apsel

Kevan M. Shokat, Ph.D.

Abstract

Cancer cells survive by co-opting intracellular growth pathways regulated through kinase signaling. Many kinases in these pathways are validated drug targets and kinase inhibitors are first-line treatment for several advanced cancers. The first generation of kinase inhibitors were intended to target single proteins. However, the highly conserved active sites of protein kinases prohibited the design of perfectly selective inhibitors. Unexpectedly, this specificity problem led to the development of clinically useful, multi-targeted kinase inhibitors. Clinically, multi-targeted inhibitors were found to have high efficacy and low toxicity. At a molecular level, this translated into simultaneous inhibition of critical nodes in a signaling network regulated by multiple inputs and levels of feedback.

Two kinase families, phosphoinositide-3-kinases (PI3Ks) and protein tyrosine kinases (PTKs), are activated by mutations and amplifications in a disproportionate number of human cancers. This suggests multi-targeted therapy inhibiting PI3Ks and PTKs may be extremely effective at blocking the signaling networks that are essential for cancer cell survival. The design of dual PI3K/PTK inhibitors is chemically challenging because PI3Ks and PTKs are members of significantly divergent kinase families. However, druggable similarities exist between these two families due to structural features essential for phosphoryl transfer with ATP as the phosphate donor.

We report the first drug-like small molecules that potently and selectively inhibit PTKs and PI3Ks. These agents were developed by exploiting structural similarities in

kinase active sites. Through iterative medicinal chemistry, kinome profiling and x-ray crystallography, the chemical and structural features that control the *in vitro* selectivity and potency of these compounds were defined. A subset of these compounds potently, and sometimes selectively, inhibit the mammalian target of rapamycin (mTOR), a Ser/Thr kinase in the PI3K family, placing mTOR in kinase space at the intersection of PI3Ks and PTKs. Subsequent cell-based experiments demonstrated these compounds inhibit their molecular targets in cells, block cancer cell proliferation and angiogenesis, and maintain activity against cells harboring mutations rendering them resistant to singly-targeted agents.

Table of Contents

List of Figures

List of Tables

List of Abbreviations

AMPPNP	5'-adenylyl-beta,gamma-imidodiphosphate
Asn	Asparagine
Asp	Aspartic acid
ATP	adenosine triphosphate
C-lobe	C-terminal lobe
CML	chronic myeloid leukemia
DGF	Asp-Phe-Gly
DME	dimethoxyethane
DMF	N,N-dimethylformamide
DNA-PK	DNA-Dependent Protein Kinase
EGFR	epidermal growth factor receptor
EphB4	EPH receptor B4
FDA	U.S. Food and Drug Administration
Gly	Glycine
Glu	Glutamic acid
GSK-3β	glycogen synthase kinase-3β
IC$_{50}$	median inhibitory concentration
Ile	Isoleucine
Lys	Lysine
Met	Methionine
mTOR	mammalian target of rapamycin
mTORC1	mTOR complex 1
mTORC2	mTOR complex 2
NIS	N-iodosuccidamide
N-lobe	N-terminal lobe

P loop	phosphate binding loop
PDGFR	platelet-derived growth factor receptor
PDK1	phosphoinositide-dependent protein kinase 1
PH	pleckstrin homology
Phe	Phenylalanine
PI3K	phosphoinositide-3-kinase
PI4Kβ	phosphatidylinositol 4-kinase β
PIKK	phosphoinositide 3-kinase-related kinase
PIP$_2$	phosphatidyl inositol-4,5-bis-phosphate
PIP$_3$	phosphatidyl inositol-3,4,5-triphosphate
PP	pyrazolopyrimidines
PP1	4-amino-1-tert-butyl-3-(p-methylphenyl) pyrazolo[3,4-d]pyrimidine
PP102	1-isopropyl-3-(quinolin-6-yl)-1H-pyrazolo[3,4-d]pyrimidin-4-amine
PP107	3-(1H-indol-6-yl)-1-isopropyl-1H-pyrazolo[3,4-d]pyrimidin-4-amine
PP110	3-(1H-indazol-6-yl)-1-isopropyl-1H-pyrazolo[3,4-d]pyrimidin-4-amine
PP118	1-isopropyl-3-(2-methylquinolin-6-yl)-1H-pyrazolo[3,4-d]pyrimidin-4-amine
PP121	1-cyclopentyl-3-(1H-pyrrolo[2,3-b]pyridin-5-yl)-1H-pyrazolo[3,4-d]pyrimidin-4-amine
PP129	1-isopropyl-3-(isoquinolin-6-yl)-1H-pyrazolo[3,4-d]pyrimidin-4-amine
PP132	1-isopropyl-3-(quinoxalin-7-yl)-1H-pyrazolo[3,4-d]pyrimidin-4-amine

PP137	3-(1H-indazol-5-yl)-1-isopropyl-1H-pyrazolo[3,4-d]pyrimidin-4-amine
PP155	4-(4-amino-1-isopropyl-1H-pyrazolo[3,4-d]pyrimidin-3-yl)-2-hydroxybenzonitrile
PP162	1-cyclopentyl-3-(H-imidazo[1,2-a]pyridin-7-yl)-1H-pyrazolo[3,4-d]pyrimidin-4-amine
PP17	6-(4-amino-1-isopropyl-1H-pyrazolo[3,4-d]pyrimidin-3-yl)naphthalen-2-ol
PP20	tert-butyl 4-(4-amino-1-isopropyl-1H-pyrazolo[3,4-d]pyrimidin-3-yl)-2-methoxyphenylcarbamate
PP242	2-(4-amino-1-isopropyl-1H-pyrazolo[3,4-d]pyrimidin-3-yl)-1H-indol-5-ol
PP257	5-(4-amino-1-isopropyl-1H-pyrazolo[3,4-d]pyrimidin-3-yl)-2-hydroxybenzonitrile
PP89	3-(1H-indol-5-yl)-1-isopropyl-1H-pyrazolo[3,4-d]pyrimidin-4-amine
PTEN	phosphatase with tensin homology
PTK	protein tyrosine kinase
RTK	receptor tyrosine kinase
S1	3-(4-amino-1-isopropyl-1H-pyrazolo[3,4-d]pyrimidin-3-yl)phenol
S2	1-methyl-3-(naphthalen-2-yl)-1H-pyrazolo[3,4-d]pyrimidin-4-amine
SAR	structure-activity relationship
Ser	Serine
THF	tetrahydrofuran
Thr	Threonine
Tyr	Tyrosine
VEGFR	vascular endothelial growth factor receptor

Chapter 1: Introduction—Establishment of lipid and protein kinases as drug targets

1.1 Kinase inhibitors in drug discovery

Over the past 10 years target-based drug discovery has become the dominant paradigm in the pharmaceutical industry (Sams-Dodd 2005; Baselga 2006). Pharmaceutical companies anticipated that target-based design, compared to the traditional phenotype-based approach, would increase efficiency through higher screening capacity and rational small molecule design (Sams-Dodd 2005). However, the rise of molecular medicine has paralleled a decline in pharmaceutical productivity (Sams-Dodd 2005; Sawyers 2006; Sebolt-Leopold and English 2006). During the same time, studies revealed several successful drugs, particularly in cancer therapy, had unanticipated targets (Frantz 2005; Sebolt-Leopold and English 2006; Wilhelm, Carter et al. 2006). Imatinib (STI-571), was one of the first examples. Approved as a single-targeted inhibitor of the Bcr-Abl tyrosine kinase for the treatment of chronic myeloid leukemia (CML), Imatinib was later found to inhibit c-KIT, platelet-derived growth factor receptor (PDGFR), and c-ARG (Joensuu, Roberts et al. 2001; Wong, McLaughlin et al. 2004; Frantz 2005; Baselga 2006). Clinical data showed that Imatinib had high efficacy and low toxicity despite these unintended targets (Druker, Sawyers et al. 2001). Additionally, Imatinib's ability to decrease proliferation of some CML cell lines depended on its ability to inhibit c-KIT, suggesting a link between multi-specificity and increased efficacy (Wong, McLaughlin et al. 2004).

Similar to Imatinib, the clinically successful multi-targeted kinase inhibitor Sorafenib was initially pursued as a single-targeted inhibitor; in the case of Sorafenib, the single target was the oncogenic Ser/Thr kinase Raf (Wilhelm, Carter et al. 2004; Wilhelm, Carter et al. 2006). Sorafenib was later found to potently inhibit several tyrosine kinases critical in tumor angiogenesis, including vascular endothelial growth factor receptor (VEGFR) and PDGFR (Wilhelm, Carter et al. 2004; Liu, Cao et al. 2006; Wilhelm, Carter et al. 2006). Sorafenib was so effective in treating advanced renal cell

carcinoma that it met approval by the U.S. Food and Drug Administration (FDA) only 5 years after the start of Phase 1 trials (Wilhelm, Carter et al. 2006). This success has been traced to the multi-targeted nature of Sorafenib: inhibition of Raf blocks tumor cell growth and inhibition of VEGFR and PDGFR blocks tumor angiogenesis (Liu, Cao et al. 2006; Wilhelm, Carter et al. 2006; Strumberg, Clark et al. 2007). This two-pronged approach enabled Sorafenib to strike at both the tumor and its microenvironment. Furthermore, like Imatinib, the success of Sorafenib has been accompanied by surprisingly low toxicity profiles in humans (Strumberg, Clark et al. 2007).

The clinical success of small molecules with multiple targets has challenged the one-drug-one-target paradigm, and both academia and pharmaceutical companies are starting to acknowledge this challenge (Frantz 2005; Hopkins, Mason et al. 2006; Stommel, Kimmelman et al. 2007; Petrelli and Giordano 2008). High-throughput, multi-targeted drug discovery programs that target sets of kinases are emerging and finding success (Frantz 2005; Garber 2006; Petrelli and Giordano 2008). In cancer, kinases have been targeted because they are central to the dysregulated intracellular signaling pathways underlying transformation (Blume-Jensen and Hunter 2001; Fabian, Biggs et al. 2005). Of particular interest are kinases in the protein tyrosine kinase (PTK)/ phosphoinositide-3-kinase (PI3K)/ mammalian target of rapamycin (mTOR) pathway, which mediates communication between cells and their environment. This tightly-regulated pathway controls the critical balance between cell survival and apoptosis (Blume-Jensen and Hunter 2001).

The PTK/PI3K/mTOR pathway (Figure 1.1) is activated when growth factors bind extracellular domains of receptor PTKs (RTKs) or transmembrane growth factor receptors that are coupled to cytoplasmic PTKs (Cantley 2002). This binding event activates the PTK to autophosphorylate on cytoplasmic tyrosine residues. The

phosphorylated tyrosine residues serve as docking sites for p85, which is the regulatory

subunit of class
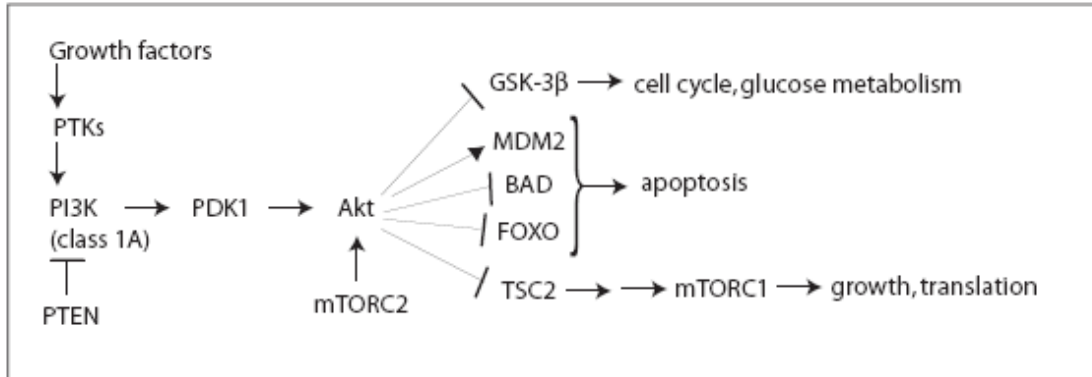
Figure 1.1 Schematic of the PTK/PI3K/mTOR Pathway. This generalized schematic
shows important signaling proteins and cellular processes that are controlled through the
PTK/PI3K/mTOR pathway.

1A PI3Ks (Cantley 2002). Class 1A PI3Ks, which include PI3Kα, PI3Kβ and PI3Kδ, are

constitutively-bound heterodimers composed of the p85 regulatory subunit and a p110

catalytic subunit (Fruman, Meyers et al. 1998). When p85 binds to activated PTKs, the

PI3K heterodimer is recruited to the membrane where p110 phosphorylates its

substrate, the membrane lipid phosphatidyl inositol-4,5-bis-phosphate (PIP$_2$), to produce

the second messenger phosphatidyl inositol-3,4,5-triphosphate (PIP$_3$) (Cantley 2002;

Vivanco and Sawyers 2002). The action of PI3K is directly antagonized by a lipid

phosphatase known as phosphatase with tensin homology (PTEN) (Cully, You et al.

2006). When PI3K is active, PIP$_3$ is generated and binds proteins with pleckstrin

homology (PH) domains, including the kinase Akt and its activator, phosphoinositide-

dependent protein kinase 1 (PDK1), recruiting them to the membrane in close proximity

of one another. PDK1 activates Akt by phosphorylating its activation loop (Thr308).

There is a second phosphorylation site on Akt at Ser473. Unlike Thr308, Ser473

phosphorylation is not required for Akt activity and only modestly increases Akt activity.

Ser473 phosphorylation is mediated by a protein complex known as mTOR complex 2 (mTORC2) (Jacinto, Facchinetti et al. 2006). The mTOR kinase is a part of this complex and it directly phosphorylates Ser473. Activated Akt has many downstream targets, including glycogen synthase kinase-3β (GSK-3β), the p53 inhibitor MDM2, the FOXO family of forkhead transcription factors, the proapoptotic protein BAD, IkB kinase (IKK) and the tumor suppressor TSC2 (tuberin), which indirectly controls cell growth and translation through mTOR complex 1 (mTORC1) (Cantley 2002; Vivanco and Sawyers 2002).

mTOR is a Ser/Thr kinase that executes the catalytic activity of mTORC1 and mTORC2. It is a central kinase in the RTK/PI3K pathway that integrates nutrient and growth factor signals to control protein translation (Guertin and Sabatini 2007). mTOR is known to play a major role in malignant transformation, though it has not been found to harbor any cancer-specific mutations (Dancey 2006). As a protein kinase in the phosphoinositide 3-kinase-related kinase (PIKK) superfamily, mTOR is evolutionary more closely related to PI3K than to tyrosine kinases (Sawyers 2003; Dancey 2006). The mTOR kinase is involved in two different protein complexes, mTORC2 and mTORC1, as described above, and mTORC2 is upstream of Akt, while mTORC1 is downstream of Akt (Guertin and Sabatini 2007). Inhibition of mTORC1 by the natural product rapamycin induces G_1 arrest in many cancer cell lines (Sawyers 2003). This result, along with many others, suggest mTOR activation is critical for the survival of many cancers.

Mutation of enzymes in the RTK/PI3K/mTOR pathway can uncouple communication between critical nodes in this pathway (Blume-Jensen and Hunter 2001). This can cause a loss of regulatory control over growth factor signaling pathways and lead to oncogenic transformation. PTK amplification and/or mutational activation is involved in many cancers, and many PTKs, including the VEGFR and the epidermal

growth factor receptor (EGFR), are validated drug targets (Druker, Sawyers et al. 2001; Frantz 2005; Sams-Dodd 2005; Garber 2006; Wilhelm, Carter et al. 2006; Petrelli and Giordano 2008; Wheatley-Price and Shepherd 2008). An estimated 15% of human cancers harbor amplifications, deletions or somatic missense mutations in the gene encoding PI3Kα, *PIK3CA* (Hennessy, Smith et al. 2005; Karakas, Bachman et al. 2006). In addition, PTEN is mutated, downregulated or epigenetically altered in the majority of cancers (Hennessy, Smith et al. 2005). In some cancers, successful PTK inhibition is dependent on functional PTEN, indicating the central importance of PI3K as an independent regulator of cancer growth (Mellinghoff, Wang et al. 2005). Overall, the RTK/PI3K/mTOR pathway harbors genomic aberrations more frequently than any other pathway in human cancer (Hennessy, Smith et al. 2005).

Small-molecule inhibitors specific to PTKs or PI3Ks have been shown to independently cause cancer regression in mouse models of human cancer (Fan, Knight et al. 2006; Wilhelm, Carter et al. 2006). Currently, there are several FDA-approved tyrosine kinase inhibitors in the clinic. There are no FDA-approved inhibitors that directly target PI3K, though several are undergoing clinical trails (Hennessy, Smith et al. 2005). Tyrosine kinase inhibitors block signaling directly upstream of PI3Ks, but spare downstream growth initiated by PI3K. In some cancer cells, this has been traced to inactivating mutations in PTEN (Nagata, Lan et al. 2004; Cully, You et al. 2006). Inactivation of PTEN uncouples PI3K from the upstream PTK signal, rendering PTK inhibitors ineffective at blocking cancer growth through the PI3K/Akt pathway. In addition, resistance to some targeted tyrosine kinase therapies is mediated through PI3K (Nagata, Lan et al. 2004). Studies provide empirical evidence that simultaneous inhibition of protein tyrosine kinases and PI3K can act synergistically to block the growth of cancer cells more completely than singly targeted agents (Klejman, Rushen et al. 2002). The wealth of genetic evidence implicating PTK/PI3K/mTOR activation in human

cancer, along with the clinical shortcomings of narrowly-targeted kinase inhibitors, provide a clear rationale for pursuing multi-targeted therapy specific against PTKs and PI3K.

1.2 Structural insights for kinase inhibitor design

Rational design of ATP-competitive kinase inhibitors requires an understanding of how the chemical groups of inhibitors can interact with structural and functional elements of kinase active sites. The following section describes key features of the catalytic domains of PTKs (sections 1.2.1 and 1.2.3) and PI3Ks (sections 1.2.2 and 1.2.3). This is a focused introduction to the critical motifs and structural elements that enable these divergent kinase families to bind ATP and ATP-analogues, while catalyzing phosphoryl transfer to very different substrates. Basic terminology and concepts are presented that are essential for understanding how kinase-inhibitor co-crystal structures informed the design of the new class of inhibitors described in Chapters 2-4.

1.2.1 Structure and function of protein kinase active sites

The architecture of the catalytic domain of protein kinases is highly conserved (Taylor, Knighton et al. 1992). It consists of two subdomains: a smaller N-terminal lobe and a larger C-terminal lobe (Figure 1.2a) (Taylor, Knighton et al. 1992; Huse and Kuriyan 2002; Noble, Endicott et al. 2004). The N-terminal lobe consists of a five-stranded β sheet and a single α helix, known as the helix αC, which is critical for catalytic activity (Huse and Kuriyan 2002). The larger C-terminal lobe is almost entirely helical. These two lobes are connected through a small linker region, known as the hinge region. The adenine of ATP binds in a deep hydrophobic cleft at the intersection of the two lobes (Taylor, Knighton et al. 1992; Adams 2001; Huse and Kuriyan 2002). Specifically, hydrogen bonding interactions between the N-6 and N-7 nitrogens of

7

adenine and backbone amides of kinase hinge region residues anchor ATP in the active site.

There are several conserved sequence motifs in protein kinases that are critical to ATP and substrate binding (Taylor, Knighton et al. 1992). The first connects strands $\beta1$ and $\beta2$ in the N-terminal lobe and is known as the phosphate binding loop, or P loop (Figure 1.2a) (Taylor, Knighton et al. 1992). The P loop contains the conserved (GXGXϕG) motif (ϕ is often Phe or Tyr), and is often called the "glycine-rich loop". (Nolen, Taylor et al. 2004). The flexibility of this motif enables the residues to position themselves so that their backbone amides can coordinate the phosphates of ATP (Huse and Kuriyan 2002).

At the base of the kinase active site, between strands $\beta6$ and $\beta7$, is a segment known as the catalytic loop, which contains conserved Asp and Asn residues (Figure 1.2a and Figure 1.2b) (Huse and Kuriyan 2002). The Asn residue coordinates a Mg^{2+} ion; the Mg^{2+} is then able to coordinate and orient the α and γ phosphates of ATP (Adams 2001; Huse and Kuriyan 2002; Kannan and Taylor 2008). In addition to binding the metal ion, the Asn residue binds the Asp residue of the catalytic loop. This Asp hydrogen bonds with the hydroxyl group of the substrate, positioning it to attack the γ-phosphate of ATP (Figure 1.2b) (Adams 2001).

A series of motifs, collectively known as the activation segment, wraps around the lip of the active site cleft and plays a critical role in positioning ATP and the protein substrate for catalysis (Figure 1.2a) (Nolen, Taylor et al. 2004). Two of the most important secondary elements of the activation segment are the magnesium-binding loop and the activation loop (Nolen, Taylor et al. 2004). The magnesium-binding loop is the most N-terminal portion of the activation segment and contains the well-conserved Asp-Phe-Gly (DGF) motif. The Asp of this loop is necessary for coordination of a Mg^{2+}

ion, which, like the Mg^{2+} ion chelated by the catalytic loop, helps position the phosphates of ATP for phosphoryl transfer (Huse and Kuriyan 2002; Nolen, Taylor et al. 2004). In the middle of the activation segment, C-terminal to the DFG motif, is the activation loop. The primary sequence and the number of phosphorylation sites of this loop is highly variable among kinases. The activation loop in active kinases are usually ordered in a phosphorylation-dependent manner, whereas, in inactive kinases, the activation loop is frequently unphosphorylated and disordered (Nolen, Taylor et al. 2004). When the activation loop is in its disordered state, the activation segment collapses into the kinase active site, occluding substrate binding and preventing catalysis (Huse and Kuriyan 2002). Phosphorylation of the loop causes a large conformational change that shifts the loop out of the active site and into position for substrate binding. As a result of this movement, the N-terminal DFG motif rotates such that the Asp is properly oriented for Mg^{2+} binding (Nolen, Taylor et al. 2004).

There is a Lys-Glu ion pair within the N-lobe of all kinases that is absolutely conserved (Figure 1.2b) (Huse and Kuriyan 2002). The Lys of this pair, which is frequently referred to as the "catalytic lysine", is buried deep in the interlobe cleft and the Glu resides within the helix αC (Huse and Kuriyan 2002). The Lys-Glu interaction results in ordering of the helix αC and positioning of the Lys side chain so that it can coordinate the α and β phosphates of ATP (Figure 1.2b). When ordered, the helix αC also is able to interact with the activation loop, helping to orient the DFG motif into its active conformation.
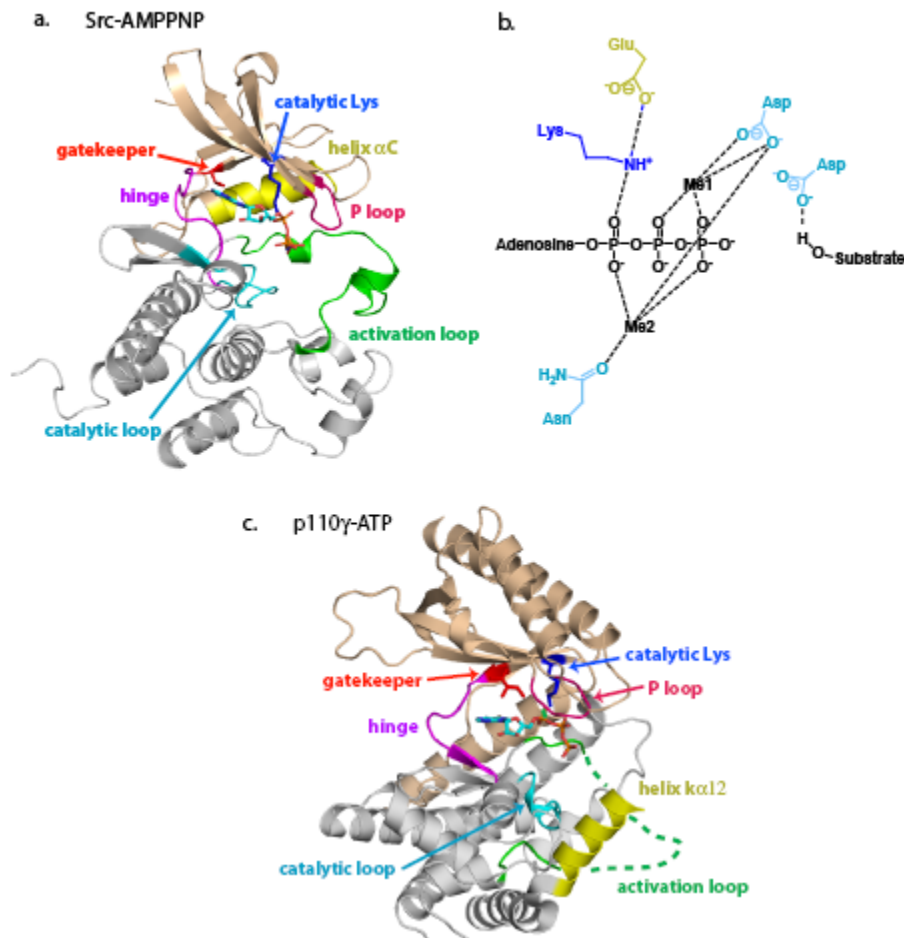
Figure 1.2 The structures of the active sites of the protein kinase Src and the phosphoinositide kinase p110γ reveal many similarities. A) and C) The catalytic domains of Src, a PTK, and p110γ, a PI3K, show the same overall kinase fold, with smaller N-terminal lobes (pink) and larger C-terminal lobes (gray). Nucleotides (5'-adenylyl-beta,gamma-imidodiphosphate (AMPPNP) in Src and ATP in p110γ) bind deep in the interlobe cleft, which is defined by hinge region residues (purple). Both kinases have the same structural elements, which include the catalytic Lys (blue), the gatekeeper residue (red), the catalytic loop (cyan), the P loop (magenta) and the activation loop (green). However, differences in shape, size and orientation of these residues and motifs are easily observed. These differences are expected given the disparate substrate specificities and modes of regulation between lipid and protein kinases. Also shown are two key helices (yellow), helix αC in Src and helix kα12 in p110γ, which are thought to be critical to conformational changes involved in kinase activation. B) A close up of the catalytic machinery of protein kinase active sites shows the conserved Lys-Glu ion pair. This ion pair is composed of the catalytic Lys (blue) and Glu (yellow) from the helix αC. Also shown are the Asp and Asn residues (cyan) of the catalytic loop, which play critical roles in coordinating metal ions and positioning the phosphates of ATP and the substrate for catalysis.

1.2.2 Structure and function of phosphoinositide-3-kinase active sites

Currently, there are crystal structures of the catalytic subunits of two PI3K isoforms: p110α and p110γ (Walker, Perisic et al. 1999; Huang, Mandelker et al. 2007). p110α is a class 1A PI3K. p110α, along with the other class 1A isoforms of PI3K, p110β and p110δ, associates with a p85 regulatory subunit and is activated through PTKs (Fruman, Meyers et al. 1998). p110γ is class 1B PI3K; it associates with a p101 regulatory subunit and is activated through G-protein coupled receptors (GPCRs) (Fruman, Meyers et al. 1998). p110α and p110γ catalyze the same reaction, converting PIP$_2$ to PIP$_3$ by transferring the terminal phosphate of ATP. Therefore, despite distinct heterodimeric partners, p110α and p110γ show little variation within their active sites. The structures of both p110α and p110γ have provided critical structural insight into class 1 PI3Ks.

Protein kinases and PI3K have little homology in their primary sequences (ex. 9% sequence homology between the kinase domains of Src and p110γ), and the size and shape of their active sites differ due to differences in substrate specificity and modes of regulation (Djordjevic and Driscoll 2002). However, PI3Ks and protein kinases are both members of the kinase super-family. Consequently, the catalytic subunits of PI3Ks share several structural features with protein kinases. The p110α and p110γ structures have a kinase fold typical of protein kinases with a smaller N-terminal lobe and a larger C-terminal lobe that are connected through hinge region residues (Figure 1.2c) (Walker, Perisic et al. 1999; Huang, Mandelker et al. 2007). The interlobe cleft creates a deep hydrophobic pocket where the adenine of ATP makes two hydrogen bonding interactions with backbone amides of the hinge region (Djordjevic and Driscoll 2002). Similar to the P-loop (or glycine-rich loop) of protein kinases, there is a loop between strands kβ3 and kβ4 of PI3K that interacts with the phosphates of ATP (Figure 1.2c) (Walker, Perisic et

al. 1999). However, in PI3Ks this loop has no glycines. Instead, the P-loop of PI3Ks has a Ser (Ser806 in p110γ) that is absolutely conserved in PI3Ks and interacts directly with the β-phosphate of ATP (Walker, Perisic et al. 1999). An N-terminal Lys, Lys883 in p110γ, interacts with the α-phosphate of ATP and is analogous to the catalytic lysine of protein kinases (Figure 1.2c) (Walker, Perisic et al. 1999).

In the C-terminal lobe, conserved Asp, Arg and Asn residues between strands kα6 and kβ9 at the base of the interlobe cleft make up the catalytic loop (Figure 1.2c). Like the residues of the catalytic loop in protein kinases, the catalytic loop residues of PI3K are important for metal ion binding (Walker, Perisic et al. 1999).

As in protein kinases, the PI3K C-terminal domain has an activation segment at the rim of the interlobe cleft that provides a platform for substrate binding (Walker, Perisic et al. 1999). The activation segment in PI3K begins with the Asp-Phe-Glu (DFG) motif, conserved in protein and lipid kinases; the Asp of the DFG (Asp 964 in p110γ) coordinates a metal ion. Following the DFG motif is the activation loop, which binds the phospholipid substrate. The activation loop in PI3K shares the function of the activation loop in protein kinases, but has a very distinct amino acid signature that is tailored for lipid substrate, rather than protein substrate, binding (Djordjevic and Driscoll 2002). In both the p110α and p110γ structures, portions of the activation loop are disordered, suggesting conformational mobility similar to protein kinase activation loops (Walker, Perisic et al. 1999; Huang, Mandelker et al. 2007).

Close to the activation segment is the C-terminal helix αK12 (Figure 1.2c). Recently, it has been suggested that conformational change of the activation loop is mediated by helix αK12 (Huang, Mandelker et al. 2007). However, the exact nature of the conformational changes in the activation loop awaits crystal structures of PI3K bound to phospholipid substrate.

1.2.3 Defining the "gatekeeper" residue

Directly N-terminal to the hinge region in both protein and lipid kinases is a residue known as the gatekeeper residue. The gatekeeper residue lies in the back wall of the ATP-binding cleft and controls access to a hydrophobic pocket (the gatekeeper pocket) that lies deep in the active site, behind the adenine-binding pocket (Figure 1.3, also shown in Figures 1.2a and 1.2c). The size of this residue is a key determinant of
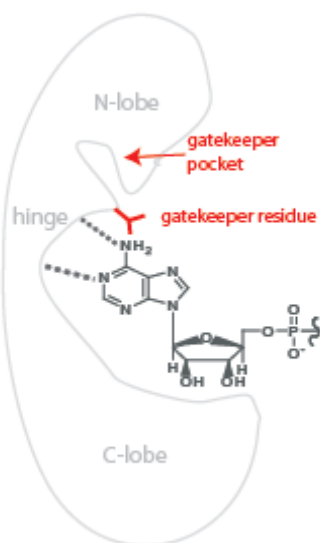
Figure 1.3 The gatekeeper residue controls access to the gatekeeper pocket. A generalized schematic of the ATP binding site in kinases shows the position of the gatekeeper residue. The hydrophobic pocket blocked by the gatekeeper residue is labeled as the gatekeeper pocket; the size and hydrophobicity of the gatekeeper residue determine which inhibitors can access the gatekeeper pocket.

kinase sensitivity to small-molecule inhibition (Liu, Bishop et al. 1999; Bishop, Ubersax et al. 2000). Small-molecule inhibitors can access the gatekeeper pocket in kinases with small gatekeeper residues, while they are sterically blocked from accessing the gatekeeper pocket in kinases with larger gatekeeper residues.

The character of the gatekeeper residue accounts for the specificity of many small-molecule kinase inhibitors. Ser/Thr kinases frequently have large, hydrophobic

gatekeeper residues, such as Phe or Met, whereas tyrosine kinases often have a small, polar gatekeeper residue, such as Thr. All clinical ATP-competitive kinase inhibitors target tyrosine kinases with Thr gatekeeper residues. Clinical resistance to kinase inhibitors has been traced to mutations in the gatekeeper residue, such as the Thr315Ile Bcr-Abl mutation found in Imatinib-resistant CML cells (Gorre, Mohammed et al. 2001). The ability for Ile, a large, hydrophobic residue to confer Imatinib resistance in these cells provides further evidence that the gatekeeper residue is critical for kinase sensitivity to inhibitors.

In contrast to tyrosine kinases, the gatekeeper residue in PI3Ks is Ile, a large hydrophobic residue (Ile879 in p110γ) and it is invariant within the PI3K family (Figure 1.2c) (Alaimo, Knight et al. 2005). The Ile gatekeeper residue is shifted further up and to the left in the active site than its counterpart in tyrosine kinases. At this position, the PI3K gatekeeper residue forms part of the ceiling at the rear of the ATP-binding pocket, helping to make the PI3K pocket distinct from protein kinases in size, shape and inhibitor sensitivity (Alaimo, Knight et al. 2005).

1.3 Significance of research

Drugs that inhibit PTKs and PI3Ks are highly sought after for cancer therapy (Hennessy, Smith et al. 2005). Currently, there are no small molecules that specifically and potently target oncogenic members of both kinase families. This thesis addresses a timely, critical question in cancer therapeutics: can effective polypharmacy be achieved through rational drug design?

Through the research described in the pages of this manuscript, a new class of small molecules is described that simultaneously and potently inhibits PTKs and PI3Ks. We use crystallographic analysis to show that these molecules achieve their specificity through rotation around a bond built into the core of the molecular scaffold, and tissue

14

culture-based experiments to suggest the vast potential of this new class of compounds in the treatment of cancer.

1.4 References

Adams, J. A. (2001). "Kinetic and catalytic mechanisms of protein kinases." Chem Rev 101(8): 2271-90.

Alaimo, P. J., Z. A. Knight, et al. (2005). "Targeting the gatekeeper residue in phosphoinositide 3-kinases." Bioorg Med Chem 13(8): 2825-36.

Baselga, J. (2006). "Targeting tyrosine kinases in cancer: the second wave." Science 312(5777): 1175-8.

Bishop, A. C., J. A. Ubersax, et al. (2000). "A chemical switch for inhibitor-sensitive alleles of any protein kinase." Nature 407(6802): 395-401.

Blume-Jensen, P. and T. Hunter (2001). "Oncogenic kinase signalling." Nature 411(6835): 355-65.

Cantley, L. C. (2002). "The phosphoinositide 3-kinase pathway." Science 296(5573): 1655-7.

Cully, M., H. You, et al. (2006). "Beyond PTEN mutations: the PI3K pathway as an integrator of multiple inputs during tumorigenesis." Nat Rev Cancer 6(3): 184-92.

Dancey, J. E. (2006). "Therapeutic targets: MTOR and related pathways." Cancer Biol Ther 5(9): 1065-73.

Djordjevic, S. and P. C. Driscoll (2002). "Structural insight into substrate specificity and regulatory mechanisms of phosphoinositide 3-kinases." Trends Biochem Sci 27(8): 426-32.

Druker, B. J., C. L. Sawyers, et al. (2001). "Activity of a specific inhibitor of the BCR-ABL tyrosine kinase in the blast crisis of chronic myeloid leukemia and acute lymphoblastic leukemia with the Philadelphia chromosome." N Engl J Med 344(14): 1038-42.

Fabian, M. A., W. H. Biggs, 3rd, et al. (2005). "A small molecule-kinase interaction map for clinical kinase inhibitors." Nat Biotechnol 23(3): 329-36.

Fan, Q. W., Z. A. Knight, et al. (2006). "A dual PI3 kinase/mTOR inhibitor reveals emergent efficacy in glioma." Cancer Cell 9(5): 341-9.

Frantz, S. (2005). "Drug discovery: playing dirty." Nature 437(7061): 942-3.

Fruman, D. A., R. E. Meyers, et al. (1998). "Phosphoinositide kinases." Annu Rev Biochem 67: 481-507.

Garber, K. (2006). "The second wave in kinase cancer drugs." Nat Biotechnol 24(2): 127-30.

Gorre, M. E., M. Mohammed, et al. (2001). "Clinical resistance to STI-571 cancer therapy caused by BCR-ABL gene mutation or amplification." Science 293(5531): 876-80.

Guertin, D. A. and D. M. Sabatini (2007). "Defining the role of mTOR in cancer." Cancer Cell 12(1): 9-22.

Hennessy, B. T., D. L. Smith, et al. (2005). "Exploiting the PI3K/AKT pathway for cancer drug discovery." Nat Rev Drug Discov 4(12): 988-1004.

Hopkins, A. L., J. S. Mason, et al. (2006). "Can we rationally design promiscuous drugs?" Curr Opin Struct Biol 16(1): 127-36.

Huang, C. H., D. Mandelker, et al. (2007). "The structure of a human p110alpha/p85alpha complex elucidates the effects of oncogenic PI3Kalpha mutations." Science 318(5857): 1744-8.

Huse, M. and J. Kuriyan (2002). "The conformational plasticity of protein kinases." Cell 109(3): 275-82.

Jacinto, E., V. Facchinetti, et al. (2006). "SIN1/MIP1 maintains rictor-mTOR complex integrity and regulates Akt phosphorylation and substrate specificity." Cell 127(1): 125-37.

Joensuu, H., P. J. Roberts, et al. (2001). "Effect of the tyrosine kinase inhibitor STI571 in a patient with a metastatic gastrointestinal stromal tumor." N Engl J Med 344(14): 1052-6.

Kannan, N. and S. S. Taylor (2008). "Rethinking pseudokinases." Cell 133(2): 204-5.

Karakas, B., K. E. Bachman, et al. (2006). "Mutation of the PIK3CA oncogene in human cancers." Br J Cancer 94(4): 455-9.

Klejman, A., L. Rushen, et al. (2002). "Phosphatidylinositol-3 kinase inhibitors enhance the anti-leukemia effect of STI571." Oncogene 21(38): 5868-76.

Liu, L., Y. Cao, et al. (2006). "Sorafenib blocks the RAF/MEK/ERK pathway, inhibits tumor angiogenesis, and induces tumor cell apoptosis in hepatocellular carcinoma model PLC/PRF/5." Cancer Res 66(24): 11851-8.

Liu, Y., A. Bishop, et al. (1999). "Structural basis for selective inhibition of Src family kinases by PP1." Chem Biol 6(9): 671-8.

Mellinghoff, I. K., M. Y. Wang, et al. (2005). "Molecular determinants of the response of glioblastomas to EGFR kinase inhibitors." N Engl J Med 353(19): 2012-24.

Nagata, Y., K. H. Lan, et al. (2004). "PTEN activation contributes to tumor inhibition by trastuzumab, and loss of PTEN predicts trastuzumab resistance in patients." Cancer Cell 6(2): 117-27.

Noble, M. E., J. A. Endicott, et al. (2004). "Protein kinase inhibitors: insights into drug design from structure." Science 303(5665): 1800-5.

Nolen, B., S. Taylor, et al. (2004). "Regulation of protein kinases; controlling activity through activation segment conformation." Mol Cell 15(5): 661-75.

Petrelli, A. and S. Giordano (2008). "From single- to multi-target drugs in cancer therapy: when aspecificity becomes an advantage." Curr Med Chem 15(5): 422-32.

Sams-Dodd, F. (2005). "Target-based drug discovery: is something wrong?" Drug Discov Today 10(2): 139-47.

Sawyers, C. L. (2003). "Will mTOR inhibitors make it as cancer drugs?" Cancer Cell 4(5): 343-8.

Sawyers, C. L. (2006). "Will kinase inhibitors have a dark side?" N Engl J Med 355(3): 313-5.

Sebolt-Leopold, J. S. and J. M. English (2006). "Mechanisms of drug inhibition of signalling molecules." Nature 441(7092): 457-62.

Stommel, J. M., A. C. Kimmelman, et al. (2007). "Coactivation of receptor tyrosine kinases affects the response of tumor cells to targeted therapies." Science 318(5848): 287-90.

Strumberg, D., J. W. Clark, et al. (2007). "Safety, pharmacokinetics, and preliminary antitumor activity of sorafenib: a review of four phase I trials in patients with advanced refractory solid tumors." Oncologist 12(4): 426-37.

Taylor, S. S., D. R. Knighton, et al. (1992). "Structural framework for the protein kinase family." Annu Rev Cell Biol 8: 429-62.

Vivanco, I. and C. L. Sawyers (2002). "The phosphatidylinositol 3-Kinase AKT pathway in human cancer." Nat Rev Cancer 2(7): 489-501.

Walker, E. H., O. Perisic, et al. (1999). "Structural insights into phosphoinositide 3-kinase catalysis and signalling." Nature 402(6759): 313-20.

Wheatley-Price, P. and F. A. Shepherd (2008). "Epidermal growth factor receptor inhibitors in the treatment of lung cancer: reality and hopes." Curr Opin Oncol 20(2): 162-75.

Wilhelm, S., C. Carter, et al. (2006). "Discovery and development of sorafenib: a multikinase inhibitor for treating cancer." Nat Rev Drug Discov 5(10): 835-44.

Wilhelm, S. M., C. Carter, et al. (2004). "BAY 43-9006 exhibits broad spectrum oral antitumor activity and targets the RAF/MEK/ERK pathway and receptor tyrosine kinases involved in tumor progression and angiogenesis." Cancer Res 64(19): 7099-109.

Wong, S., J. McLaughlin, et al. (2004). "Sole BCR-ABL inhibition is insufficient to eliminate all myeloproliferative disorder cell populations." Proc Natl Acad Sci U S A 101(50): 17456-61.

Chapter 2:
Development of ATP-competitive small molecules that inhibit phosphoinositide-3-kinases and protein tyrosine kinases

2.1   Introduction

Currently, all FDA-approved multi-kinase inhibitors target members of the same kinase family. The ability to rationally design a molecule that is promiscuous within a kinase family is not surprising given the sequence homology that defines protein families. However, the ability to use rational design to create inhibitors that target two distinct kinase families is less clear. Structural and sequence alignments of the catalytic domains of Src, a PTK, and PI3K, a phosphoinositide kinase, reveal little homology, in contrast to Src and Hck, which are members of the Src kinase family, or Src and VEGFR which are members of different tyrosine kinase families (Figure 2.1). The lack of homology between protein kinases and phosphoinositide kinases reflects differences in substrate specificity and modes of regulation (Djordjevic and Driscoll 2002). However, Src, like PI3K, functions in phosphoryl transfer using ATP as a substrate. Sequence comparison shows common motifs, such as the DFG motif and the catalytic lysine (Figure 2.1b); and structural comparison reveals a common overall topology in the kinase catalytic domains (Figure 2.1a). More specifically, the active sites share a modular composition that includes a hydrophobic region in the vicinity of the gatekeeper residue (described in detail below), an adenine pocket that interacts with the backbone of hinge region residues, an affinity pocket occupied by the conserved catalytic lysine and a hydrophobic region at the active-site entrance (Djordjevic and Driscoll 2002; Knight, Chiang et al. 2004; Knight, Gonzalez et al. 2006; Liu and Gray 2006). By exploiting both modular and sequence similarities between PI3Ks and PTKs, we were able to rationally design inhibitors that specifically and potently target these disparate protein families.

21

a.

Src Hck   Src VEGFR2   Src p110γ

b.

```
                    G-rich loop                    Cat. Lys              Helix αC
p110γ   804  CKVMA.SK.KKPLWLEFKCADPTALSNETIGIIFKHG..........DDLRQD..MLILQILRIM
  Src   270  EVKLGQGCFGEVWMGTWNG.........TTRVAIKTLKP..GTMSPE.APLQEAQVMKKLR....
  Hck   270  EKKLGAGQFGEVWMATYNK.........HTKVAVKTMKP..GSMSVE.APLAEANVMKTLQ....
VEGFR2  837  GKPLGRGAFGQVIEADAFGID...KTATCRTVAVKMLKEGATHSEHR.ALMSELKILIHIGH...

                                      Gatekeeper  Hinge
p110γ   852  ESIWETESLDLCLLPY.GCISTG..DKIGMIEIVKDATTIAKIQQSTVGNTG........AFKDE
  Src   319  .........HEKLVQLYAVVSEE..PIYIVTEYMS.KGSLLDFLKGETG............KYLR
  Hck   319  .........HDKLVKLHAVVTKE..PIYIITEFMA.KGSLLDFLKSDEG............SKQP
VEGFR2  895  .........HLNVVNLLGACTKPGGPLMVIVEFCK.FGNLSTYLRSKRNEFVPYK......DFLT

                                                                  Cat. Asp
p110γ   906  VLSHWLKEKCPIEEKFQAAVERFVYSCAGYCVATFV..LGIGDRHNDNIMISETGNLFHIDFGH
  Src   360  ................LPQLVDMAAQIASGMAYVERMNYVHRDLRAANILVGENLVCKVADFGL
  Hck   360  ................LPKLIDFSAQIAEGMAFIEQRNYIHRDLRAANILVSASLVCKIADFGL
VEGFR2  944  ................LEHLICYSFQVAKGMEFLASRKCIHRDLAARNILLSEKNVVKICDFGL
```

c.

Pair	Relationship	Sequence Identity (KD)	Backbone RMSD (KD)
Src - Hck	Src family kinases	67%	0.76 Å
Src - VEGFR	Tyrosine kinases	36%	2.3 Å
Src - p110γ	Kinases	9%	4.3 Å

Figure 2.1 Structure and sequence comparison of tyrosine kinases and PI3-K a) Kinase domains were aligned by the residues for the universal core as defined by Scheef and Bourne to demonstrate the high structural homology among tyrosine kinases and compare this to the low structural homology between tyrosine and phosphoinositide kinases. B) Sequence alignments of the kinase domains of phosphoinositide 3-kinase p110γ, and tyrosine kinases Src, Hck and VEGFR show phosphoinositide kinases are significantly divergent, though they share some key motifs (eg. DFG). C) Pairwise sequence identity and backbone RMSD values quantify the sequence and structural divergence between tyrosine kinases and phosphoinositide kinase.

2.2   Inhibitor screen identifies two hits

We selected a panel of 20 small molecules from a library of protein kinase inhibitors based on an aryl-pyrazolopyrimidine scaffold. This is the scaffold of 4-amino-1-*tert*-butyl-3-(p-methylphenyl) pyrazolo[3,4-d]pyrimidine (PP1), a well-known inhibitor of the Src family of protein tyrosine kinases (Hanke, Gardner et al. 1996; Liu, Bishop et al. 1999). We tested the PP1 derivatives against α, β, δ and γ isoforms of p110, the catalytic subunit of PI3K, in *in vitro* kinase assays. This screen identified two inhibitors, 3-(4-amino-1-isopropyl-1H-pyrazolo[3,4-d]pyrimidin-3-yl)phenol (S1) and 1-methyl-3-(naphthalen-2-yl)-1H-pyrazolo[3,4-d]pyrimidin-4-amine (S2), that inhibited various PI3Ks at low micromolar (μM) potency (Figure 2.2a, Appendix 1).

2.3   X-ray crystallography reveals inhibitor binding mode in a lipid kinase

S1 and S2 were sent to our collaborator Roger Williams at MRC Cambridge, who solved the crystal structures of these compounds bound to PI3Kγ. The crystal structure revealed the inhibitor binding mode. The main features contributing to PI3K binding are features conserved in protein kinases (Figure 2.2b).

The pyrazolopyrimidine scaffolds of S1 and S2 occupy the adenine region, with the N-5 nitrogen and the exocyclic amine making hydrogen bonds with the amide backbone of hinge region residues. Hinge region hydrogen bonds are common to kinase inhibitors (Hanke, Gardner et al. 1996; Liu, Bishop et al. 1999; Knight and Shokat 2007). The pyrazolopyrimidine satisfies these interactions in a manner similar to the adenine of ATP. The R_2 and R_1 groups, which interact with the active site entrance and a deep hydrophobic pocket, respectively, showed potential to be optimized.

In the structure of S1 bound to p110γ, the catalytic lysine (Lys833), a residue conserved in protein kinases, bends towards the inhibitor, making a hydrogen

23
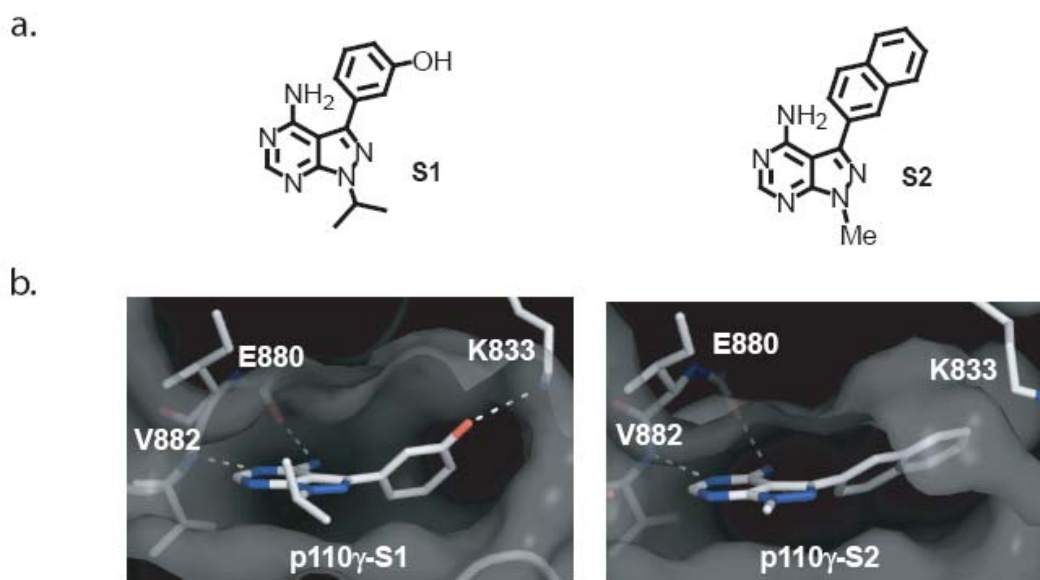
Figure 2.2 X-ray crystallography reveals inhibitor interactions with the lipid kinase p110γ. a) Pyrazolopyrimidines S1 and S2, known protein kinase inhibitors, were low micromolar inhibitors of PI3K. b) S1 and S2 bound to p110γ show interactions with hinge region and deep hydrophobic pocket; these interactions are typical of protein kinase inhibitors.

bond with the R_1-hydroxy of S1 (Figure 2.2b). In contrast, in the p110γ/S2 co-crystal structure, the catalytic lysine reaches away from the inhibitor, augmenting the size of the deep hydrophobic pocket. This creates more space for the napthyl moiety of the R_1 group in S2, enhancing the hydrophobic interactions between S2 and the deep hydrophobic pocket. We hypothesized that both the hydrogen bonding interactions observed in the S1/p110γ co-crystal structure and the extensive hydrophobic interactions observed in the S2/p110γ co-crystal structure might be enhanced by modifying the electronics, hydrogen bonding substituents and/or size of R_1.

The deep hydrophobic pocket that is in the vicinity of the aryl portion of R_1 is adjacent to the gatekeeper residue. The gatekeeper is a residue that controls access to a pre-existing cavity in the back of the ATP-binding pocket. This residue is an important determinant of kinase sensitivity to inhibitors (Liu, Bishop et al. 1999; Bishop, Ubersax et

al. 2000; Shah and Sawyers 2003; Alaimo, Knight et al. 2005; Zhang, Kenski et al. 2005). PI3K has an Ile gatekeeper residue, whereas many tyrosine kinases (ex. EGFR, HCK, PDGFR) have a Thr gatekeeper residue (Liu, Bishop et al. 1999; Alaimo, Knight et al. 2005). Both of these gatekeeper residues are small beta-branched amino acids, however Ile is hydrophobic and Tyr is polar and has hydrogen bonding capacity. We anticipated that a medicinal chemistry effort with R_1 derivatization could yield an aryl group whose binding interactions with the catalytic lysine and the hydrophobic gatekeeper pocket would be optimized and specific to PI3K and PTKs.

The R_2 isopropyl of S1 and the R_2 methyl of S2 occupy the entrance to the ATP binding pocket, below Met804, a residue known to be conformationally mobile (Knight, Gonzalez et al. 2006). Therefore, we anticipated that derivatization of R_2 may have unpredictable conformational effects in the lipid kinase, affecting inhibitor potency. In addition, the size of the active-site entrance is smaller in PI3K than PTKs. This is evidenced by the ability of PP1 (*t*-butyl at R_2) to inhibit Src family kinases but not PI3K (Appendix 1). We hypothesized that systematic derivatization of R_2 would reveal an R_2 ideal in size and conformation for dual-specificity inhibition.

2.4   Inhibitor target profiles guide compound development

Using two simple synthetic schemes (Figure 2.3) we made a diverse compound library of pyrazolopyrimidines (PP). As compounds were synthesized they were tested *in vitro* against the purified kinase domains of p110α, p110β, p110δ, p110γ, DNA-Dependent Protein Kinase (DNA-PK), mTOR, phosphatidylinositol 4-kinase β (PI4Kβ), Abl, Hck, Src, Src(T338I), VEGFR, EGFR and EPH receptor B4 (EphB4)
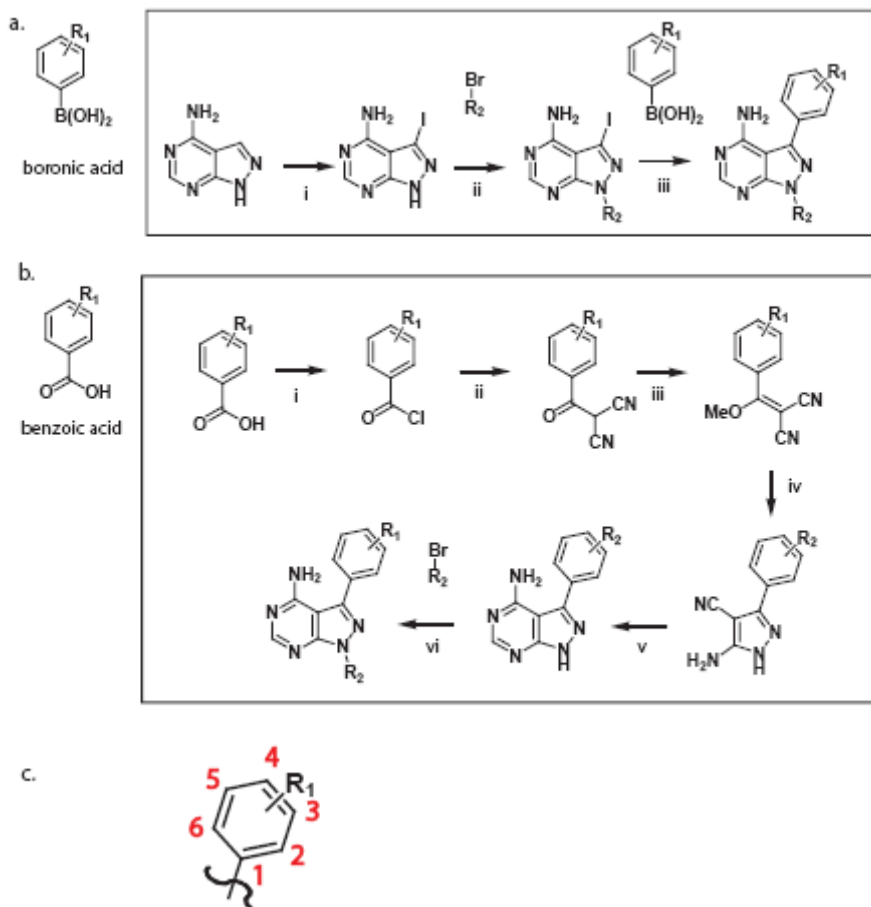
Fig. 2.3 Synthetic scheme a) Synthetic scheme based on boronic acid availability. i. NIS, DMF, 50˚C; ii. alkyl halide, K_2CO_3, DMF, 80˚C; iii. Boronic acid, $Pd(PPh_3)_4$, EtOH, DME. sat. $NaCO_3$, 90˚C. b) Synthetic scheme based on benzoic acid availability. i. Benzoic acid, DMF, CH_2Cl_2, 0˚C; ii. Oxalyl chloride, 37˚C; iii. malononitrile, NaH, THF, 0˚C - 37˚C; iv. $NaHCO_3$, $(CH_3)_2SO_4$, 1,4 dioxane, H_2O, 90˚C; v. hydrazine, EtOH, 37˚C; vi. formamide, 180˚C; vii. alkyl halide, K_2CO_3, DMF, 80˚C. c) To facilitate discussion of the SAR data, the R_1 carbon attached to the pyrazole is defined as the 1-position and the subsequent numbering is shown.

(Appendix 1). The medicinal chemistry effort was divided into two broad categories: phenol derivatives of S1 and napthyl derivatives of S2 (Figure 2.4a, Appendix 1).

2.5   Inhibitors yield sharp structure-activity relationship (SAR) data

Our synthetic efforts were guided by the target profiles of the compounds, which showed sharp SAR data (Figure 2.4, Figure 2.5). To facilitate the discussion of the SAR data, the R_1 carbon attached to the pyrazole is defined as the 1-position, as shown in Figure 2.3c. Derivatization of S1 at the R_1 position revealed that PTKs were inhibited more potently by 3-phenol than 4-phenol. Lipid kinases were inhibited equally by 3- and 4-phenol and, overall, 3-phenol conferred the greatest dual potency. As an example, the 4-phenol compound 5-(4-amino-1-isopropyl-1H-pyrazolo[3,4-d]pyrimidin-3-yl)-2-hydroxybenzonitrile (PP257) is a selective lipid kinase inhibitor but the 3-phenol compound 4-(4-amino-1-isopropyl-1H-pyrazolo[3,4-d]pyrimidin-3-yl)-2-hydroxybenzonitrile (PP155), inhibits lipid and protein kinases potently. SAR analysis also showed that potency against both targets is abolished by the addition of a substituent at the 2-position of the phenol and enhanced by the addition of a halogen at the 4- or 5- positions (F < Cl < Br, in order of increasing potency). Halogen substitution at the 4-position enhanced potency more than halogen substitution at the 5-position, and substitution of a small electron-donating group (ex. methoxy or methyl) at the 4-position of the phenol enhanced potency against both targets.

Sharp SAR data was also found for S2 derivatization at the R_1 position. The lipid kinases were more potently inhibited by large hydrophobic moieties that had diminished hydrogen bonding capacity, whereas the protein kinases were less tolerant of these compounds. For example, 6-(4-amino-1-isopropyl-1H-pyrazolo[3,4-d]pyrimidin-3-yl)naphthalen-2-ol (PP17), a 6-hydroxy-napthyl compound which combines the napthyl of S2 with the hydrogen bonding capacity of S1, showed greatest potency against

27

protein kinases and moderate potency against the lipid kinases. In contrast, 1-isopropyl-3-(quinolin-6-yl)-1H-pyrazolo[3,4-d]pyrimidin-4-amine (PP102), a 6-quinoline, was one of the most selective and potent compounds against lipid kinases, and was significantly less potent against protein kinases when compared to the S1 derivatives. Strikingly, movement of the nitrogen in the quinoline moiety to any other position significantly decreased or, in the case of the 6-isoquinoline, 1-isopropyl-3-(isoquinolin-6-yl)-1H-pyrazolo[3,4-d]pyrimidin-4-amine (PP129), completely abolished potency against the protein kinases and lipid kinases (Figure 2.5). Addition of exocyclic substituents to the quinoline (ex. the methyl-quinoline, 1-isopropyl-3-(2-methylquinolin-6-yl)-1H-pyrazolo[3,4-d]pyrimidin-4-amine (PP118)) or addition of heteroatoms (ex. the quinoxiline, 1-isopropyl-3-(quinoxalin-7-yl)-1H-pyrazolo[3,4-d]pyrimidin-4-amine (PP132)) diminished potency against the lipid kinases and abolished potency against the protein kinases.

Indole derivatives were also synthesized in an effort to combine the desirable chemical properties of S1 and S2. Compounds with an aza-indole, such as 1-cyclopentyl-3-(1H-pyrrolo[2,3-b]pyridin-5-yl)-1H-pyrazolo[3,4-d]pyrimidin-4-amine (PP121) at the R_1 position conferred the greatest dual potency, whereas changing R_1 to an imidazole-pyridine, such as 3-(H-imidazo[1,2-a]pyridin-7-yl)-1-isopropyl-1H-pyrazolo[3,4-d]pyrimidin-4-amine (PP161), completely abolished potency against both targets. The 5-indole (ex. 3-(1H-indol-5-yl)-1-isopropyl-1H-pyrazolo[3,4-d]pyrimidin-4-amine (PP89)) retained potency against tyrosine kinases, but lost potency against the lipid kinases. In contrast, the 6-indole, 3-(1H-indol-6-yl)-1-isopropyl-1H-pyrazolo[3,4-
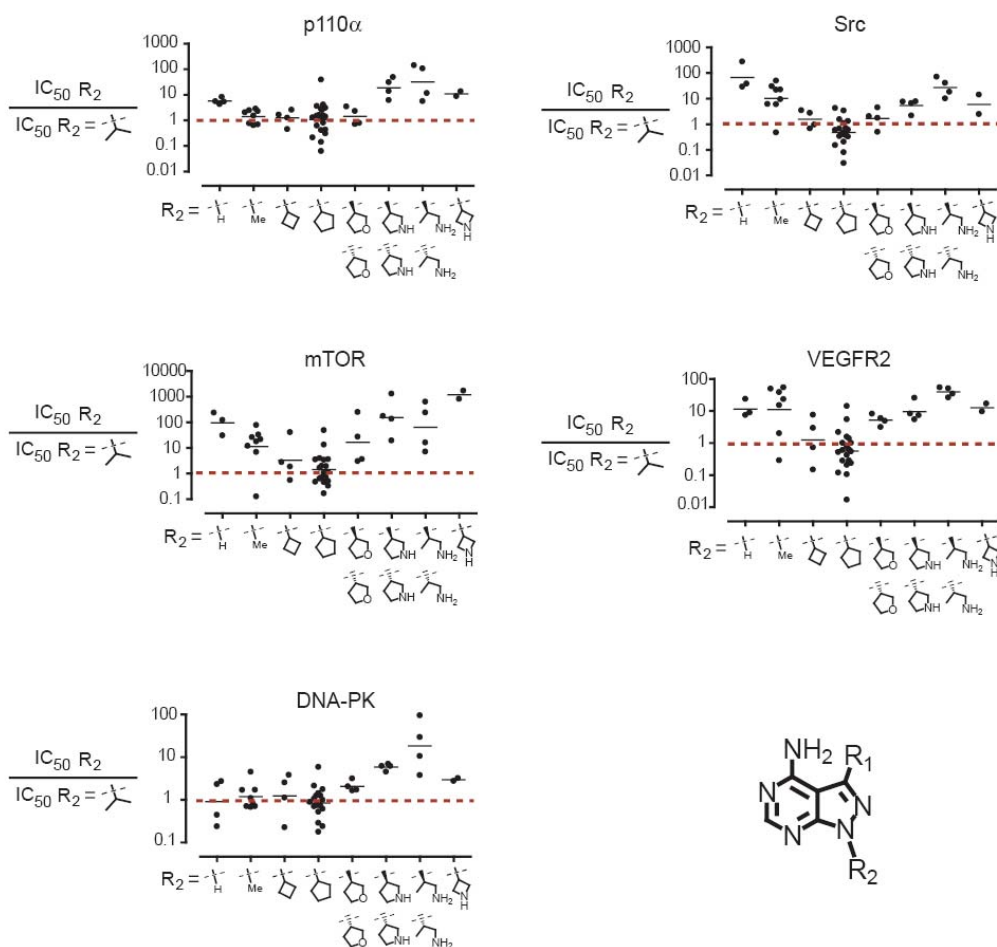
Figure 2.4 IC$_{50}$ analysis of PP inhibitors derivatized at the R$_2$ position shows sharp SAR data. Few R$_2$ groups are more potent than isopropyl at the R$_2$ position against tyrosine or phosphoinsitide kinases. Those of equal or greater potency than isopropyl are largely cyclopentyl groups.

29
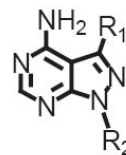
d]pyrimidin-4-amine (PP107), retained potency against only Src-family kinases. Addition

of a nitrogen to the indole to make the indazole (3-(1H-indazol-6-yl)-1-isopropyl-1H-

pyrazolo[3,4-d]pyrimidin-4-amine (PP110) or 3-(1H-indazol-5-yl)-1-isopropyl-1H-
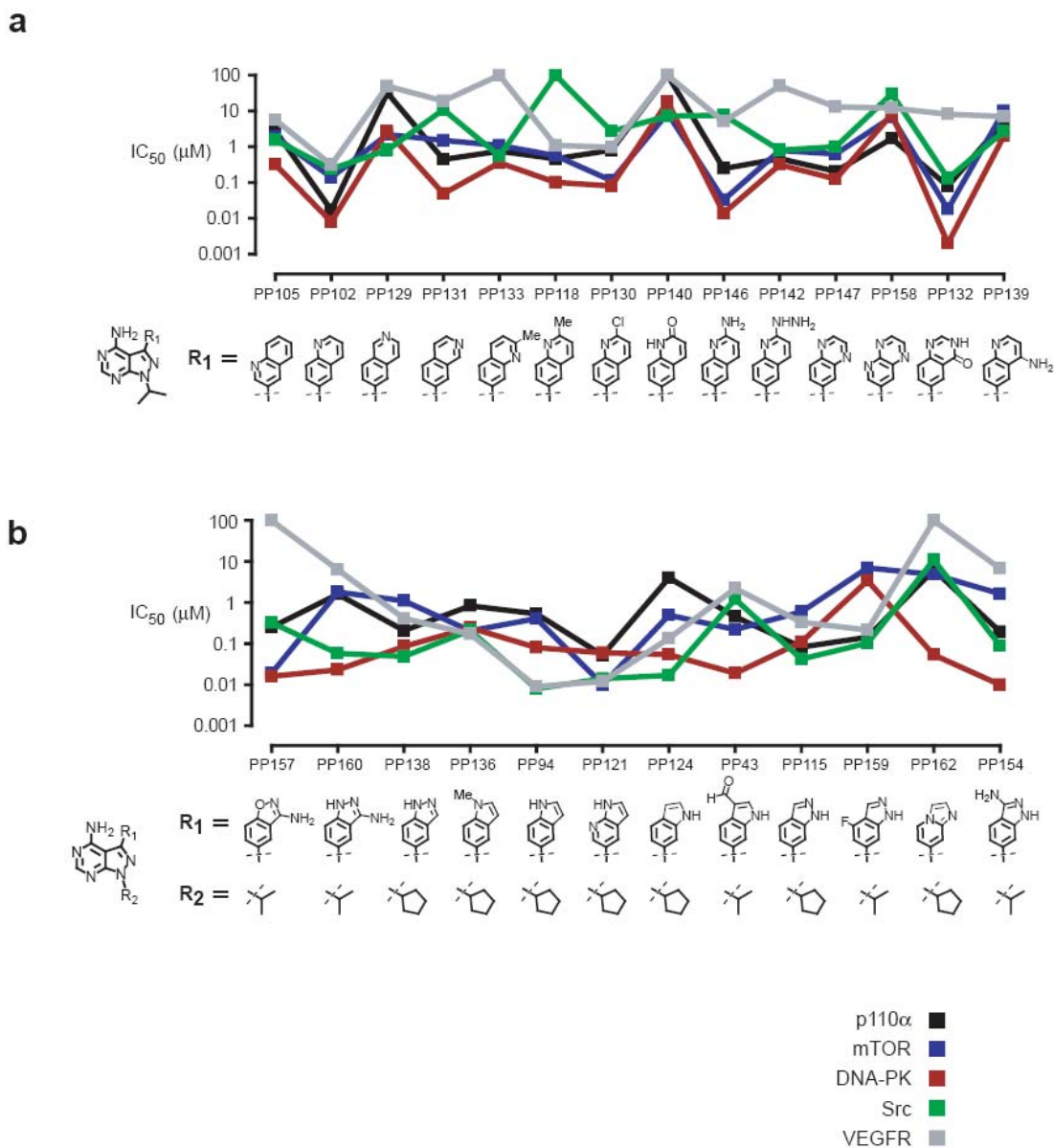
Figure 2.5 R₁ derivatization shows sharp SAR data. Small changes in the chemical structure result in large changes in potency and target profiles.

pyrazolo[3,4-d]pyrimidin-4-amine (PP137)) enhanced lipid kinase activity and had little effect on protein kinase activity. The addition of exocyclic substituents to the indole or indazole diminished dual potency.

The SAR at the R_2 position was R_1-dependent, though many of the trends were similar in the S1 and S2 derivatives. Branched residues at the alpha carbon increased potency against both targets (methylene consistently abolished potency). For alkyl rings, ring size affected potency. Cyclopentyl conferred greater potency than other alkyl rings (cyclobutyl, cyclohexyl etc.). The addition of heteroatoms (N or O) to straight-chain or cyclic R_1 groups consistently diminished potency.

A methyl at the R_2 position was tolerated by the lipid kinases but not the protein kinases. Cyclopentyl at the R_2 position enhanced potency against the protein kinases and slightly diminished potency against the lipid kinases. Overall, isopropyl conferred the greatest dual-specificity inhibition. However, the compound with the profile that displayed the most desirable target profile as a dual-specificity inhibitor was PP121, which has an aza-indole moiety at the R_1 position and a cyclopentyl moiety at the R_2 position.

Through an iterative process that included chemical synthesis, kinase activity profiling and SAR analysis, we were able to develop pyrazolopyrimidines (PP inhibitors) with a continuum of activity against lipid and protein tyrosine kinases (Figure. 2.6a). The specificities ranged from tert-butyl 4-(4-amino-1-isopropyl-1H-pyrazolo[3,4-d]pyrimidin-3-yl)-2-methoxyphenylcarbamate (PP20), selective for protein kinases, to PP121, potent against lipid and protein kinases, to compounds selective for kinase in PI3K related family, such as 2-(4-amino-1-isopropyl-1H-pyrazolo[3,4-d]pyrimidin-3-yl)-1H-indol-5-ol (PP242) which is mTOR selective, and 1-cyclopentyl-3-(H-imidazo[1,2-a]pyridin-7-yl)-1H-pyrazolo[3,4-d]pyrimidin-4-amine (PP162), which is DNA-PK selective. Significantly, PP242 is the first selective, ATP-competitive mTOR inhibitor to be described.
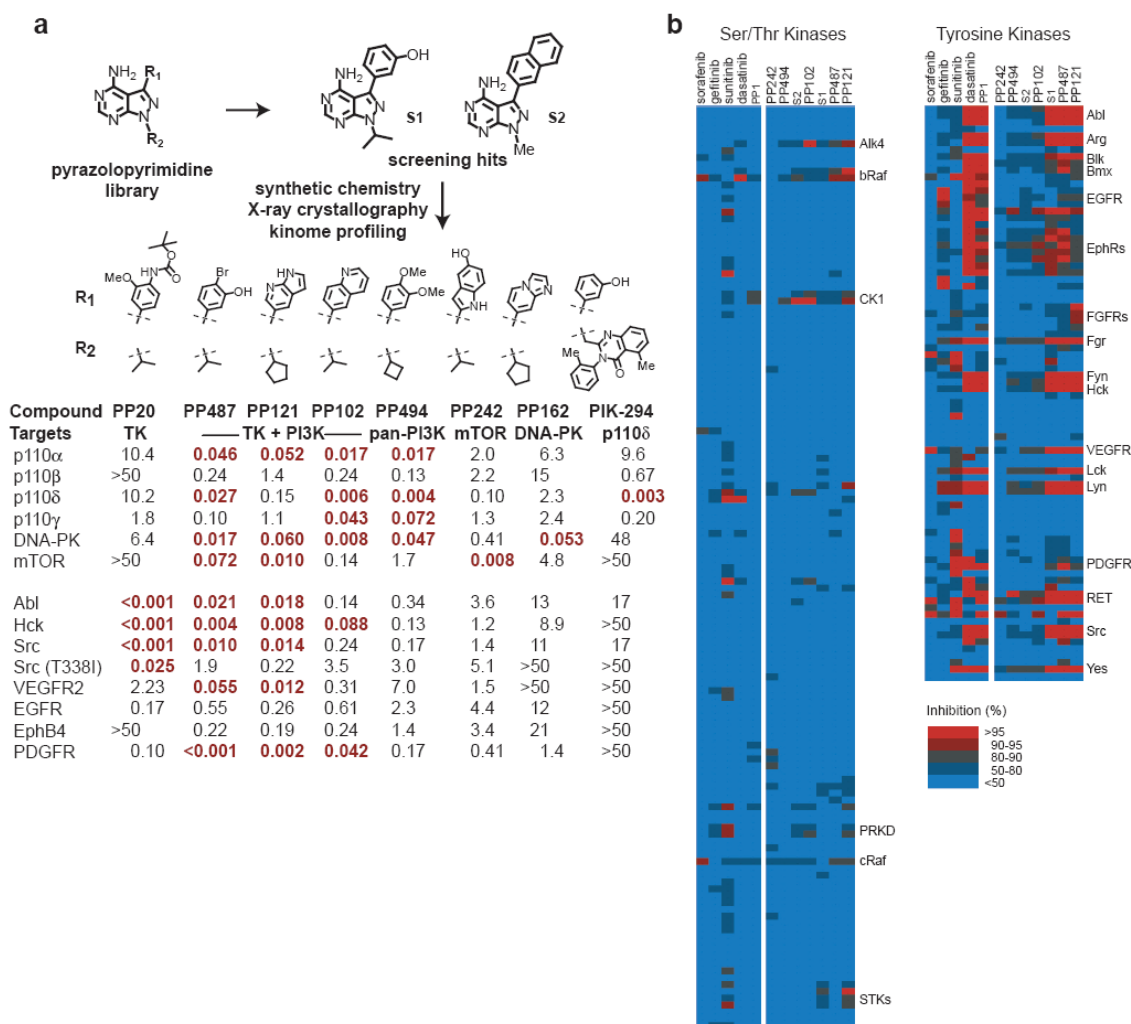
Figure 2.6 Kinase target profiles of PP inhibitors. a) Through directed chemical optimization, pyrazolopyrimidines were synthesized with a spectrum of activity against tyrosine kinases and phosphoinositide kinases. b) Screening a panel of PP inhibitors against 219 protein kinases revealed selectivity profiles similar to PP1, which a selective Src-family kinase inhibitor with a pyrazolopyrimidine scaffold, and several clinical kinase inhibitors.

2.6.   Kinome-wide inhibitor profiling reveals compounds selectivity

To verify the selectivity of the PP compounds against desired lipid and protein

tyrosine kinases, the most potent inhibitors were profiled at 1μM against a

panel of 219 protein kinases. All compounds screened showed selectively for protein

tyrosine kinases (Figure 2.6b), that mirrored the selectivity of the Src-family kinase

32

inhibitor PP1 and several clinical kinase inhibitors. The PP compounds had little effect

on Ser/Thr kinases.

2.7   Co-crystal structures of Src/dual-specificity inhibitors reveal PTK binding mode

To understand how the PP compounds achieved potency against both lipid and

protein tyrosine kinases we solved co-crystal structures of Src bound to several PP

inhibitors. This work was done in collaboration with Jimmy Blair, a fellow graduate

student. As with the lipid kinase/PP inhibitor co-crystal structures, the backbone of the

hinge region of Src makes hydrogen bonds with the PP inhibitor scaffold that are critical

for high-affinity inhibitor binding. However, the binding of the compounds in the active

site of Src is shifted up and to the left relative to the how the compounds are bound in

the lipid kinase (Figure 2.7a). This places the inhibitors deeper into the active site of Src

and positions the R_1 aryl moieties below the Thr gatekeeper residue (Thr338) where they

can access the deep hydrophobic pocket in the back of the Src active site. In the lipid

kinase where the gatekeeper residue (Ile879) is located further up and to the left in the

active site, the location of the compound toward the front of the active site places the

aryl portion of the R_1 substituent below the gatekeeper residue and into a deep

hydrophobic pocket, where it strengthens hydrophobic interactions between the R_1

moiety and the lipid kinase (Figure 2.7a).   In order to achieve this mode of binding, the

bond between the pyrazolopyrimidine core and the R_1 subsitutent is rotated ~90º in the

lipid kinase when compared to the protein kinase (Figure 2.7a). This rotatable bond,

which is intrinsic to
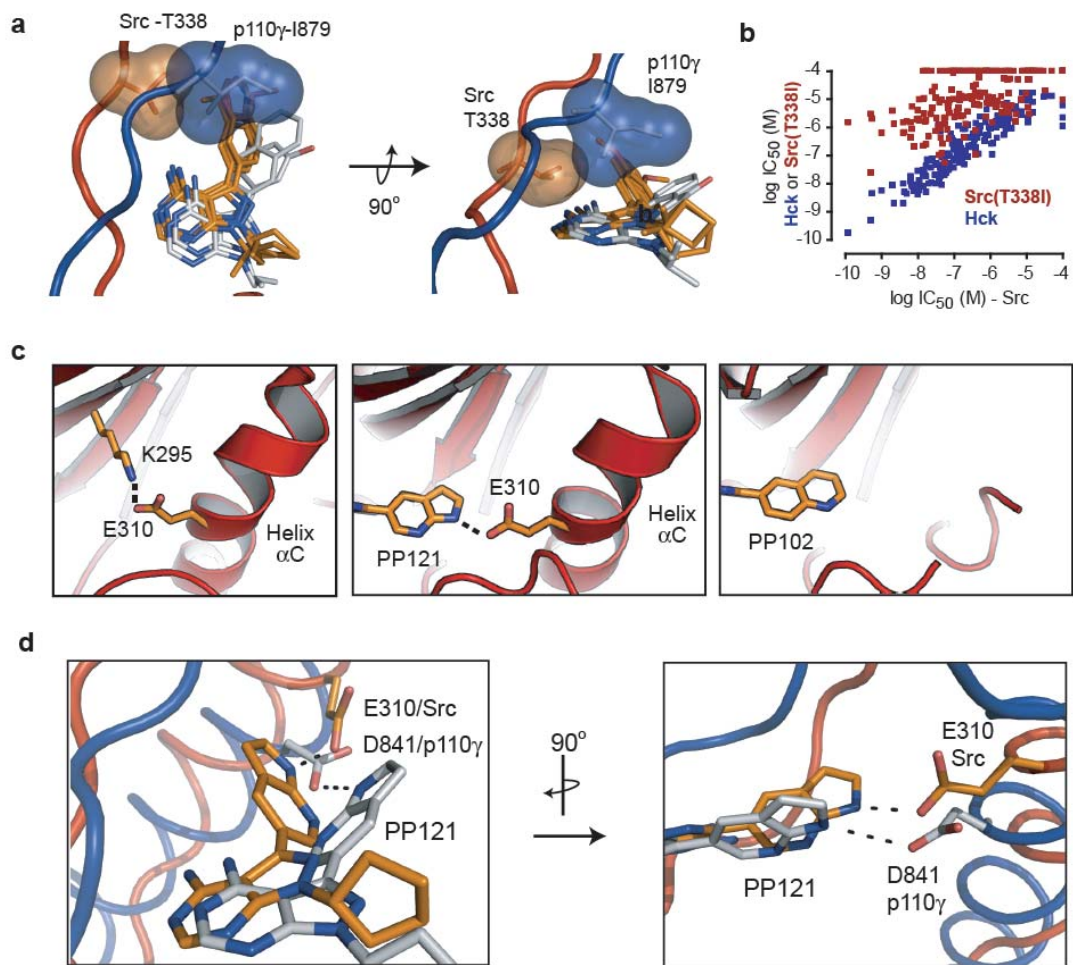
Fig. 2.7 Co-crystal structures of dual-specificity inhibitors bound to p110γ and Src reveal inhibitor binding mode and explain SAR data. a) Backbone regions of p110γ and Src were aligned in structures with PP inhibitors bound, showing the displacement of PP inhibitors further into the lipid kinase pocket than the protein kinase pocket, the rotation of the molecular scaffold that allows binding to both kinase families, and the position of the gatekeeper residue. b) *In vitro* kinase assays confirm the importance of the gatekeeper in PP inhibitor binding. c) The structure of PP121 bound to Src shows PP121 hydrogen bonds with E310, ordering helix αC and providing structural rational for the potency of this compounds compared to other compounds, such as PP102, which cannot make the same interaction. f) Modeling suggests PP121 can make a similar interaction with D841 in p110γ.

the pyrazolopyrimidine scaffold, allows the R_1 moiety to access the hydrophobic pockets that exist in distinct regions of the Src and p110γ active sites.

The importance of the gatekeeper residue in compound binding was confirmed *in vitro.* Dual-specificity inhibitors were tested against the purified kinase domain of Src containing a sterically forbidding T338I gatekeeper mutation. The T338I mutation abolished inhibitor potency (Figure 2.7b). This provided definitive evidence that the small gatekeeper residue of tyrosine kinases enables the selectivity of these compounds, and also provides a structural rational for the lack of activity of these compounds against Ser/Thr kinases, which typically have larger gatekeeper residues, such as Met or Phe (Hanke, Gardner et al. 1996).

The crystal structure of Src with PP121, the potent dual-specificity inhibitor, revealed a hydrogen bonding interaction between the indole nitrogen of the aza-indole inhibitor and E310 of the αC helix in Src (Figure 2.7c). This hydrogen bond mimics the bond between the catalytic lysine (K295 in Src) and E310 on the helix αC of the apo structure of Src (Figure 2.7c) (Huse and Kuriyan 2002). The hydrogen bonding interaction and the ordering of helix αC are necessary for placing Src in an active confirmation, and provide an explanation for the potency of PP121, which would be expected to bind more tightly in the active site than compounds such as PP102, which lack the ability to make this hydrogen bonding interaction (Figure 2.7c). Although we do not have the structure of PP121 bound to the lipid kinase, a model generated by replacing the R_1 group of S1 with an azaindole in the p110γ co-crystal structure suggests a similar interaction is possible in PI3K (Figure 2.7d).

2.8 Conclusion

Through iterative chemical synthesis and kinome screening we developed a panel of pyrazolopyrimidines with a continuum of activity against protein tyrosine kinases and phosphoinositide kinases. To our knowledge, these are the first compounds with selectivity and specificity for these distantly-related kinases. Using crystallographic analysis we discovered that the rotatable bond between the aryl- R_1 moiety and the pyrazolopyrimidine scaffold was the critical component of the small molecules that enabled dual-specificity inhibition.

2.9 Experimental Procedures

2.9.1 Synthetic methods

All RP-HPLC was carried out on either a Varian ProStar solvent delivery system or a Ranin SD-200 solvent delivery system each equipped with a Zorbax 300-SB C18 column. The column was eluted with $CH_3CN/H_2O/0.1\%TFA$ (1-100% gradient), which was monitored by UV at λ=260 nm. ^{1}H and ^{13}C NMR were recorded on a Varian Innova 400 spectrometer at 400 MHz and 100 MHz, respectively. [1]H chemical shifts are reported in δ (ppm) as s (singlet), d (doublet), t (triplet), q (quartet), m (multiplet) or br (broad) and are referenced to the residual solvent peak. Low resolution electrospray ionization LC/MS (ESI-MS) were recorded on a Waters Micromass ZQ equipped with a Waters 2695 Separations module using an XTerra MS C18 3.6µm column (Waters).

Synthesis of 1H-pyrazolo[3,4-d]pyrimidin-4-amine **(BA18)**

A solution of 250 mL of formamide and 3-amino-4-pyrazolecarbonitrile (25 g, 0.231 mol) was heated to 180°C overnight under an argon atmosphere. Reaction was cooled and 400 mL of dH$_2$O were added. The resulting solid was filtered and rinsed with

cold dH$_2$O. White solid precipitate was collected and dried *in vacuo* overnight to yield

BA18 (39 g, 100% yield). ^{1}H NMR (DMSO-*d$_6$*) δ 8.13 (s, 1H), 8.07 (s, 1H), 7.6 (br); ^{13}C

NMR (DMSO-*d$_6$*) δ 163.5, 158.6, 156.4, 133.1, 100.2; ESI-MS (M+H)$^+$ *m/z* calcd 136.1,

found 136.1.

Synthesis of 3-iodo-1H-pyrazolo[3,4-d]pyrimidin-4-amine **(BA19)**

A solution of 3H-pyrazolo[3,4-d]pyrimidin-4-amine (10g, 0.074 mol) and n-iodo-

succinamide (25 g, 0.111 mol) in DMF (80mL) was heated to 80°C overnight under an

argon atmosphere. The resulting solid was filtered and rinsed with cold EtOH. Product

was dried *in vacuo* overnight to yield BA19 (24 g, 100% yield). ^{1}H NMR (DMSO-*d$_6$*) δ

11.06 (br, 1H), 8.17 (s, 1H); ^{13}C NMR (DMSO-*d$_6$*) δ 157.6, 156.0, 155.2, 102.5, 89.8;

ESI-MS (M+H)$^+$ *m/z* calcd 262.0, found 262.0

Synthesis of 3-iodo-1-isopropyl-1H-pyrazolo[3,4-d]pyrimidin-4-amine **(PP12)**

A solution of 3-iodo-1H-pyrazolo[3,4-d]pyrimidin-4-amine (2 g, 0.0077 mol) and

K$_2$CO$_3$ (4.2g, 0.031 mol) in DMF (50 mL) was brought to 80°C under an argon

atmosphere. Isopropylbromide (1.0g, 0.0084 mol) was added with a syringe. Reaction

was refluxed under argon atmosphere for 2 hours. Solid K$_2$CO$_3$ was removed by

filtration. Solvent was partially removed *in vacuo*. Sodium citrate (50 mL) was added

and reaction was extracted with EtOAc. Organic phases concentrated *in vacuo* and

purified using silica gel column chromatography [MeOH—CH$_2$Cl$_2$, 5:95] yielding PP12

(1.68 g, 72% yield). ^{1}H NMR (CDCl$_3$) δ 8.31 (s, 1H), 5.99 (br, 2H), 5.07 (m, *J*=6.6 Hz,

1H); ^{13}C NMR (CDCl$_3$) δ 157.5, 155.9, 153.2, 104.2, 85.6, 49.9, 22.2; ESI-MS (M+H)$^+$

m/z calcd 304.0, found 304.1. ESI-HRMS (M+H)$^+$ *m/z* calcd 304.0059, found 304.0049.

Synthesis of 1-cyclopentyl-3-iodo-1H-pyrazolo[3,4-d]pyrimidin-4-amine **(BA80)**

A solution of 3-iodo-1H-pyrazolo[3,4-d]pyrimidin-4-amine (400 mg, 1.53 mmol) and K_2CO_3 (1 g, 6 mmol) in DMF (5 mL) was stirred at room temperature under an argon atmosphere. Iodocyclopentane (1.0g, 0.0084 mol) was added with a syringe. Reaction was refluxed under argon atmosphere for 2 hours. Solid K_2CO_3 was removed by filtration. Solvent was partially removed *in vacuo*. Sodium citrate (50 mL) was added and reaction was extracted with EtOAc. Organic phases concentrated *in vacuo* and purified using silica gel column chromatography [MeOH—CH_2Cl_2, 5:95] yielding B80 (300 mg, 60% yield). ESI-MS (M+H)$^+$ *m/z* calcd 330.0, found 330.0.

Synthesis of 3-iodo-1-methyl-1H-pyrazolo[3,4-d]pyrimidin-4-amine (**BA109**).

A solution of 3-iodo-1H-pyrazolo[3,4-d]pyrimidin-4-amine (2 g, 7.69 mmol) and K_2CO_3 (4.25 g, 30.8 mmol) in DMF (5 mL) was stirred at room temperature under an argon atmosphere. Iodomethane (1.17 mL, 7.69 mmol) was added with a syringe. Reaction was stirred under an argon atmosphere at room temperature for 2 hours. Solid K_2CO_3 was removed by filtration. Solvent was partially removed *in vacuo*. Sodium citrate (50 mL) was added and reaction was extracted with EtOAc. Organic phases concentrated *in vacuo* and purified using silica gel column chromatography [MeOH—CH_2Cl_2, 5:95] yielding BA109 (212 mg, 10% yield). ^{1}H NMR (CDCl$_3$) δ 8.31 (s, 1H), 4.07 (s, 3H); ESI-MS (M+H)$^+$ *m/z* calcd 275.9, found 275.9

General synthetic method for **PP14-15, PP17, PP20, PP21, BA22, PP23, BA24, PP26, PP30-PP32, PP34, PP35, PP38-PP46, PP48-PP49; PP52-PP56, PP59, PP60; PP62-PP66, PP262, PP85, PP86, PP89, PP91, PP95, PP96, PP102, PP105-PP108, PP110, PP118, PP128-PP135, PP139, PP140, PP143, PP145, PP149-PP153, PP156, PP158 and PP161:**

A solution of boronic acid (2.5 equivalents) in EtOH (1.65 mL) was added to a solution of 3-iodo-1-isopropyl-1H-pyrazolo[3,4-d]pyrimidin-4-amine (**BA12**, 1 equivalent) in DME (6 mL). Pd(PPh$_3$)$_4$ (8 mg, 0.08 mmol) and saturated Na$_2$CO$_3$ (0.95 mL) were added and the reaction was heated to 90°C under an argon atmosphere overnight (Suzuki reaction). After cooling, the reaction was extracted with saturated NaCl and CH$_2$Cl$_2$. Organic phases were combined, concentrated *in vacuo* and purified by RP-HPLC (MeCN:H$_2$O:0.1% TFA) to yield desired products. Products were analyzed by LC-MS, ^{1}H NMR and ESI-HRMS.

General synthetic scheme for **BA81, PP88, PP94, PP90,PP92, PP97, PP112, PP115, PP121, PP122, PP124, PP138, PP141, PP144 and PP162.**

A solution of boronic acid (2.5 equivalents) in EtOH (1.65 mL) was added to a solution of 1-cyclopentyl-3-iodo-1H-pyrazolo[3,4-d]pyrimidin-4-amine (**BA80**, 1 equivalent) in DME (6 mL). Pd(PPh$_3$)$_4$ (8 mg, 0.08 mmol) and saturated Na$_2$CO$_3$ (0.95 mL) were added and the reaction was heated to 90°C under an argon atmosphere overnight (Suzuki reaction). After cooling, the reaction was extracted with saturated NaCl and CH$_2$Cl$_2$. Organic phases were combined, concentrated *in vacuo* and purified by RP-HPLC (MeCN:H$_2$O:0.1% TFA) to yield desired products. Products were analyzed by LC-MS, ^{1}H NMR and ESI-HRMS.

General synthetic scheme for **PP111, PP114, PP116, PP117, PP119, PP120, PP148**.

A solution of boronic acid (2.5 equivalents) in EtOH (1.65 mL) was added to a solution of 3-iodo-1-methyl-1H-pyrazolo[3,4-d]pyrimidin-4-amine (**BA109**, 1 equivalent) in DME (6 mL). Pd(PPh$_3$)$_4$ (8 mg, 0.08 mmol) and saturated Na$_2$CO$_3$ (0.95 mL) were added and the reaction was heated to 90°C under an argon atmosphere overnight (Suzuki reaction). After cooling, the reaction was extracted with saturated NaCl and CH$_2$Cl$_2$.

Organic phases were combined, concentrated *in vacuo* and purified by RP-HPLC

(MeCN:H$_2$O:0.1% TFA) to yield desired products. Products were analyzed by LC-MS.

Synthesis of 4-(4-Amino-1-isopropyl-1H-pyrazolo[3,4-d]pyrimidin-3-yl)-

benzenesulfonamide **(PP14)**

Benzenesulfonamide-4-boronic acid pinacol ester (23 mg, 0.08 mmol) and 3-

iodo-1-isopropyl-1H-pyrazolo[3,4-d]pyrimidin-4-amine (20 mg, 0.07 mmol) were coupled

via the Suzuki reaction to yield PP14 (2.2 mg, 10% yield). ESI-MS (M+H)[+] *m/z* calcd

333.1, found 333.1. ESI-HRMS (M+H)[+] *m/z* calcd 333.1134, found 333.1126.

Synthesis of 4-(4-amino-1-isopropyl-1H-pyrazolo[3,4-d]pyrimidin-3-yl)-2-methoxyphenol

(PP15)

2 methoxy-4-(4,4,5,5-tetramethyl-1,3-2-dioxaborolan-2-yl) phenol (19 mg, 0.08

mmol) and 3-iodo-1-isopropyl-1H-pyrazolo[3,4-d]pyrimidin-4-amine (20 mg, 0.07 mmol)

were coupled via the Suzuki reaction to yield PP15 (4.3 mg, 20% yield). ^{1}H NMR

(DMSO-d_6) δ 9.39 (br), 8.34 (s, 1H), 7.16 (d, *J*=2.3 Hz, 1H), 7.08 (dd, *J*=8.0 Hz, *J*=2.1

Hz, 1H), 6.939 (d, *J*=8.0 Hz, 1H); ESI-MS (M+H)[+] *m/z* calcd 300.1, found 300.2. . ESI-

HRMS (M+H)[+] *m/z* calcd 300.1461, found 300.1462.

Synthesis of 6-(4-amino-1-isopropyl-1H-pyrazolo[3,4-d]pyrimidin-3-yl)naphthalen-2-ol

(PP17)

6-hydroxynaphthalen-2-yl-2-boronic acid (15 mg, 0.08 mmol) and 3-iodo-1-

isopropyl-1H-pyrazolo[3,4-d]pyrimidin-4-amine (20 mg, 0.07 mmol) were coupled via the

Suzuki reaction to yield PP17 (4.8 mg, 23% yield). ^{1}H NMR (CD$_3$OD) δ 8.37 (s, 1H), 8.08

(s, 1H), 7.86 (d, *J*=8.6 Hz, 2H), 7.71 (dd, *J*=8.7 Hz, *J*=1.5 Hz, 1H), 7.22 (d, *J*=2.4Hz, 1H),

7.18 (dd, *J*=8.9, *J*=2.4, 1H), 5.24 (m, *J*=6.6 Hz, 1H), 1.62 (d, *J*=6.6 Hz, 6H); ESI-MS

(M+H)$^+$ *m/z* calcd 320.1, found 320.1. ESI-HRMS (M+H)$^+$ *m/z* calcd 320.1511, found

320.1499.

Synthesis of tert-butyl 4-(4-amino-1-isopropyl-1H-pyrazolo[3,4-d]pyrimidin-3-yl)-2-

methoxyphenylcarbamate **(PP20)**

        4-N-Boc-amino-3-methoxy-benzeneboronic acid (48 mg, 0.18 mmol) and 3-iodo-

1-isopropyl-1H-pyrazolo[3,4-d]pyrimidin-4-amine (50 mg, 0.18 mmol) were coupled via

the Suzuki reaction to yield PP20. ^{1}H NMR (CDCl$_3$) δ 8.22 (s, 1H), 7.82 (d, J=8.3 Hz,

1H), 7.64 (s, 1H), 7.32 (s, 1H), 6.37 (br), 5.29 (m, *J*=6.7 Hz, 1H), 4.00 (s, 3H), 1.63 (d,

J=6.6 Hz, 6H), 1.53 (s, 9H); ESI-MS (M+H)$^+$ *m/z* calcd 399.2, found 399.1.

Synthesis of 3-(4-amino-3-methoxyphenyl)-1-isopropyl-1H-pyrazolo[3,4-d]pyrimidin-4-

amine (**PP202**)

        A solution of tert-butyl 4-(4-amino-1-isopropyl-1H-pyrazolo[3,4-d]pyrimidin-3-yl)-

2-methoxyphenylcarbamate (**PP20**) (20 mg, 0.05 mmol) in CH$_2$Cl$_2$, TFA, S(CH$_2$)$_2$, H$_2$O

(45:45:5:5) (1 mL) was stirred at room temperature for 15 minutes. NaHCO$_3$ (2 mL) was

added until reaction was alkaline. Reaction was extracted with H$_2$O and CH$_2$Cl$_2$.

Organic phases were combined, concentrated *in vacuo* and purified by RP-HPLC

(MeCN:H$_2$O:0.1% TFA) to yield PP202. ESI-HRMS (M+H)$^+$ *m/z* calcd 299.1620, found

299.1609.

Synthesis of 2-amino-5-(4-amino-1-isopropyl-1H-pyrazolo[3,4-d]pyrimidin-3-yl)phenol

(PP203)

        PP20 (tert-butyl 4-(4-amino-1-isopropyl-1H-pyrazolo[3,4-d]pyrimidin-3-yl)-2-

methoxyphenylcarbamate, 7 mg, 0.018 mmol) was dissolved in CH$_2$Cl$_2$ (2.5 mL) and

stirred under an argon atmosphere at room temperature. BBr$_3$ (0.500 mL) was added slowly with a syringe. The reaction mixture was stirred overnight, under argon at room temperature. BBr$_3$ was removed *in vacuo* and the remaining solid was purified by RP-HPLC (MeCN:H$_2$O:0.1% TFA) to yield PP203.

Synthesis of 5-(4-amino-1-isopropyl-1H-pyrazolo[3,4-d]pyrimidin-3-yl)pyridine-2-carbonitrile **(PP21)**

2-cyanopyridine 5-boronic acid pinocol ester (18 mg, 0.08 mmol) and 3-iodo-1-isopropyl-1H-pyrazolo[3,4-d]pyrimidin-4-amine (20 mg, 0.07 mmol) were coupled via the Suzuki reaction to yield PP21 (2.5 mg, 14% yield). ^{1}H NMR (CDCl$_3$) δ 9.06 (d, *J*=1.43 Hz, 1H), 8.30 (s, 1H), 8.18 (dd, *J*=1.73 Hz, *J*=1.73 Hz, 1H), 7.92 (d, *J*=8.5 Hz, 1H), 5.26 (m, *J*=6.50 Hz, 1H), 1.64 (d, *J*=6.5 Hz, 6H); ESI-MS (M+H)$^+$ *m/z* calcd 280.1, found 280.1. ESI-HRMS (M+H)$^+$ *m/z* calcd 280.1311, found 280.1299.

Synthesis of 3-(3-(benzyloxy)-5-fluorophenyl)-1-isopropyl-1H-pyrazolo[3,4-d]pyrimidin-4-amine (**BA22**).

(3-Benzyloxy-5-fluorophenyl)boronic acid (29 mg, 5.80 mmol) and 3-iodo-1-isopropyl-1H-pyrazolo[3,4-d]pyrimidin-4-amine (20 mg, 0.07 mmol) were coupled via the Suzuki reaction to yield 15.6 mg (60% yield). ESI-MS (M+H)$^+$ *m/z* calcd 378.1, found 378.0.

Synthesis of 3-(4-amino-1-isopropyl-1H-pyrazolo[3,4-d]pyrimidin-3-yl)-5-fluorophenol **(PP22)**

A solution of 3-(3-(benzyloxy)-5-fluorophenyl)-1-isopropyl-1H-pyrazolo[3,4-d]pyrimidin-4-amine (**BA22**, 15 mg, 0.04 mmol) in MeOH (0.9 mL) was flushed with argon. Pd on activated carbon (10 mL) was carefully added while keeping reaction

42

under an argon atmosphere. Reaction was flushed with H_2 gas and left under H_2 atmosphere overnight at room temperature. The reaction was filtered through celite and rinsed with MeOH to yield PP22 (15 mg, 100% yield). ^1H NMR (CD_3OD) δ 8.37 (s, 1H), 6.96 (s, 1H), 6.92 (d, *J*=9.0 Hz, 1H), 6.70 (d, *J*=10.5 Hz, 1H), 5.21 (m, *J*=6.7 Hz, 1H), 1.61 (d, *J*=6.6 Hz, 6H); ESI-MS (M+H)$^+$ *m/z* calcd 288.1, found 288.1; ESI-HRMS (M+H)$^+$ *m/z* calcd 288.1275, found 288.1275.

Synthesis of 1-isopropyl-3-(3,4-dimethoxyphenyl)-1H-pyrazolo[3,4-d]pyrimidin-4-amine **(PP23)**

      3,4-Dimethoxyphenylboronic acid (24 mg, 0.13 mmol) and 3-iodo-1-isopropyl-1H-pyrazolo[3,4-d]pyrimidin-4-amine (20 mg, 0.07 mmol) were coupled via the Suzuki reaction to yield PP23 (13.1 mg, 60% yield). ^1H NMR ($CDCl_3$) δ 8.24 (s, 1H), 7.15 (m, 2H), 7.04 (m, 1H), 5.19 (m, *J*=7.1Hz, 1H), 3.97 (s, 6H), 1.64 (d, *J*=6.6 Hz, 6H) ; ESI-MS (M+H)$^+$ *m/z* calcd 314.0, found 314.1; ESI-HRMS (M+H)$^+$ *m/z* calcd 314.1617, found 314.1632.

Synthesis of tert-butyl 2-(4-amino-1-isopropyl-1H-pyrazolo[3,4-d]pyrimidin-3-yl)-5-(benzyloxy)-1H-indole-1-carboxylate **(BA24)**

      5-Benzyloxy-1-BOC-indole-2-boronic acid (303mg, 0.83 mmol) and 3-iodo-1-isopropyl-1H-pyrazolo[3,4-d]pyrimidin-4-amine were coupled via the Suzuki reaction to yield BA24. ESI-MS (M+H)$^+$ *m/z* calcd 499.2, found 499.2.

Synthesis of 2-(4-amino-1-isopropyl-1H-pyrazolo[3,4-d]pyrimidin-3-yl)-1H-indol-5-ol **(PP242)**

PP242 (3-(4-fluoro-3-methoxyphenyl)-1-isopropyl-1H-pyrazolo[3,4-d]pyrimidin-4-amine, 30 mg, 0.10 mmol) was dissolved in a solution of formic acid (4.5 mL, 10 equivalents) and HCl (0.45 mL, 1 equivalent). The reaction was heated and stirred for one hour under an argon atmosphere. The reaction was then concentrated *in vacuo* and purified by RP-HPLC (MeCN:H$_2$O:0.1% TFA) to yield PP242. ESI-MS (M+H)$^+$ *m/z* calcd 309.1, found 309.1.

Synthesis of (3-(4-amino-1-isopropyl-1H-pyrazolo[3,4-d]pyrimidin-3-yl)phenyl)methanol **(PP26)**

(3-Hydroxymethylphenyl)boronic acid (24 mg, 0.13 mmol) and 3-iodo-1-isopropyl-1H-pyrazolo[3,4-d]pyrimidin-4-amine (20 mg, 0.07 mmol) were coupled via the Suzuki reaction to yield PP26 (8.4 mg, 42% yield). ^{1}H NMR (CDCl$_3$) δ 11.53 (br), 8.22 (s, 1H), 7.71 (s, 1H), 7.56-7.53 (m, 3H), 6.29 (br), 5.20 (m, *J*=6.6 Hz, 1H), 4.81 (s, 2H), 1.63 (d, *J*=6.6 Hz, 6H); ESI-MS (M+H)$^+$ *m/z* calcd 283.1, found 284.2; ESI-HRMS (M+H)$^+$ *m/z* calcd 284.1511, found 284.1519.

Synthesis of 3-(4-amino-1-isopropyl-1H-pyrazolo[3,4-d]pyrimidin-3-yl)-N-(4,5-dihydrothiazol-2-yl)benzamide **(PP30)**

[3-((4,5-dihydrothiazol-2-yl)carbamoyl)phenyl]boronic acid (19 mg, 0.08 mmol) and 3-iodo-1-isopropyl-1H-pyrazolo[3,4-d]pyrimidin-4-amine (20 mg, 0.07 mmol) were coupled via the Suzuki reaction to yield PP30 (17.8 mg, 67% yield).
ESI-HRMS (M+H)$^+$ *m/z* calcd 382.1450, found 382.1467.

Synthesis of 1-(4-(4-amino-1-isopropyl-1H-pyrazolo[3,4-d]pyrimidin-3-yl)phenyl)ethanone **(PP31)**

4-Acetylphenylboronic acid (12.7 mg, 0.08 mmol) in EtOH (3.3 mL) and 3-iodo-1-isopropyl-1H-pyrazolo[3,4-d]pyrimidin-4-amine (20 mg, 0.07 mmol) were coupled via the Suzuki reaction to yield PP31 (12.9 mg, 62% yield). ^{1}H NMR (CD$_3$OD) δ 8.33 (s, 1H), 8.21 (dt, J=8.6 Hz, 2.1 Hz, 2H), 7.89 (dt, J=8.0 Hz, J=1.4 Hz, 2H), 5.21 (m, J=6.9 Hz, 1H), 2.71 (s, 3H), 1.62 (d, J=7.0 Hz, 6H); ESI-HRMS (M+H)$^+$ m/z calcd 296.1511, found 296.1520.

Synthesis of N-(4-(4-amino-1-isopropyl-1H-pyrazolo[3,4-d]pyrimidin-3-yl)-2-chlorophenyl)acetamide **(PP32)**

(4-Aminocarbonyl-3-chlorophenyl)boronic acid (16 mg, 0.08 mmol) and 3-iodo-1-isopropyl-1H-pyrazolo[3,4-d]pyrimidin-4-amine (20 mg, 0.07 mmol) in DME (12 mL). Pd(PPh$_3$)$_4$ (16 mg, 0.014 mmol) were coupled via the Suzuki reaction to yield PP32 (9.7 mg, 42% yield). ^{1}H NMR (CD$_3$OD) δ 8.41 (s, 1H), 7.85 (m, 1H), 7.23 (m, 1H), 5.26 (m, J=6.6 Hz, 1H), 1.63 (d, J=7.1 Hz, 6H); ESI-MS (M+H)$^+$ m/z calcd 331.1, found 331.1; ESI-HRMS (M+H)$^+$ m/z calcd 331.1074, found 331.1085.

Synthesis of 5-(4-amino-1-isopropyl-1H-pyrazolo[3,4-d]pyrimidin-3-yl)-3-methylthiophene-2-carbaldehyde **(PP34)**

5-Formyl-3-methylthiophene-2-boronic acid (26 mg, 0.14 mmol) and 3-iodo-1-isopropyl-1H-pyrazolo[3,4-d]pyrimidin-4-amine (40 mg, 0.13 mmol) were coupled via the Suzuki reaction to yield PP34 (14.7 mg, 38% yield). ^{1}H NMR (CDCl$_3$) δ 9.48 (s, 1H), 7.80 (s, 1H), 6.80 (s, 1H), 4.77 (m, J=6.7 Hz, 1H), 1.92 (s, 3H), 1.17 (d, J=6.7 Hz, 6H); ESI-MS (M+H)$^+$ m/z calcd 302.1, found 302.0; ESI-HRMS (M+H)$^+$ m/z calcd 302.1076, found 302.1090.

Synthesis of 5-(4-amino-1-isopropyl-1H-pyrazolo[3,4-d]pyrimidin-3-yl)furan-3-carbaldehyde **(PP35)**

4-Formylfuran-2-boronic acid (20 mg, 0.14 mmol) and 3-iodo-1-isopropyl-1H-pyrazolo[3,4-d]pyrimidin-4-amine (40 mg, 0.13 mmol) were coupled via the Suzuki reaction to yield PP35 (13.5 mg, 39% yield). ^{1}H NMR (CDCl$_3$) δ 8.24 (s, 1H), 7.59 (s, 1H), 7.08 (s, 1H), 5.49 (s, 1H), 5.09 (m, J=6.6 Hz, 1H), 1.54 (d, J=7.0 Hz, 6H); ESI-MS (M+H)$^+$ m/z calcd 272.1, found 272.1; ESI-HRMS (M+H)$^+$ m/z calcd 272.1147, found 272.1157.

Synthesis of N-[3-(4-Amino-1-isopropyl-1H-pyrazolo[3,4-d]pyrimidin-3-yl)-phenyl]-methanesulfonamide **(PP38)**

3-Methanesulfonylaminophenylboronic acid (32 mg, 0.15 mmol) and 3-iodo-1-isopropyl-1H-pyrazolo[3,4-d]pyrimidin-4-amine to yield PP38 were coupled via the Suzuki reaction to yield PP38 (24.3 mg, 54% yield). ^{1}H NMR (CD$_3$OD) δ 8.36 (s, 1H), 7.63 (m, 1H), 7.56 (m, 1H), 7.38 (m, 1H), 5.23 (m, J=6.4 Hz, 1H), 3.05 (s, 3H), 1.60 (d, J=6.7 Hz, 6H); ESI-MS (M+H)$^+$ m/z calcd 347.1, found 347.0; ESI-HRMS (M+H)$^+$ m/z calcd 347.1290, found 347.1302.

Synthesis of 3-(4-amino-1-isopropyl-1H-pyrazolo[3,4-d]pyrimidin-3-yl)benzonitrile **(PP39)**

3-Cyanophenylboronic acid (23 mg, 0.15 mmol) and 3-iodo-1-isopropyl-1H-pyrazolo[3,4-d]pyrimidin-4-amine were coupled via the Suzuki reaction to yield PP39 (14.9 mg, 41% yield). ^{1}H NMR (CDCl$_3$) δ 8.26 (s, 1H), 8.02 (s, 1H), 7.86 (m, J=9.1, 2H), 7.7 (t, J=7.9, 1H), 5.22 (m, J=6.6 Hz, 1H), 1.63 (d, J=7.0 Hz, 6H); ESI-MS (M+H)$^+$ m/z calcd 279.1, found 279.0. ESI-HRMS (M+H)$^+$ m/z calcd 279.1358, found 279.1367.

Synthesis of N-[4-(4-Amino-1-isopropyl-1H-pyrazolo[3,4-d]pyrimidin-3-yl)-phenyl]-methanesulfonamide **(PP40)**

4-Methanesulfonylaminophenylboronic acid (24 mg, 0.11 mmol) and 3-iodo-1-isopropyl-1H-pyrazolo[3,4-d]pyrimidin-4-amine (30 mg, 0.10 mmol) were coupled via the Suzuki reaction to yield PP40 (0.9 mg, 3% yield). ESI-MS (M+H)[+] m/z calcd 347.1, found 347.0. ESI-HRMS (M+H)[+] m/z calcd 347.1290, found 347.1290.

Synthesis of 3-(4-Amino-1-isopropyl-1H-pyrazolo[3,4-d]pyrimidin-3-yl)-benzenesulfonamide **(PP41)**

Benzenesulfonamide-3-boronic acid pinacol ester (31 mg, 0.11 mmol) and 3-iodo-1-isopropyl-1H-pyrazolo[3,4-d]pyrimidin-4-amine (30 mg, 0.10 mmol) were coupled via the Suzuki reaction to yield PP41 (9.2 mg, 28% yield). ESI-MS (M+H)[+] m/z calcd 333.1, found 333.0. ESI-HRMS (M+H)[+] m/z calcd 333.1134, found 333.1134.

Synthesis of 2-(4-amino-1-isopropyl-1H-pyrazolo[3,4-d]pyrimidin-3-yl)benzo[b]thiophene-5-carbaldehyde **(PP42)**

5-Formylbenzo[b]thiophene-2-boronic acid pinacol ester (31 mg, 0.11 mmol) and 3-iodo-1-isopropyl-1H-pyrazolo[3,4-d]pyrimidin-4-amine (30 mg, 0.10 mmol) were coupled via the Suzuki reaction to yield PP42 (15.2 mg, 45% yield). ^{1}H NMR (CD$_3$OD) δ 8.38 (s, 1H), 8.02 (s, 1H), 7.96 (d, J=8.6 Hz, 1H), 7.78 (s, 1H), 7.51 (dd, J=8.6 Hz, J=1.5 Hz, 1H), 5.53 (s, 1H), 5.23 (m, J=7.1 Hz, 1H), 1.61 (d, J=6.6 Hz, 6H); ESI-MS (M+H)[+] m/z calcd 338.1, found 338.0. ESI-HRMS (M+H)[+] m/z calcd 338.1076, found 338.1084.

Synthesis of 5-(4-amino-1-isopropyl-1H-pyrazolo[3,4-d]pyrimidin-3-yl)-1H-indole-3-carbaldehyde **(PP43)**

N-Boc-3-formyl-5-indoleboronic acid pinacol ester (40 mg, 0.11 mmol) and 3-iodo-1-isopropyl-1H-pyrazolo[3,4-d]pyrimidin-4-amine (30 mg, 0.10 mmol) were coupled via the Suzuki reaction. The TFA from purification hydrolyzed the Boc to yield PP43. ^{1}H NMR (CDCl$_3$) δ 10.11 (s, 1H), 9.03 (br), 8.66 (s, 1H), 8.23 (s, 1H), 7.99 (d, J=2.8 Hz, 1H), 7.64 (d, J=8.8 Hz, 1H), 7.58 (dd, J=8.3 Hz, J=1.7 Hz, 1H), 5.22 (m, J=6.7 Hz, 1H), 1.65 (d, J=6.7 Hz, 6H); ESI-MS (M+H)$^+$ m/z calcd 321.1, found 321.0. ESI-HRMS (M+H)$^+$ m/z calcd 321.1464, found 321.1473.

Synthesis of 3-(benzo[c][1,2,5]oxadiazol-6-yl)-1-isopropyl-1H-pyrazolo[3,4-d]pyrimidin-4-amine **(PP44)**

Benzo[c][1,2,5]oxadiazole-5-boronic acid (18 mg, 0.11 mmol) and 3-iodo-1-isopropyl-1H-pyrazolo[3,4-d]pyrimidin-4-amine (30 mg, 0.10 mmol) were coupled via the Suzuki reaction to yield PP44. ^{1}H NMR (CDCl$_3$) δ 8.32 (s, 1H), 8.14 (t, J=1.7 Hz, 1H), 8.08 (dd, J=9.0 Hz, J=0.7 Hz, 1H), 7.86 (dd, J=9.4 Hz, J=1.2 Hz, 1H), 5.26 (m, J=6.6 Hz, 1H), 1.64 (d, J=7.03 Hz, 6H); ESI-MS (M+H)$^+$ m/z calcd 296.1, found 296.1. ESI-HRMS (M+H)$^+$ m/z calcd 296.1260, found 296.1260.

Synthesis of 2-(4-(4-amino-1-isopropyl-1H-pyrazolo[3,4-d]pyrimidin-3-yl)phenyl)acetonitrile **(PP45)**

(4-Cyanomethylphenyl)boronic acid (18 mg, 0.11 mmol) and 3-iodo-1-isopropyl-1H-pyrazolo[3,4-d]pyrimidin-4-amine (30 mg, 0.10 mmol) were coupled via the Suzuki reaction to yield PP45. ^{1}H NMR (CDCl$_3$) δ 8.30 (s, 1H), 7.72 (d, J=7.9 Hz, 2H), 7.54 (d, J=7.7 Hz, 2H), 5.20 (m, J=6.7 Hz, 1H), 3.86 (s, 2H), 1.62 (d, J=6.7 Hz, 6H); ESI-MS (M+H)$^+$ m/z calcd 293.1, found 293.1. ESI-HRMS (M+H)$^+$ m/z calcd 293.1515, found 293.1561.

Synthesis of 2-(3-(4-amino-1-isopropyl-1H-pyrazolo[3,4-d]pyrimidin-3-yl)phenyl)acetonitrile **(PP46)**

(3-Cyanomethylphenyl)boronic acid (18 mg, 0.11 mmol) and 3-iodo-1-isopropyl-1H-pyrazolo[3,4-d]pyrimidin-4-amine (30 mg, 0.10 mmol) were coupled via the Suzuki reaction to yield PP46. ^{1}H NMR (CDCl$_3$) δ 8.24 (s, 1H), 7.70 (s, 1H), 7.6 (m, 2H), 7.55 (m, 2H), 5.21 (m, *J*=6.6 Hz, 1H), 3.88 (s, 2H), 1.63 (d, *J*=6.7 Hz, 6H); ESI-MS (M+H)$^+$ *m/z* calcd 293.1, found 293.1. ESI-HRMS (M+H)$^+$ *m/z* calcd 293.1515, found 293.1523.

Synthesis of 1-isopropyl-3-(4-methoxyphenyl)-1H-pyrazolo[3,4-d]pyrimidin-4-amine **(PP48)**

(4-Methoxyphenylboronic acid (17 mg, 0.11 mmol) and 3-iodo-1-isopropyl-1H-pyrazolo[3,4-d]pyrimidin-4-amine (30 mg, 0.10 mmol) were coupled via the Suzuki reaction to yield PP48 (4.5mg, 16% yield). ^{1}H NMR (CDCl$_3$) δ 8.22 (s, 1H), 7.57 (d, *J*=8.5 Hz, 2H), 7.09 (d, *J*=8.7 Hz, 2H), 6.24 (br), 5.18 (m, *J*=6.6 Hz, 1H), 3.89 (s, 3H), 1.62 (d, *J*=6.6 Hz, 6H); ESI-MS (M+H)$^+$ *m/z* calcd 284.1, found 284.1; ESI-HRMS (M+H)$^+$ *m/z* calcd 284.1512, found 284.1521.

Synthesis of 1-isopropyl-3-(3-methoxyphenyl)-1H-pyrazolo[3,4-d]pyrimidin-4-amine **(PP49)**

3-Methoxyphenylboronic acid (17 mg, 0.11 mmol) and 3-iodo-1-isopropyl-1H-pyrazolo[3,4-d]pyrimidin-4-amine (30 mg, 0.10 mmol) were coupled via the Suzuki reaction to yield PP49. ^{1}H NMR (CDCl$_3$) δ 8.23 (s, 1H), 7.49 (t, *J*=7.9 Hz, 1H), 7.19 (m, 1H), 7.17 (d, *J*=1.7 Hz, 1H), 7.08 (dd, *J*=8.4 Hz, *J*=2.4 Hz, 1H), 6.35 (br), 5.20 (m, *J*=6.6

Hz, 1H), 3.89 (s, 3H), 1.63 (d, *J*=6.7 Hz, 6H); ESI-MS (M+H)⁺ *m/z* calcd 284.1, found

284.0; ESI-HRMS (M+H)⁺ *m/z* calcd 284.1515, found 284.1521.

Synthesis of 1-isopropyl-3-(pyridin-3-yl)-1H-pyrazolo[3,4-d]pyrimidin-4-amine **(PP52)**

      3-Pyridinylboronic acid (15 mg, 0.14 mmol) and 3-iodo-1-isopropyl-1H-

pyrazolo[3,4-d]pyrimidin-4-amine (40 mg, 0.13 mmol) were coupled via the Suzuki

reaction to yield PP52. ¹H NMR (CDCl₃) δ 9.27 (s, 1H), 8.73 (d, *J*=3.85 Hz, 1H), 8.50 (d,

J=7.7 Hz, 1H), 8.23 (s, 1H), 7.82 (t, *J*=5.8 Hz, 1H), 5.25 (m, *J*=6.9 Hz, 1H), 1.64 (d,

J=6.7 Hz, 6H); ESI-MS (M+H)⁺ *m/z* calcd 255.1, found 255.0; ESI-HRMS (M+H)⁺ *m/z*

calcd 255.1358, found 255.1365.

Synthesis of 1-isopropyl-3-(pyrimidin-5-yl)-1H-pyrazolo[3,4-d]pyrimidin-4-amine **(PP53)**

      5-Pyrimidinylboronic acid (15 mg, 0.14 mmol) and 3-iodo-1-isopropyl-1H-

pyrazolo[3,4-d]pyrimidin-4-amine (40 mg, 0.13 mmol) were coupled via the Suzuki

reaction to yield PP53. ¹H NMR (CDCl₃) δ 9.40 (s, 1H), 9.09 (s, 2H), 8.30 (s, 1H), 5.62

(m, *J*=6.3 Hz, 1H), 1.64 (d, *J*=6.7 Hz, 6H); ESI-MS (M+H)⁺ *m/z* calcd 256.1, found 256.1;

ESI-HRMS (M+H)⁺ *m/z* calcd 256.1311, found 256.1320.

Synthesis of 3-(2,3-dihydrobenzo[b][1,4]dioxin-6-yl)-1-isopropyl-1H-pyrazolo[3,4-

d]pyrimidin-4-amine **(PP54)**

      2,3-dihydro-1,4-benzodioxin-6-ylboronic acid (26 mg, 0.14 mmol) and 3-iodo-1-

isopropyl-1H-pyrazolo[3,4-d]pyrimidin-4-amine (40 mg, 0.13 mmol) were coupled via the

Suzuki reaction to yield PP54 (6 mg, 15% yield). ¹H NMR (CDCl₃) δ 8.21 (s, 1H), 7.13 (d,

J=1.9 Hz, 1H), 7.07 (dd, *J*=8.2 Hz, *J*=1.9 Hz, 1H), 5.15 (m, *J*=7.0 Hz, 1H), 4.30 (s, 4H),

1.58 (d, *J*=7.2 Hz, 6H); ESI-MS (M+H)⁺ *m/z* calcd 312.1, found 312.0; ESI-HRMS

(M+H)⁺ *m/z* calcd 312.1460, found 312.1470.

Synthesis of 1-(3-(4-amino-1-isopropyl-1H-pyrazolo[3,4-d]pyrimidin-3-

yl)phenyl)ethanone **(PP55)**

      3-Acetylphenylboronic acid (23 mg, 0.14 mmol) and 3-iodo-1-isopropyl-1H-

pyrazolo[3,4-d]pyrimidin-4-amine (40 mg, 0.13 mmol) were coupled via the Suzuki

reaction to yield PP55 (7 mg, 18% yield). ¹H NMR (CDCl₃) δ 8.26 (s, 2H-overlapping

protons), 8.12 (d, *J*=7.4 Hz, 1H), 7.85 (d, *J*=7.1 Hz, 1H), 7.71 (t, *J*=7.8 Hz, 1H), 5.23 (m,

J=6.6 Hz, 1H), 2.68 (s, 3H), 1.64 (d, *J*=6.65 Hz, 6H); ESI-MS (M+H)⁺ *m/z* calcd 296.1,

found 296.1; ESI-HRMS (M+H)⁺ *m/z* calcd 296.1511, found 296.1520.

Synthesis of 4-(4-amino-1-isopropyl-1H-pyrazolo[3,4-d]pyrimidin-3-yl)phenol **(PP56)**

      4-Hydroxyphenylboronic acid and 3-iodo-1-isopropyl-1H-pyrazolo[3,4-

d]pyrimidin-4-amine (40 mg, 0.13 mmol) were coupled via the Suzuki reaction to yield

PP56 (12 mg, 32% yield). ¹H NMR (CDCl₃) δ 8.23 (s, 1H), 7.50 (m, *J*=8.7 Hz, 2H), 7.00

(m, *J*=8.5 Hz, 2H), 5.19 (m, *J*=6.6 Hz, 1H), 1.62 (d, *J*=7.0 Hz, 6H); ESI-MS (M+H)⁺ *m/z*

calcd 270.1, found 270.1; ESI-HRMS (M+H)⁺ *m/z* calcd 270.1355, found 270.1355.

Synthesis of 4-(4-amino-1-isopropyl-1H-pyrazolo[3,4-d]pyrimidin-3-yl)-2-fluorophenol

(PP59)

      3-fluoro-4-hydroxyphenylboronic acid (103 mg, 0.66 mmol) and 3-iodo-1-

isopropyl-1H-pyrazolo[3,4-d]pyrimidin-4-amine (100 mg, 0.33 mmol) were coupled via

the Suzuki reaction to yield PP59 (26 mg, 27% yield). ¹H NMR (CDCl₃) δ 8.25 (s, 1H),

7.37 (dd, *J*=10.6 Hz, *J*=1.8 Hz, 7.26 (d, *J*=8.7 Hz, 1H), 7.14 (t, *J*=8.3 Hz, 1H), 5.12 (t, *J*=6.7 Hz, 1H) 1.54 (d, *J*=6.7 Hz, 6H); ESI-MS (M+H)$^+$ *m/z* calcd 288, found 288.

Synthesis of 4-(4-amino-1-isopropyl-1H-pyrazolo[3,4-d]pyrimidin-3-yl)-3-methylphenol **(PP60)**

4-hydroxy-2-methylphenylboronic acid (110 mg, 0.66 mmol) and 3-iodo-1-isopropyl-1H-pyrazolo[3,4-d]pyrimidin-4-amine (100 mg, 0.33 mmol) were coupled via the Suzuki reaction to yield PP60 (42 mg, 22% yield). ^{1}H NMR (CDCl$_3$) δ 8.34 (s, 1H), 7,23 (s, 1H), 6.86 (d, *J*=2.3 Hz, 1H), 6.81 (dd, *J*=8.2 Hz, *J*=2.8 Hz, 1H), 5.18 (m, *J*=6.6 Hz, 1H), 2.26 (s, 3H), 2.4 (d, *J*=6.7 Hz, 6H); ESI-MS (M+H)$^+$ *m/z* calcd 284, found 284.

Synthesis of 3-(4-fluoro-3-methoxyphenyl)-1-isopropyl-1H-pyrazolo[3,4-d]pyrimidin-4-amine **(PP62)**

4-fluoro-3-methoxyphenylboronic acid (61 mg, 0.36 mmol) and 3-iodo-1-isopropyl-1H-pyrazolo[3,4-d]pyrimidin-4-amine (90 mg, 0.30 mmol) were coupled via the Suzuki reaction to yield PP62 (40 mg, 44% yield). ^{1}H NMR (CDCl$_3$) δ 8.33 (s, 1H), 7.27 (dd, *J*=8.1 Hz, *J*=2.3 Hz, 1H), 7.21 (d, *J*=10.6 Hz, 1H), 7.17 (dd, *J*=4.4 Hz, *J*=1.8 Hz, 1H), 5.17 (m, *J*=6.5 Hz, 1H), 3.95 (s, 3H); ESI-MS (M+H)$^+$ *m/z* calcd 302, found 302.

Synthesis of 5-(4-amino-1-isopropyl-1H-pyrazolo[3,4-d]pyrimidin-3-yl)-2-fluorophenol **(PP262)**

A solution of PP62 (3-(4-fluoro-3-methoxyphenyl)-1-isopropyl-1H-pyrazolo[3,4-d]pyrimidin-4-amine, 30 mg, 0.10 mmol) was dissolved in CH$_2$Cl$_2$ (5 mL) and stirred under an argon atmosphere. BBr$_3$ (500uL, 0.5 mol) was added slowly with a syringe, while stirring. The reaction was stirred at room temperature for 3 hours then

concentrated *in vacuo* and purified using silica gel column chromatography [MeOH—CH$_2$Cl$_2$, 2:98] to yield PP262 (23 mg, 44% yield). ^{1}H NMR (CDCl$_3$) δ 8.34 (s, 1H), 7.35 (dd, *J*=8.1 Hz, *J*=1.5 Hz, 1H), 7.21 (d, *J*=10.3 Hz, 1H), 7.18 (dd, *J*=4.4 Hz, 1.4 Hz, 1H), 5.18 (m, *J*=6.5 Hz, 1H), 1.59 (d, *J*=6.7 Hz, 6H); ESI-MS (M+H)$^+$ *m/z* calcd 288.1, found 288.1.

Synthesis of 3-(2,5-difluoro-4-methoxyphenyl)-1-isopropyl-1H-pyrazolo[3,4-d]pyrimidin-4-amine **(PP63)**

2,5-difluoro-4-methoxyphenylboronic acid (84 mg, 0.45 mmol) and 3-iodo-1-isopropyl-1H-pyrazolo[3,4-d]pyrimidin-4-amine (54 mg, 0.18 mmol) were coupled via the Suzuki reaction to yield PP63 (50 mg, 17% yield). ^{1}H NMR (CDCl$_3$) δ 8.35 (s, 1H), 7.35 (dd, *J*=11.0 Hz, *J*=6.9, 1H), 6.87 (dd, *J*=11.0 Hz, *J*=7.0, 1H), 5.18 (m, *J*=6.5 Hz, 1H), 3.95 (s, 3H), 1.59 (d, *J*=6.8 Hz, 6H); ESI-MS (M+H)$^+$ *m/z* calcd 320.1, found 320.0.

Synthesis of 4-(4-amino-1-isopropyl-1H-pyrazolo[3,4-d]pyrimidin-3-yl)-2,5-difluorophenol **(PP93)**

3-(2,5-difluoro-4-methoxyphenyl)-1-isopropyl-1H-pyrazolo[3,4-d]pyrimidin-4-amine (BA63) (20 mg, 0.06 mmol) was dissolved in CH$_2$Cl$_2$ (2mL) and BBr$_3$ (0.630 mL, 0.63 mmol) was added slowly with a syringe, while stirring. The reaction was stirred at room temperature for overnight then concentrated *in vacuo* and purified using by RP-HPLC (MeCN:H$_2$O:0.1% TFA) to yield PP93 (6.7 mg, 35% yield). ^{1}H NMR (CDCl$_3$) δ 8.27 (s, 1H), 7.37 (dd, *J*=10.4 Hz, *J*=6.7 Hz, 1H), 7.00 (dd, *J*=10.6 Hz, *J*=7.0 Hz, 1H), 5.21 (m, *J*=6.5 Hz, 1H), 1.62 (d, *J*=6.5 Hz, 6H); ESI-MS (M+H)$^+$ *m/z* calcd 306.1, found 306.0.

Synthesis of 1-isopropyl-3-(3,4,5-trimethoxyphenyl)-1H-pyrazolo[3,4-d]pyrimidin-4-amine **(PP64)**

3,4,5-trimethoxyphenylboronic acid (123 mg, 0.58 mmol) and 3-iodo-1-isopropyl-1H-pyrazolo[3,4-d]pyrimidin-4-amine (70 mg, 0.23 mmol) were coupled via the Suzuki reaction to yield PP64 (70 mg, 89% yield). ^{1}H NMR (CDCl$_3$) δ 8.34 (s, 1H), 6.88 (s, 2H), 5.16 (m, J=6.7 Hz, 1H), 3.91 (s, 6H), 3.88 (s, 3H), 1.59 (d, J=6.7 Hz, 6H); ESI-MS (M+H)$^+$ m/z calcd 344.1, found 344.0.

Synthesis of 1-isopropyl-3-(2,3-dimethoxyphenyl)-1H-pyrazolo[3,4-d]pyrimidin-4-amine **(PP65)**

2,3-dimethoxyphenylboronic acid (105 mg, 0.58 mmol) and 3-iodo-1-isopropyl-1H-pyrazolo[3,4-d]pyrimidin-4-amine (70 mg, 0.23 mmol) were coupled via the Suzuki reaction to yield to yield PP65 (63 mg, 88% yield). ^{1}H NMR (CDCl$_3$) δ 8.31 (s, 1H), 7.18 (d, J=7.6 Hz, 1H), 7.14 (dd, J=7.8 Hz, J=1.9 Hz, 1H), 7.02 (dd, J=8.1 Hz, J=1.8 Hz, 1H), 5.17 (m, J=6.5 Hz, 1H), 3.92 (s, 3H), 3.68 (s, 3H), 1.59 (d, J=6.5 Hz, 6H); ESI-MS (M+H)$^+$ m/z calcd 314.1, found 314.1.

Synthesis of 1-isopropyl-3-(2,4-dimethoxypyrimidin-5-yl)-1H-pyrazolo[3,4-d]pyrimidin-4-amine **(PP66)**

2,4-dimethoxypyrimidin-5-yl-5-boronic acid (106 mg, 0.58 mmol) and 3-iodo-1-isopropyl-1H-pyrazolo[3,4-d]pyrimidin-4-amine (70 mg, 0.23 mmol) were coupled via the Suzuki reaction to yield to yield PP66. ^{1}H NMR (CDCl$_3$) δ 8.46 (s, 1H), 8.32 (s, 1H), 5.16 (m, J=6.5 Hz, 1H), 4.06 (s, 3H), 4.05 (s, 3H), 1.57 (d, J=6.5 Hz, 6H); ESI-MS (M+H)$^+$ m/z calcd 316.1, found 316.0.

Synthesis of 3-(3-bromo-5-methoxyphenyl)-1-isopropyl-1H-pyrazolo[3,4-d]pyrimidin-4-amine **(PP85)**

2-(3-bromo-5-methoxyphenyl)-4,4,5,5-tetramethyl-1,3,2-dioxaborolane (137 mg, 0.43 mmol) and 3-iodo-1-isopropyl-1H-pyrazolo[3,4-d]pyrimidin-4-amine (65 mg, 0.216 mmol) were coupled via a Suzuki reaction to yield PP85 (28mg, 36% yield). ^{1}H NMR (CDCl$_3$) δ 8.25 (s, 1H), 7.38 (t, *J*=1.5 Hz, 1H), 7.20 (t, *J*=2.1 Hz, 1H), 7.09 (m, 1H), 5.19 (m, *J*=6.7 Hz, 1H), 3.87 (s, 3H), 1.61 (d, *J*=6.6 Hz, 6H); ESI-MS (M+H)[+] *m/z* calcd 362.1, found 362.0.

Synthesis of 3-(4-amino-1-isopropyl-1H-pyrazolo[3,4-d]pyrimidin-3-yl)-5-bromophenol (**PP87**)

3-(3-bromo-5-methoxyphenyl)-1-isopropyl-1H-pyrazolo[3,4-d]pyrimidin-4-amine (**PP85**, 0.1 mmol) was dissolved in CH$_2$Cl$_2$ (1 mL) and BBr$_3$ (1 mL, 1 mol) was added slowly with a syringe, while stirring. The reaction was stirred at room temperature for 35 minutes then concentrated *in vacuo* and purified using by RP-HPLC (MeCN:H$_2$O:0.1% TFA) to yield PP87 (10.7 mg, 31% yield). ^{1}H NMR (CDCl$_3$) δ 8.23 (s, 1H), 7.33 (m, 1H), 7.20 (m, 1H), 7.13 (m, 1H), 5.18 (m, *J*=7.1 Hz, 1H), 1.61 (d, *J*=6.5 Hz, 6H); ESI-MS (M+H)[+] *m/z* calcd 348.0, found 348.0.

Synthesis of tert-butyl 5-(4-amino-1-isopropyl-1H-pyrazolo[3,4-d]pyrimidin-3-yl)-1H-indole-1-carboxylate **(PP86)**

Tert-butyl 5-(4,4,5,5-tetramethyl-1,3,2-dioxaborolan-2-yl)-1H-indole-1-carboxylate (212 mg, 0.61 mmol) and 3-iodo-1-isopropyl-1H-pyrazolo[3,4-d]pyrimidin-4-amine (75 mg, 0.25 mmol) were coupled via a Suzuki reaction to yield PP86 (9.3 mg, 9% yield). ^{1}H NMR (CD$_3$OD) δ 8.34 (s, 1H), 8.30 (d, *J*=8.4 Hz, 1H), 7.89 (d, *J*=1.7 Hz, 1H), 7.68 (d,

J=3.7 Hz, 1H), 7.62 (dd, *J*=8.5 Hz, *J*=2.0 Hz, 1H), 6.65 (d, *J*=3.5 Hz, 1H), 5.20 (m, *J*=7.1 Hz, 1H), 1.70 (s, 9H), 1.62 (d, *J*=7.0 Hz, 6H); ESI-MS (M+H)$^+$ *m/z* calcd 362.1, found 362.0.

Synthesis of 3-(1H-indol-5-yl)-1-isopropyl-1H-pyrazolo[3,4-d]pyrimidin-4-amine **(PP89)**

Tert-butyl 5-(4-amino-1-isopropyl-1H-pyrazolo[3,4-d]pyrimidin-3-yl)-1H-indole-1-carboxylate (**PP86**, 9 mg, 0.022 mmol) was dissolved in 50:50 CH$_2$Cl$_2$:TFA and stirred for one hour at room temperature. The reaction mixture was concentrated *in vacuo* and purified using by RP-HPLC (MeCN:H$_2$O:0.1% TFA) to yield PP89 (4.8 mg, 75% yield). ^{1}H NMR (CDCl$_3$) δ 8.56 (br), 8.21 (s, 1H), 7.96 (s, 1H), 7.58 (d, *J*=7.6 Hz, 1H), 7.43 (dd, *J*=8.1 Hz, *J*=1.4 Hz, 1H), 7.34 (t, *J*=2.6 Hz, 1H), 6.65 (m, 1H), 6.42 (br), 5.20 (m, *J*=6.7 Hz, 1H), 1.64 (d, *J*=6.8 Hz, 1H); ESI-MS (M+H)$^+$ *m/z* calcd 293.1, found 293.0.

Synthesis of 3-(1H-indol-4-yl)-1-isopropyl-1H-pyrazolo[3,4-d]pyrimidin-4-amine **(PP91)**

1H-indol-4-yl-4-boronic acid (40 mg, 0.25 mmol) and 3-iodo-1-isopropyl-1H-pyrazolo[3,4-d]pyrimidin-4-amine (30 mg, 0.1 mmol) were coupled via a Suzuki reaction to yield PP91 (14.6 mg, 50% yield). ^{1}H NMR (CDCl$_3$) δ 8.76 (br, 1H), 8.24 (s, 1H), 7.58 (d, *J*=7.3 Hz, 1H), 7.36 (m, 1H), 7.35 (m, 1H), 7.34 (s, 1H), 6.57 (s, 1H), 5.25 (m, *J*=6.9 Hz, 1H), 1.67 (d, *J*=6.5 Hz, 6H); ESI-MS (M+H)$^+$ *m/z* calcd 293.1, found 293.1.

Synthesis of 3-(2,3-dihydrobenzofuran-5-yl)-1-isopropyl-1H-pyrazolo[3,4-d]pyrimidin-4-amine **(PP95)**

2,3-dihydro-1-benzofuran-5-ylboronic acid (38 mg, 0.23 mmol) and 3-iodo-1-isopropyl-1H-pyrazolo[3,4-d]pyrimidin-4-amine (30 mg, 0.1 mmol) were coupled via a Suzuki reaction to yield PP95 (15.7 mg, 59% yield). ^{1}H NMR (CDCl$_3$) δ 11.68 (br), 8.21

(s, 1H), 7.49 (s, 1H), 7.37 (d, J=8.2 Hz, 1H), 6.95 (d, J=8.2 Hz, 1H), 5.18 (m, J=7.0 Hz, 1H), 4.69 (t, J=8.6 Hz, 2H), 3.31 (t, J=8.6 Hz, 2H), 1.62 (d, J=7.0 Hz, 6H); ESI-MS (M+H)[+] *m/z* calcd 296.1, found 296.1.

Synthesis of 3-(benzofuran-5-yl)-1-isopropyl-1H-pyrazolo[3,4-d]pyrimidin-4-amine **(PP96)**

5-(4,4,5,5-tetramethyl-1,3,2-dioxaborolan-2-yl)-1-benzofuran (56 mg, 0.23 mmol) in EtOH (1.65 mL) and 3-iodo-1-isopropyl-1H-pyrazolo[3,4-d]pyrimidin-4-amine (30 mg, 0.1 mmol) were coupled via a Suzuki reaction to yield PP96 (19 mg, 72% yield). ^{1}H NMR (CDCl₃) δ 8.24 (s, 1H), 7.89 (d, J=1.5 Hz, 1H), 7.75 (d, J=2.2 Hz, 1H), 7.69 (d, J=8.8 Hz, 1H), 7.57 (dd, J=8.4 Hz, J=1.8 Hz, 1H), 6.87 (dd, J=2.2 Hz, J=0.7 Hz, 1H), 5.20 (m, J=7.0 Hz, 1H), 1.63 (d, J=7.0 Hz, 6H); ESI-MS (M+H)[+] *m/z* calcd 296.1, found 296.1.

Synthesis of 1-isopropyl-3-(quinolin-6-yl)-1H-pyrazolo[3,4-d]pyrimidin-4-amine **(PP102)**

6-(4,4,5,5-tetramethyl-1,3,2-dioxaborolan-2-yl)quinoline (63 mg, 0.25 mmol) and 3-iodo-1-isopropyl-1H-pyrazolo[3,4-d]pyrimidin-4-amine (30 mg, 0.1 mmol) were coupled via a Suzuki reaction to yield PP102 (27.5 mg, 19 % yield). ^{1}H NMR (CDCl₃) δ 9.0 (dd, J=1.5 Hz, J=4.1 Hz, 1H), 8.42 (s, 1H), 8.29 (s, 1H), 8.27 (d, J=7.3 Hz, , 1H), 8.18 (d, J=2.0 Hz, 1H), 8.09 (dd, J=2.1 Hz, J=8.7 Hz, 1H), 7.50 (dd, J=4.3 Hz, J=8.3 Hz, 1H), 5.44 (br, 2H), 5.24 (m, J=6.4 Hz, 1H), 1.64 (d, J=6.7 Hz, 6H); ESI-MS (M+H)[+] *m/z* calcd 305.14, found 305.10. ESI-HRMS (M+H)[+] *m/z* calcd 305.1515, found 305.1504.

Synthesis of 1-isopropyl-3-(quinolin-3-yl)-1H-pyrazolo[3,4-d]pyrimidin-4-amine **(PP105)**

Quinolin-3-yl-3-boronic acid (43 mg, 0.25 mmol) and 3-iodo-1-isopropyl-1H-pyrazolo[3,4-d]pyrimidin-4-amine (30 mg, 0.1 mmol) were coupled via a Suzuki reaction to yield PP105 (45 mg, 85% yield). ^{1}H NMR (CDCl$_3$) δ 9.24 (d, J=2.2 Hz, 1H), 8.44 (d, J=2.2 Hz, 1H), 8.34 (s, 1H), 8.15 (d, J=8.4 Hz, 1H), 7.90 (d, J=8.1 Hz, 1H), 7.79 (t, J=7.0 Hz, 1H), 7.63 (t, J=7.7 Hz, 1H), 5.23 (m, J=6.6 Hz, 1H), 1. 3 (d, J=6.6 Hz, 6H); ESI-MS (M+H)$^+$ m/z calcd 305.14, found 305.10.

Synthesis of 3-(1H-indol-6-yl)-1-isopropyl-1H-pyrazolo[3,4-d]pyrimidin-4-amine **(PP107)**

Indole-6-boronic acid (40.25 mg, 0.25 mmol) in and 3-iodo-1-isopropyl-1H-pyrazolo[3,4-d]pyrimidin-4-amine (30 mg, 0.1 mmol) were coupled via a Suzuki reaction to yield PP107 (22 mg, 42% yield). ^{1}H NMR (CDCl$_3$) δ 8.30 (s, 1H), 7.84 (d, J=8.1 Hz, 1H), 7.72 (s, 1H), 7.39 (m, 1H), 7.37 (d, J=2.9 Hz, 1H), 6.66 (m, 1H), 5.22 (m, J=6.6 Hz, 1H), 1.65 (d, J=6.6 Hz, 1H); ESI-MS (M+H)$^+$ m/z calcd 293.14, found 293.10.

Synthesis of 1-isopropyl-3-(1H-pyrrolo[2,3-b]pyridin-5-yl)-1H-pyrazolo[3,4-d]pyrimidin-4-amine **(PP108)**

7-azaindole-5-boronic acid (61 mg, 0.25 mmol) and 3-iodo-1-isopropyl-1H-pyrazolo[3,4-d]pyrimidin-4-amine (30 mg, 0.1 mmol) were coupled via a Suzuki reaction to yield PP108 (34 mg, 65% yield). ^{1}H NMR (CDCl$_3$) δ 8.66 (s, 2H, overlapping singlets), 8.25 (s, 1H), 7.60 (d, J=2.6 Hz, 1H), 6.81 (d, J=2.6 Hz, 1H), 5.25 (m, J=7.0 Hz, 1H), 1.64 (d, J=7.0 Hz, 6H); ESI-MS (M+H)$^+$ m/z calcd 294.14, found 294.10.

Synthesis of 3-(1H-indazol-6-yl)-1-isopropyl-1H-pyrazolo[3,4-d]pyrimidin-4-amine **(PP110)**

6-indazolboronic acid (30 mg, 0.18 mmol) and 3-iodo-1-isopropyl-1H-pyrazolo[3,4-d]pyrimidin-4-amine (22 mg, 0.074 mmol) were coupled via a Suzuki reaction to yield PP110 (15.5 mg, 40% yield). ^{1}H NMR (CDCl$_3$) δ 8.28 (s, 1H), 8.22 (s, 1H), 8.01 (d, J=8.4 Hz, 1H), 7.87 (s, 1H), 7.47 (d, J=8.1 Hz, 1H), 5.24 (m, J=6.6 Hz, 1H), 6.65 (d, J=7.0 Hz, 6H), ESI-MS (M+H)$^+$ m/z calcd 294.14, found 294.10.

Synthesis of 1-isopropyl-3-(2-methylquinolin-6-yl)-1H-pyrazolo[3,4-d]pyrimidin-4-amine
(PP118)

2-methyl-6-(4,4,5,5-tetramethyl-1,3,2-dioxaborolan-2-yl)quinoline (**ZK507**, 10 mg, 0.04 mmol) and 3-iodo-1-isopropyl-1H-pyrazolo[3,4-d]pyrimidin-4-amine (5 mg, 0.015 mmol) were coupled via a Suzuki reaction to yield PP118 (8 mg, 97% yield). ^{1}H NMR (CDCl$_3$) δ 8.76 (m, 2H), 8.32 (m, 1H), 8.30 (s, 1H), 7.72 (m, 1H), 7.26 (s, 2H), 5.26 (m J=6.9 Hz, 1H), 3.11 (s, 3H), 1.65 (d, J=6.9 Hz, 6H); ESI-MS (M+H)$^+$ m/z calcd 319.16, found 319.10.

Synthesis of 1-isopropyl-3-(isoquinolin-6-yl)-1H-pyrazolo[3,4-d]pyrimidin-4-amine
(PP129)

A solution of isoquinolin-6-yl-6-boronic acid (**PP127**, 29 mg, 0.165 mmol) and 3-iodo-1-isopropyl-1H-pyrazolo[3,4-d]pyrimidin-4-amine (20 mg, 0.07 mmol) were coupled via a Suzuki reaction to yield PP129 (30 mg, 34% yield).

Synthesis of 3-(2-chloroquinolin-6-yl)-1-isopropyl-1H-pyrazolo[3,4-d]pyrimidin-4-amine
(PP130)

2-chloroquinolin-6-yl-6-boronic acid (**ZK526**, 60 mg, 0.28 mmol) and 3-iodo-1-isopropyl-1H-pyrazolo[3,4-d]pyrimidin-4-amine (20 mg, 0.07 mmol) were coupled via a Suzuki reaction to yield PP130 (11 mg, 28% yield). ^{1}H NMR (CDCl$_3$) δ 8.28 (s, 1H), 8.25 (d, J=8.4 Hz, 1H), 8.22 (d, J=8.8 Hz, 1H), 8.12 (d, J=1.8 Hz, 1H), 8.05 (dd, J=8.8 Hz, J=1.8 Hz, 1H), 7.54 (d, J=8.8 Hz, 1H), 5.26 (m, J=6.6 Hz, 1H), 1.66 (d, J=6.6 Hz, 6H); ESI-MS (M+H)$^+$ *m/z* calcd 339.1, found 339.0.

Synthesis of 1-isopropyl-3-(isoquinolin-7-yl)-1H-pyrazolo[3,4-d]pyrimidin-4-amine

(PP131)

Isoquinolin-7-yl-7-boronic acid (**ZK528**, 48 mg, 0.28 mmol) in EtOH (1.65 ml) and 3-iodo-1-isopropyl-1H-pyrazolo[3,4-d]pyrimidin-4-amine (20 mg, 0.07 mmol) were coupled via a Suzuki reaction to yield PP131 (14 mg, 38% yield). ^{1}H NMR (CDCl$_3$) δ 8.78 (s, 1H), 8.57 (d, J=8.4 Hz, 1H), 8.48 (d, J=8.4 Hz, 1H), 8.28-8.25 (m, 3H (overlapping spectra)), 8.20 (d, J=5.5 Hz, 1H), 5.28 (m, J=6.6 Hz, 1H), 1.66 (d, J=6.6 Hz, 6H).

Synthesis of 1-isopropyl-3-(quinoxalin-7-yl)-1H-pyrazolo[3,4-d]pyrimidin-4-amine

(PP132)

Quinoxalin-6-yl-6-boronic acid (**ZK515**, 30 mg, 0.18 mmol) and 3-iodo-1-isopropyl-1H-pyrazolo[3,4-d]pyrimidin-4-amine (20 mg, 0.07 mmol) were coupled via a Suzuki reaction to yield PP132 (23 mg, 62% yield). ^{1}H NMR (CDCl$_3$) δ 8.95 (m, 2H), 8.40 (d, J=2.2 Hz, 1H), 8.34 (d, J=8.4 Hz, 1H), 8.28 (s, 1H), 8.12 (dd, J=8.8 Hz, J=1.8 Hz, 1H), 5.27 (m, J=6.6 Hz, 1H), 1.67 (d, J=6.6 Hz, 6H); ESI-MS (M+H)$^+$ *m/z* calcd 306.14, found 306.10.

Synthesis of 1-isopropyl-3-(2-methylquinolin-7-yl)-1H-pyrazolo[3,4-d]pyrimidin-4-amine

(PP133)

2-methylquinolin-7-yl-7-boronic acid (**ZK531**, 40 mg, 0.21 mmol) and 3-iodo-1-isopropyl-1H-pyrazolo[3,4-d]pyrimidin-4-amine (20 mg, 0.07 mmol) were coupled via a Suzuki reaction to yield PP133 (32 mg, 84% yield). ^{1}H NMR (CDCl$_3$) δ 8.38 (s, 1H), 8.26 (s, 1H), 8.22 (d, J=8.4 Hz, 1H), 8.01 (d, J=8.4 Hz, 1H), 7.87 (dd, J=8.1 Hz, J=1.5 Hz, 1H), 7.44 (d, J=8.4 Hz, 1H), 5.24 (s, J=6.6 Hz, 1H), 2.82 (s, 3H), 1.65 (d, J=6.6 Hz, 6H);ESI-MS (M+H)$^+$ m/z calcd 319.16, found 319.10.

Synthesis of 3-(2-chloroquinolin-3-yl)-1-isopropyl-1H-pyrazolo[3,4-d]pyrimidin-4-amine

(PP134)

2-chloroquinolin-3-yl-3-boronic acid (72 mg, 0.35 mmol) and 3-iodo-1-isopropyl-1H-pyrazolo[3,4-d]pyrimidin-4-amine (40 mg, 0.14 mmol) were coupled via a Suzuki reaction to yield PP134 (16 mg, 20% yield). ^{1}H NMR (CDCl$_3$) δ 8.37 (s, 1H), 8.26 (s, 1H), 8.10 (d, J=9.2 Hz, 1H), 7.91 (m, 1H), 7.88 (m, 1H), 7.68 (m, 1H); 5.26 (m, J=6.6 Hz, 1H), 1.66 (d, J=6.6 Hz, 6H);ESI-MS (M+H)$^+$ m/z calcd 339.1, found 339.0.

Synthesis of 1-isopropyl-3-(1-methyl-1H-indol-5-yl)-1H-pyrazolo[3,4-d]pyrimidin-4-amine

(PP135)

1-methyl-5-(4,4,5,5-tetramethyl-1,3,2-dioxaborolan-2-yl)-1H-indole (27 mg, 0.11 mmol) and 3-iodo-1-isopropyl-1H-pyrazolo[3,4-d]pyrimidin-4-amine (20 mg, 0.07 mmol) were coupled via a Suzuki reaction to yield PP135 (11 mg, 30% yield). ^{1}H NMR (CDCl$_3$) δ 8.20 (s, 1H), 7.89 (m, 1H), 7.50 (d, J=8.6 Hz, 1H), 7.46 (dd, J=8.4 Hz, J=1.5 Hz, 1H), 7.19 (d, J=2.9 Hz, 1H), 6.58 (d, J=2.9 Hz, 1H), 5.20 (m, J=6.6 Hz, 1H), 3.88 (s, 3H), 1.64 (d, J=6.6 Hz, 6H); ESI-MS (M+H)$^+$ m/z calcd 307.2, found 307.0.

Synthesis of 3-(1H-indazol-5-yl)-1-isopropyl-1H-pyrazolo[3,4-d]pyrimidin-4-amine

(PP137)

1H-indazol-5-yl-5-boronic acid (33 mg, 0.21 mmol) in and 3-iodo-1-isopropyl-1H-pyrazolo[3,4-d]pyrimidin-4-amine (25 mg, 0.08 mmol) were coupled via a Suzuki reaction to yield PP137 (9 mg, 21% yield). ^{1}H NMR (CD$_3$OD) δ 8.41 (s, 1H), 8.22 (s, 1H), 8.16 (t, J=1.5 Hz, 1H), 7.78 (m, 2H (overlapping peaks)), 5.27 (m, J=6.6 Hz, 1H), 1.64 (d, J=6.6 Hz, 6H); ESI-MS (M+H)$^+$ m/z calcd 294.1, found 294.4.

Synthesis of 1-isopropyl-3-(pyrido[3,2-b]pyrazin-7-yl)-1H-pyrazolo[3,4-d]pyrimidin-4-amine **(PP139)**

Pyrido[3,2-b]pyrazin-7-yl-7-boronic acid (**ZK533**, 17 mg, 0.10 mmol) and 3-iodo-1-isopropyl-1H-pyrazolo[3,4-d]pyrimidin-4-amine (15 mg, 0.05 mmol) were coupled via a Suzuki reaction to yield PP139 (4 mg, 15% yield). ^{1}H NMR (CDCl$_3$) δ 9.56 (d, J=2.2 Hz, 1H), 9.16 (d, J=1.8 Hz, 1H), 9.05 (d, J=1.8 Hz, 1H), 8.72 (d, J=2.6 Hz, 1H), 8.33 (s, 1H), 5.28 (m, J=7.0 Hz, 1H), 1.67 (d, J=7.0 Hz, 6H); ESI-MS (M+H)$^+$ m/z calcd 307.1, found 307.4.

Synthesis of 6-(4-amino-1-isopropyl-1H-pyrazolo[3,4-d]pyrimidin-3-yl)quinolin-2(1H)-one **(PP140)**

2-hydroxyquinolin-6-yl-6-boronic acid (**ZK535**, 31 mg, 0.14 mmol) and 3-iodo-1-isopropyl-1H-pyrazolo[3,4-d]pyrimidin-4-amine (20 mg, 0.07 mmol) were coupled via a Suzuki reaction to yield PP140. ^{1}H NMR (CDCl$_3$) δ 8.25 (s, 3H), 7.89 (d, J=9.2 Hz, 1H), 7.88 (s, 1H), 7.81 (dd, J=8.4 Hz, J=1.5 Hz, 1H), 7.58 (d, J=8.4 Hz, 1H), 6.80 (d, J=9.5 Hz, 1H), 5.22 (m, J=7.0 Hz, 1H), 1.64 (d, J=7.0 Hz, 6H); ESI-MS (M+H)$^+$ m/z calcd 321.1, found 321.4.

Synthesis of 6-(4-amino-1-isopropyl-1H-pyrazolo[3,4-d]pyrimidin-3-yl)-4H-chromen-4-one **(PP143)**

6-(4,4,5,5-tetramethyl-1,3,2-dioxaborolan-2-yl)-4H-chromen-4-one (56 mg, 0.24 mmol) and 3-iodo-1-isopropyl-1H-pyrazolo[3,4-d]pyrimidin-4-amine (25 mg, 0.083 mmol) were coupled via a Suzuki reaction to yield PP143 (12 mg, 26% yield). ^{1}H NMR (CD$_3$OD) δ 8.46 (d, *J*=2.2 Hz, 1H), 8.40 (s, 1H), 8.27 (d, *J*=6.2 Hz, 1H), 8.16 (dd, *J*=8.8 Hz, *J*=2.2 Hz, 1H), 7.83 (d, *J*=8.8 Hz, 1H), 6.47 (d, *J*=6.2 Hz, 1H), 5.26 (m, *J*=6.6 Hz, 1H), 1.64 (d, *J*=6.6 Hz, 6H); ESI-MS (M+H)$^+$ *m/z* calcd 322.1, found 322.4.

Synthesis of tert-butyl 6-(4-amino-1-isopropyl-1H-pyrazolo[3,4-d]pyrimidin-3-yl)quinolin-4-ylcarbamate **(PP145)**

Tert-butyl quinolin-4-ylcarbamate boronic acid (95 mg, 0.33 mmol) and 3-iodo-1-isopropyl-1H-pyrazolo[3,4-d]pyrimidin-4-amine (50 mg, 0.17 mmol) were coupled via a Suzuki reaction to yield PP145 (20 mg, 18% yield). ESI-MS (M+H)$^+$ *m/z* calcd 420.2, found 420.5.

Synthesis of 6-(4-amino-1-isopropyl-1H-pyrazolo[3,4-d]pyrimidin-3-yl)quinolin-4-amine **(PP147)**

A solution of tert-butyl 6-(4-amino-1-isopropyl-1H-pyrazolo[3,4-d]pyrimidin-3-yl)quinolin-4-ylcarbamate (**PP145**, 15 mg, 0.04 mmol) was dissolved in 50% TFA in CH$_2$Cl$_2$ and stirred at room temperature for 90 minutes. The reaction was concentrated *in vacuo* and purified by RP-HPLC (MeCN:H$_2$O:0.1% TFA) to yield BA147 (3 mg, 14% yield). ^{1}H NMR (CD$_3$OD) δ 8.71 (d, *J*=1.8 Hz, 1H), 8.39 (s, 1H), 8.38 (d, *J*=6.6 Hz, 1H), 8.29 (dd, *J*=8.8

Hz, *J*=1.8 Hz, 1H), 8.03 (d, *J*=8.8 Hz, 1H), 6.92 (d, *J*=7.0 Hz, 1H), 5.26 (m, *J*=6.6 Hz, 1H), 1.64 (d, *J*=6.6 Hz, 6H); ESI-MS (M+H)⁺ *m/z* calcd 320.2, found 320.4.

Synthesis of 4-(4-amino-1-isopropyl-1H-pyrazolo[3,4-d]pyrimidin-3-yl)-2,6-difluorobenzaldehyde **(PP149)**

3,5-difluoro-4-formyl-phenylboronic acid (150 mg, 0.83 mmol) and 3-iodo-1-isopropyl-1H-pyrazolo[3,4-d]pyrimidin-4-amine (100 mg, 0.33 mmol) were coupled via a Suzuki reaction to yield PP149 (33 mg, 31% yield). ESI-MS (M+H)⁺ *m/z* calcd 318.1, found 318.4.

Synthesis of 5-(4-amino-1-isopropyl-1H-pyrazolo[3,4-d]pyrimidin-3-yl)-2-fluorobenzonitrile **(PP150)**

4-cyano-3-fluorophenylboronic acid (136 mg, 0.83 mmol) and 3-iodo-1-isopropyl-1H-pyrazolo[3,4-d]pyrimidin-4-amine (100 mg, 0.33 mmol) were coupled via a Suzuki reaction to yield PP150 (50 mg, 51% yield). ESI-MS (M+H)⁺ *m/z* calcd 297.1, found 297.4.

Synthesis of 4-(4-amino-1-isopropyl-1H-pyrazolo[3,4-d]pyrimidin-3-yl)-2-fluorobenzonitrile **(PP151)**

4-cyano-3-fluorophenylboronic acid (135 mg, 0.83 mmol) and 3-iodo-1-isopropyl-1H-pyrazolo[3,4-d]pyrimidin-4-amine (100 mg, 0.33 mmol) were coupled via a Suzuki reaction to yield PP151 (47 mg, 48 % yield). ESI-MS (M+H)⁺ *m/z* calcd 297.1, found 297.4.

Synthesis of 4-(4-amino-1-isopropyl-1H-pyrazolo[3,4-d]pyrimidin-3-yl)-2-fluorobenzaldehyde **(PP152)**

3-fluoro-4-formylphenyl boronic acid (140 mg, 0.83 mmol) and 3-iodo-1-isopropyl-1H-pyrazolo[3,4-d]pyrimidin-4-amine (100 mg, 0.33 mmol) were coupled via a Suzuki reaction to yield PP152 (25 mg, 25 % yield). ^{1}H NMR (DMSO-d_6) δ 10.30 (s, 1H), 8.27 (s, 1H), 7.98 (t, J=7.7 Hz, 1H), 7.69 (dd, J=8.1 Hz, J=1.1 Hz, 1H), 7.62 (dd, J=11.4 Hz, J=1.5 Hz, 1H), 5.09 (m, J=6.6 Hz, 1H), 1.50 (d, J=6.6 Hz, 1H), 1.50 (J=6.6 Hz, 6H); ESI-MS (M+H)$^{+}$ m/z calcd 300.1, found 300.4.

Synthesis of 5-(4-amino-1-isopropyl-1H-pyrazolo[3,4-d]pyrimidin-3-yl)-1H-benzo[d]imidazol-2(3H)-one **(PP156)**

5-(4,4,5,5-tetramethyl-1,3,2-dioxaborolan-2-yl)-1H-benzo[d]imidazol-2(3H)-one (54 mg, 0.21 mmol) and 3-iodo-1-isopropyl-1H-pyrazolo[3,4-d]pyrimidin-4-amine (100 mg, 0.33 mmol) were coupled via a Suzuki reaction to yield PP156 (6 mg, 14 % yield). ^{1}H NMR (CD$_3$OD) δ 8.36 (s, 1H), 7.40 (m, 1H), 7.39 (m, 1H), 7.26 (d, J=8.4 Hz, 1H), 5.23 (m, J=6.6 Hz, 1H), 1.62 (d, J=6.6 Hz, 6H).

Synthesis of 6-(4-amino-1-isopropyl-1H-pyrazolo[3,4-d]pyrimidin-3-yl)quinazolin-4(3H)-one **(PP158)**

3,4-dihydro-4-oxoquinazolin-6-yl-6-boronic acid (**ZK532**, 30 mg, 0.16 mmol) and 3-iodo-1-isopropyl-1H-pyrazolo[3,4-d]pyrimidin-4-amine (25 mg, 0.08 mmol) were coupled via a Suzuki reaction to yield PP158 (8 mg, 20 % yield). ^{1}H NMR (CD$_3$OD) δ 8.57 (d, J=1.8 Hz, 1H), 8.41 (s, 1H), 8.23 (s, 1H), 8.22 (dd, J=8.4 Hz, J=2.2 Hz, 1H), 7.92 (d, J=8.4 Hz, 1H), 5.27 (m, J=6.6 Hz, 1H), 1.64 (d, J=6.6 Hz, 6H); ESI-MS (M+H)$^{+}$ m/z calcd 322.1, found 322.4.

Synthesis of 3-(H-imidazo[1,2-a]pyridin-7-yl)-1-isopropyl-1H-pyrazolo[3,4-d]pyrimidin-4-amine **(PP161)**

Imidazo[1,2-a]pyridine-6-boronic acid (33 mg, 0.21 mmol) and 3-iodo-1-isopropyl-1H-pyrazolo[3,4-d]pyrimidin-4-amine (25 mg, 0.08 mmol) were coupled via a Suzuki reaction to yield PP161 (26 mg, 81 % yield). ^{1}H NMR (CD$_3$OD) δ 9.22 (t, J=1.1 Hz, 1H), 8.45 (s, 1H), 8.37 (d, J=1.5, 1H), 8.30 (dd, J=9.2 Hz, J=1.5 Hz, 1H), 8.18 (d, J=2.2 Hz, 1H), 8.15 (d, J=9.5 Hz, 1H), 5.30 (m, J=6.6 Hz, 1H), 1.64 (d, J=7.0 Hz, 6H); ESI-MS (M+H)$^+$ *m/z* calcd 294.1, found 294.4.

Synthesis of 1-(3-(4-amino-1-isopropyl-1H-pyrazolo[3,4-d]pyrimidin-3-yl)phenyl)ethanone **(BA81, PP81 & PP281)**

Tert-butyl 2-methoxy-4-(4,4,5,5-tetramethyl-1,3,2-dioxaborolan-2-yl)phenylcarbamate (200 mg, 0.76 mmol) in EtOH (3.3 mL) and 1-cyclopentyl-3-iodo-1H-pyrazolo[3,4-d]pyrimidin-4-amine (100 mg, 0.30 mmol) were coupled via the Suzuki reaction to yield BA81. BA81 was dissolved in 50:50 CH$_2$Cl$_2$:TFA and stirred for one hour at room temperature. The reaction mixture was concentrated *in vacuo* and purified using by RP-HPLC (MeCN:H$_2$O:0.1% TFA) to yield PP81. PP81 was dissolved in CH$_2$Cl$_2$ (2mL) and BBr$_3$ (4 mL, 4 mol) was added slowly with a syringe, while stirring. The reaction was stirred at room temperature for 2 hours then concentrated *in vacuo* and purified using by RP-HPLC (MeCN:H$_2$O:0.1% TFA) to yield PP281.

Synthesis of tert-butyl 5-(4-amino-1-cyclopentyl-1H-pyrazolo[3,4-d]pyrimidin-3-yl)-1H-indole-1-carboxylate **(PP88)**

Tert-butyl 5-(4,4,5,5-tetramethyl-1,3,2-dioxaborolan-2-yl)-1H-indole-1-carboxylate (130 mg, 0.38 mmol) and 1-cyclopentyl-3-iodo-1H-pyrazolo[3,4-d]pyrimidin-4-amine (**BA80**, 50 mg, 0.15 mmol) were couple via a Suzuki reaction to yield PP88. ^{1}H NMR

(CD$_3$OD) δ 8.36 (d, *J*=6.6 Hz, 1H), 8.35 (s, 1H), 7.93 (d, *J*=1.9 Hz, 1H), 7.77 (d, *J*=3.7 Hz, 1H), 7.65 (dd, *J*=8.3 Hz, *J*=1.9 Hz, 1H), 6.77 (d, *J*=3.7 Hz, 1H), 5.38 (m, *J*=7.4 Hz, 1H), 2.22 (m, 4H), 2.05 (m, 2H), 1.82 (m, 2H); ESI-MS (M+H)$^+$ *m/z* calcd 419.2, found 419.1.

Synthesis of 3-(1H-indol-5-yl)-1-cyclopentyl-1H-pyrazolo[3,4-d]pyrimidin-4-amine **(PP94)**

Tert-butyl 5-(4-amino-1-cyclopentyl-1H-pyrazolo[3,4-d]pyrimidin-3-yl)-1H-indole-1-carboxylate (PP88) was dissolved in 50:50 CH$_2$Cl$_2$:TFA and stirred for one hour at room temperature. The reaction mixture was concentrated *in vacuo* and purified using by RP-HPLC (MeCN:H$_2$O:0.1% TFA) to yield PP94 (6.3 mg). ^{1}H NMR (CDCl$_3$) δ 8.23 (s, 1H), 7.90 (s, 1H), 7.57 (d, *J*=8.4 Hz, 1H), 7.43 (dd, *J*=8.4 Hz, *J*=1.5 Hz, 1H), 7.35 (t, *J*=2.9 Hz, 1H), 6.65 (m, 1H), 5.33 (m, *J*=7.7 Hz, 1H), 2.22 (m, 4H), 2.03 (m, 2H), 1.77 (m, 2H); ESI-MS (M+H)$^+$ *m/z* calcd 319.1, found 319.2.

Synthesis of 1-cyclopentyl-3-(3,4-dimethoxyphenyl)-1H-pyrazolo[3,4-d]pyrimidin-4-amine **(PP90)**

3,4-dimethoxyphenylboronic acid (41 mg, 0.23 mmol) and 1-cyclopentyl-3-iodo-1H-pyrazolo[3,4-d]pyrimidin-4-amine (**BA80**, 30 mg, 0.09 mmol) were coupled via a Suzuki reaction to yield PP90 (8.4 mg, 28% yield). ^{1}H NMR (CDCl$_3$) δ 8.22 (s, 1H), 7.15 (dd, *J*=7.0 Hz, *J*=2.0 Hz, 1H), 7.14 (s, 1H), 7.03 (d, *J*=8.8 Hz, 1H), 5.31 (m, *J*=7.6 Hz, 1H), 3.96 (s, 3H), 3.95 (s, 3H), 2.20 (m, 4H), 2.02 (m, 2H), 1.77 (m, 2H); ESI-MS (M+H)$^+$ *m/z* calcd 340.2, found 340.1.

Synthesis of 1-cyclopentyl-3-(1H-indol-4-yl)-1H-pyrazolo[3,4-d]pyrimidin-4-amine **(PP92)**

1H-indol-4-yl-4-boronic acid (30 mg, 0.19 mmol) and 1-cyclopentyl-3-iodo-1H-pyrazolo[3,4-d]pyrimidin-4-amine (**BA80**, 25 mg, 0.076 mmol) were coupled via a Suzuki reaction to yield PP92 (23 mg, 95% yield). ^{1}H NMR (CDCl$_3$) δ 8.74 (br, 1H), 8.23 (s, 1H), 7.58 (d, J=7.3 Hz, 1H), 7.37 (m, 1H), 7.35 (m, 1H), 7.33 (m, 1H), 6.57 (m, 1H), 5.38 (m, J=7.4 Hz, 1H), 2.25 (m, 4H), 2.03 (m, 2H), 1.79 (m, 2H); ESI-MS (M+H)$^+$ *m/z* calcd 319.2, found 319.1.

Synthesis of 3-(benzofuran-5-yl)-1-cyclopentyl-1H-pyrazolo[3,4-d]pyrimidin-4-amine (**PP97**)

5-(4,4,5,5-tetramethyl-1,3,2-dioxaborolan-2-yl)-1-benzofuran (37 mg, 0,071 mmol)) and1-cyclopentyl-3-iodo-1H-pyrazolo[3,4-d]pyrimidin-4-amine (**BA80**, 25 mg, 0.076 mmol) were coupled via a Suzuki reaction to yield PP97 (16 mg, 83% yield). ^{1}H NMR (CDCl$_3$) δ 8.23 (s, 1H), 7.88 (s, 1H), 7.77 (d, J=2.2 Hz, 1H), 7.70 (d, J=8.4 Hz, 1H), 7.56 (dd, J=8.4 Hz, J=1.8 Hz, 1H), 6.88 (m, 1H), 5.34 (m, J=7.3 Hz, 1H), 2.21 (m, 4H), 2.02 (m, 2H), 1.78 (m, 2H) ; ESI-MS (M+H)$^+$ *m/z* calcd 320.1, found 320.0.

Synthesis of 1-cyclopentyl-3-(quinolin-6-yl)-1H-pyrazolo[3,4-d]pyrimidin-4-amine (**PP112**)

6-(4,4,5,5-tetramethyl-1,3,2-dioxaborolan-2-yl)quinoline (58 mg, 0.23 mmol) and 1-cyclopentyl-3-iodo-1H-pyrazolo[3,4-d]pyrimidin-4-amine (**BA80**, 30 mg, 0.09 mmol) were coupled via a Suzuki reaction to yield PP112 (42 mg, 84% yield). ^{1}H NMR (CDCl$_3$) δ 9.22 (d, J=3.7 Hz, 1H), 8.75 (d, J=8.1 Hz, 1H), 8.59 (d, J=8.8 Hz, 1H), 8.32 (d, J=1.8 Hz, 1H), 8.26 (dd, J=8.8 Hz, J=1.5 Hz, 1H), 7.88 (dd, J=8.4 Hz, J=4.8 Hz, 1H). 5.40 (m, J=7.3 Hz, 1H), 2.23 (m, 4H), 2.04 (m, 2H), 1.80 (m, 2H); ESI-MS (M+H)$^+$ *m/z* calcd 331.2, found 331.1.

Synthesis of 1-cyclopentyl-3-(1H-indazol-6-yl)-1H-pyrazolo[3,4-d]pyrimidin-4-amine **(PP115)**

6-indazolboronic acid (25 mg, 0.15 mmol) and 1-cyclopentyl-3-iodo-1H-pyrazolo[3,4-d]pyrimidin-4-amine (**BA80**, 20 mg, 0.06 mmol) were coupled via a Suzuki reaction to yield PP115 (18 mg, 56% yield). ^{1}H NMR (CDCl$_3$) δ 8.28 (s, 1H), 8.21 (s, 1H), 8.49 (d, J=8.1 Hz, 1H), 7.85 (s, 1H), 7.45 (dd, J=8.1 Hz, J=0.7 Hz, 1H), 5.36 (m, J=7.4 Hz, 1H), 2.23 (m, 4H), 2.03 (m, 2H), 1.78 (m, 2H); ESI-MS (M+H)$^+$ m/z calcd 320.2, found 320.0.

Synthesis of 1-cyclopentyl-3-(1H-pyrrolo[2,3-b]pyridin-5-yl)-1H-pyrazolo[3,4-d]pyrimidin-4-amine **(PP121)**

5-(4,4,5,5-tetramethyl-1,3,2-dioxaborolan-2-yl)-1H-pyrrolo[2,3-b]pyridine (44 mg, 0.15 mmol) and 1-cyclopentyl-3-iodo-1H-pyrazolo[3,4-d]pyrimidin-4-amine (**BA80**,20 mg, 0.06 mmol) were coupled via a Suzuki reaction to yield PP121 (27 mg, 80% yield). ^{1}H NMR (DMSO-d_6) δ 11.83 (br, 1H), 8.48 (d, J=2.1 Hz, 1H), 8.24 (s, 1H), 8.19 (d, J=1.79 Hz, 1H), 7.57 (d, J=3.2 Hz, 1H), 6.57 (d, J=3.2 Hz, 1H), 5.25 (m, J=7.4 Hz, 1H), 2.09 (m, 4H), 1.91 (m, 2H), 1.70 (m, 2H); ^{13}C NMR (DMSO-d_6) δ 158.9, 156.1, 154.5, 149.0, 143.1, 142.8, 128.5, 127.8, 121.7, 120.2, 101.1, 98.4, 57.5, 32.5, 24.9; ESI-MS (M+H)$^+$ m/z calcd 320.2, found 320.0. ESI-HRMS (M+H)$^+$ m/z calcd 320.1624, found 320.1609.

Synthesis of 1-cyclopentyl-3-(quinolin-3-yl)-1H-pyrazolo[3,4-d]pyrimidin-4-amine **(PP122)**

Quinolin-3-yl-3-boronic acid (26 mg, 0.15 mmol) and1-cyclopentyl-3-iodo-1H-pyrazolo[3,4-d]pyrimidin-4-amine (**BA80**, 20 mg, 0.06 mmol) were coupled via a Suzuki reaction to yield PP122 (26 mg, 78% yield). ^{1}H NMR (CDCl$_3$) δ 9.65 (d, J=2.2 Hz, 1H),

9.08 (d, *J*=1.5 Hz, 1H), 8.38 (d, *J*=8.8 Hz, 1H), 8.23 (s, 1H), 8.19 (d, *J*=7.7 Hz, 1H), 8.05 (m, 1H), 7.90 (m, 1H), 5.41 (m, *J*=7.3 Hz, 1H), 2.24 (m, 4H), 2.04 (m, 2H), 1.81 (m, 2H).

Synthesis of 1-cyclopentyl-3-(1H-indol-6-yl)-1H-pyrazolo[3,4-d]pyrimidin-4-amine **(PP124)**

Indole-6-boronic acid (25 mg, 0.15 mmol) in and 1-cyclopentyl-3-iodo-1H-pyrazolo[3,4-d]pyrimidin-4-amine (**BA80**, 20 mg, 0.06 mmol) were coupled via a Suzuki reaction to yield PP124 (20 mg, 62% yield). ¹H NMR (CD₃OD) δ 8.36 (m, 1H), 7.76 (d, *J*=7.9 Hz, 1H), 7.73 (s, 1H), 7.39 (m, 1H), 7.33 (d, *J*=8.3 Hz, 1H), 5.38 (m, *J*=7.4 Hz, 1H), 2.20 (m, 4H), 2.02 (m, 2H), 1.79 (m, 2H).

Synthesis of 1-cyclopentyl-3-(1-methyl-1H-indol-5-yl)-1H-pyrazolo[3,4-d]pyrimidin-4-amine **(PP136)**

1-methyl-5-(4,4,5,5-tetramethyl-1,3,2-dioxaborolan-2-yl)-1H-indole (49 mg, 0.19 mmol) and 1-cyclopentyl-3-iodo-1H-pyrazolo[3,4-d]pyrimidin-4-amine (**BA80**, 25 mg, 0.075 mmol) were coupled via a Suzuki reaction to yield PP136 (16 mg, 38% yield). ¹H NMR (CDCl₃) δ 8.20 (s, 1H), 7.88 (m, 1H), 7.50 (d, *J*=8.4 Hz, 1H), 7.45 (dd, *J*=8.1 Hz, *J*=1.8 Hz, 1H), 7.19 (d, *J*=2.9 Hz, 1H), 6.58 (dd, *J*=2.9 Hz, *J*=0.7 Hz, 1H), 5.32 (m, *J*=7.7 Hz, 1H), 3.88 (s, 3H), 2.22 (m, 4H), 2.03 (m, 2H), 1.78 (m, 2H); ESI-MS (M+H)⁺ *m/z* calcd 333.2, found 333.0.

Synthesis of 1-cyclopentyl-3-(1H-indazol-5-yl)-1H-pyrazolo[3,4-d]pyrimidin-4-amine **(PP138)**

1H-indazol-5-yl-5-boronic acid (25mg, 0.15 mmol) in EtOH (1.65 ml) was added to a solution of 1-and cyclopentyl-3-iodo-1H-pyrazolo[3,4-d]pyrimidin-4-amine (**BA80**, 20 mg,

0.06 mmol) were coupled via a Suzuki reaction to yield PP138 (16 mg, 54% yield). ^{1}H NMR (CD$_3$OD δ 8.41 (s, 1H), 8.21 (s, 1H), 8.14 (t, *J*=1.5 Hz, 1H), 7.77 (m, 2H (overlapping peaks)), 5.42 (m, *J*=7.7 Hz, 1H), 2.23 (m, 4H), 2.05 (m, 2H), 1.82 (m, 2H); ESI-MS (M+H)$^+$ *m/z* calcd 320.2, found 320.5.

Synthesis of 6-(4-amino-1-cyclopentyl-1H-pyrazolo[3,4-d]pyrimidin-3-yl)quinolin-2(1H)-one **(PP141)**

2-hydroxyquinolin-6-yl-6-boronic acid (**ZK353**, 25mg, 0.15 mmol) and 1-cyclopentyl-3-iodo-1H-pyrazolo[3,4-d]pyrimidin-4-amine (**BA80**,20 mg, 0.06 mmol) were coupled via a Suzuki reaction to yield PP141. ^{1}H NMR (CDCl$_3$) δ 8.26 (s, 1H), 7.87 (d, *J*=6.2 Hz, 1H), 7.85 (d, *J*=1.5 Hz, 1H), 7.79 (dd, *J*=8.4 Hz, *J*=1.8 Hz, 1H), 7.52 (d, *J*=8.4 Hz, 1H), 6.80 (d, *J*=9.5 Hz, 1H), 5.34 (m, *J*=7.7 Hz, 1H), 2.21 (m, 4H), 2.02 (m, 2H), 1.79 (m, 2H); ESI-MS (M+H)$^+$ *m/z* calcd 347.2, found 347.5.

Synthesis of 6-(4-amino-1-cyclopentyl-1H-pyrazolo[3,4-d]pyrimidin-3-yl)-4H-chromen-4-one **(PP144)**

6-(4,4,5,5-tetramethyl-1,3,2-dioxaborolan-2-yl)-4H-chromen-4-one (25mg, 0.15 mmol) and 1-cyclopentyl-3-iodo-1H-pyrazolo[3,4-d]pyrimidin-4-amine (**BA80**, 20 mg, 0.06 mmol) were coupled via a Suzuki reaction to yield PP144 (25 mg, 89% yield). ^{1}H NMR (CDCl$_3$) δ 8.48 (d, *J*=2.2 Hz, 1H), 8.24 (s, 1H), 8.00 (dd, *J*=8.8 Hz, *J*=2.2 Hz, 1H), 7.91 (d, *J*=6.2 Hz, 1H), 7.67 (d, *J*=8.4 Hz, 1H), 6.36 (d, *J*=6.2 Hz, 1H), 5.35 (m, *J*7.7 Hz, 1H), 2.20 (m, 4H), 2.02 (m, 2H), 1.78 (m, 2H); ESI-MS (M+H)$^+$ *m/z* calcd 348.1, found 348.4.

Synthesis of 1-cyclopentyl-3-(H-imidazo[1,2-a]pyridin-7-yl)-1H-pyrazolo[3,4-d]pyrimidin-4-amine **(PP162)**

Imidazo[1,2-a]pyridine-6-boronic acid (**BA80**, 25 mg, 0.15 mmol) and 1-cyclopentyl-3-iodo-1H-pyrazolo[3,4-d]pyrimidin-4-amine (BA80, 20 mg, 0.06 mmol) were coupled via a Suzuki reaction to yield PP162. ^{1}H NMR (CD$_3$OD) δ 8.45 (s, 1H), 8.37 (d, J=2.2 Hz, 1H), 8.29 (dd, J=9.5 Hz, J=1.5 Hz, 1H), 8.18 (d, J=2.2 Hz, 1H), 8.15 (dt, J=1.5 Hz, J=1.1 Hz, 1H), 5.46 (m, J=7.3 Hz, 1H), 2.23 (m, 4H), 2.04 (m, 2H), 1.84 (m, 2H); ESI-MS (M+H)$^+$ *m/z* calcd 320.2, found 320.4.

Synthesis of 1-methyl-3-(quinolin-6-yl)-1H-pyrazolo[3,4-d]pyrimidin-4-amine **(PP111)**

6-(4,4,5,5-tetramethyl-1,3,2-dioxaborolan-2-yl)quinoline (46mg, 0.18 mmol) in EtOH (1.65 ml) was added to a solution of 3-iodo-1-methyl-1H-pyrazolo[3,4-d]pyrimidin-4-amine (**BA109**, 20mg, 0.07 mmol) were coupled via a Suzuki reaction to yield PP111 (13 mg, 37% yield). ^{1}H NMR (CDCl$_3$) δ 9.16 (dd, J=4.8 Hz, J=1.5 Hz, 1H), 8.51 (m, 1H), 8.49 (m, 1H), 8.31 (s, 1H), 8.21 (d, J=2.2 Hz, 1H), 8.13 (dd, J=8.8 Hz, 1.8 Hz, 1H), 7.74 (dd, J=8.4 Hz, 4.4 Hz, 1H), 4.20 (s, 3H); ESI-MS (M+H)$^+$ *m/z* calcd 277.1, found 277.1.

Synthesis of 3-(2-ethoxynaphthalen-6-yl)-1-methyl-1H-pyrazolo[3,4-d]pyrimidin-4-amine **(PP116)**

6-ethoxy-2-naphthaleneboronic acid (39mg, 0.18 mmol) and 3-iodo-1-methyl-1H-pyrazolo[3,4-d]pyrimidin-4-amine (**BA109**, 20mg, 0.07 mmol) were coupled via a Suzuki reaction to yield PP116 (19 mg, 63% yield). ^{1}H NMR (CDCl$_3$) δ 8.26 (s, 1H), 8.02 (s, 1H), 7.91 (d, J=8.4 Hz, 1H), 7.81 (d, J=8.8 Hz, 1H), 7.66 (dd, J=8.4 Hz, 1.8 Hz, 1H), 7.27 (dd, J=8.1 Hz, J=2.6 Hz, 1H), 7.20 (s, 1H), 4.20 (q, J=7.0 Hz, 2H), 4.16 (s, 3H), 1.52 (t, J=7.0 Hz, 3H); ESI-MS (M+H)$^+$ *m/z* calcd 320.1, found 320.1.

Synthesis of 3-(1H-indol-6-yl)-1-methyl-1H-pyrazolo[3,4-d]pyrimidin-4-amine **(PP119)**

Indole-6-boronic acid (29mg, 0.18 mmol) in EtOH (1.65 ml) and 3-iodo-1-methyl-1H-pyrazolo[3,4-d]pyrimidin-4-amine (**BA109**, 20mg, 0.07 mmol) were coupled via a Suzuki reaction to yield PP119 (25 mg, 71% yield). ^{1}H NMR (CDCl$_3$) δ 8.25 (s, 1H), 7.83 (d, J=8.1 Hz, 1H), 7.69 (d, J=0.7 Hz, 1H), 7.38 (m, 1H), 7.34 (dd, J=8.1 Hz, J=1.5 Hz, 1H), 6.67 (m, 1H), 4.14 (s, 3H); ESI-MS (M+H)$^+$ *m/z* calcd 265.1, found 265.1.

Synthesis of 1-methyl-3-(1H-pyrrolo[2,3-b]pyridin-5-yl)-1H-pyrazolo[3,4-d]pyrimidin-4-amine **(PP120)**

7-azaindole-5-boronic acid (53 mg, 0.18 mmol) and 3-iodo-1-methyl-1H-pyrazolo[3,4-d]pyrimidin-4-amine (**BA109**, 20mg, 0.07 mmol) were coupled via a Suzuki reaction to yield PP120 (11 mg, 31% yield). ^{1}H NMR (CDCl$_3$) δ 8.58 (d, J=1.8 Hz, 1H), 8.42 (d, J=1.8 Hz, 1H), 8.31 (s, 1H), 7.61 (dd, J=3.3 Hz, J=2.2 Hz, 1H), 6.77 (dd, J=3.3 Hz, J=1.8 Hz, 1H), 4.18 (s, 3H); ESI-MS (M+H)$^+$ *m/z* calcd 266.1, found 266.0.

Synthesis of 6-(4-amino-1-methyl-1H-pyrazolo[3,4-d]pyrimidin-3-yl)-4H-chromen-4-one **(PP148)**

6-(4,4,5,5-tetramethyl-1,3,2-dioxaborolan-2-yl)-4H-chromen-4-one (50 mg, 0.18 mmol) and 3-iodo-1-methyl-1H-pyrazolo[3,4-d]pyrimidin-4-amine (**BA109**, 20mg, 0.07 mmol were coupled via a Suzuki reaction to yield PP148 (6 mg, 28% yield). ^{1}H NMR (DMSO-d$_6$) δ 8.36 (d, J=6.2 Hz, 1H), 8.29 (d, 1H), 8.25 (d, J=3.3 Hz, 1H), 8.06 (dd, J=8.8 Hz, J=2.2 Hz, 1H), 7.80 (d, J=8.8 Hz, 1H), 6.42 (d, J=5.9 Hz, 1H), 3.98 (s, 3H); ESI-MS (M+H)$^+$ *m/z* calcd 294.1, found 294.4.

Synthesis of 5-(4-amino-1-cyclopentyl-1H-pyrazolo[3,4-d]pyrimidin-3-yl)-2-ethoxyphenol (**PP98**)

1-cyclopentyl-3-(4-ethoxy-3-methoxyphenyl)-1H-pyrazolo[3,4-d]pyrimidin-4-amine (PP359, 25 mg, 0,071 mmol) was dissolved in CH_2Cl_2 (5 mL) and stirred at -10°C under an argon atmosphere. After 30 minutes, reaction was brought to 0°C and stirred for 2.5 hours. Reaction was stirred for additional 4 hours at room temperature, then concentrated *in vacuo* and purified by RP-HPLC (MeCN:H_2O:0.1% TFA) to yield PP98 (3 mg, 13% yield). ^{1}H NMR (CDCl$_3$) δ 7.23 (d, *J*=2.2 Hz, 1H), 7.07 (dd, *J*=8.1 Hz, *J*=2.2 Hz, 1H), 5.31 (m, *J*=7.3 Hz, 1H), 4.22 (m, 2H), 2.33 (m, 4H), 1.99 (m, 2H), 1.75 (m, 2H), 1.51 (m, 3H); ESI-MS (M+H)$^+$ *m/z* calcd 340.1, found 340.1.

Synthesis of 2-(4-(4-amino-1-isopropyl-1H-pyrazolo[3,4-d]pyrimidin-3-yl)-2-methoxyphenylamino)propan-1-ol (**PP99**)

3-(4-amino-3-methoxyphenyl)-1-isopropyl-1H-pyrazolo[3,4-d]pyrimidin-4-amine (pp202) (30 mg, 0.10 mmol) was dissolved in DMF (0.400 mL). K_2CO_3 (55 mg, 0.4 mmol) was added and reaction was stirred at 70°C. 3-bromo-1-propanol (0.050 mL, 0.6 mmol) was added and reaction was stirred overnight. Solid K_2CO_3 was removed by filtration. Solvent was partially removed *in vacuo*. Sodium citrate (50 mL) was added and reaction was extracted with saturated NaCl and CH_2Cl_2. Organic phases concentrated *in vacuo* and purified by RP-HPLC (MeCN:H_2O:0.1% TFA) to yield PP99 (8.4 mg, 24% yield). ESI-MS (M+H)$^+$ *m/z* calcd 357.2, found 357.1.

Synthesis of 3-(2-(hydrazine)quinolin-6-yl)-1-isopropyl-1H-pyrazolo[3,4-d]pyrimidin-4-amine (**PP142**)

3-(2-chloroquinolin-6-yl)-1-isopropyl-1H-pyrazolo[3,4-d]pyrimidin-4-amine (PP130, 20 mg, 0.05 mmol) was dissolved in 1 ml EtOH under an argon atmosphere.

Hydrazine (1.6 ml, 33 mmol) was added by syringe and reaction was heated to 90°C for 6.5 hours. Crude reaction was cooled, concentrated *in vacuo* and purified by RP-HPLC (MeCN:H$_2$O:0.1% TFA) to yield PP142 (12 mg, 61% yield). ^{1}H NMR (CDCl$_3$) δ 8.27 (s, 1H), 8.20 (d, *J*=8.8 Hz, 1H), 8.02-7.97 (m, 3H (overlapping spectra)), 7.84 (d, *J*=10.6 Hz, 1H), 5.24 (m, *J*=7.0 Hz, 1H), 1.64 (d, *J*=6.6 Hz, 6H); ESI-MS (M+H)$^+$ *m/z* calcd 335.2, found 335.5.

Synthesis of 6-(4-amino-1-isopropyl-1H-pyrazolo[3,4-d]pyrimidin-3-yl)quinolin-2-amine (**PP146**)

3-(2-chloroquinolin-6-yl)-1-isopropyl-1H-pyrazolo[3,4-d]pyrimidin-4-amine (PP130, 50 mg, 0.15 mmol), acetamide (174 mg, 3.0 mmol) and K$_2$CO$_3$ (104 mg, 0.75 mmol) were combined and heated to 200°C under an argon atmosphere for one hour. Reaction was cooled, then extracted with H$_2$O and CH$_2$Cl$_2$. Organic phases were combined, concentrated *in vacuo* and purified by RP-HPLC (MeCN:H$_2$O:0.1% TFA) to yield PP146 (22 mg, 46 % yield). ^{1}H NMR (CD$_3$OD) δ 8.48 (d, *J*=9.2 Hz, 1H), 8.37 (s, 1H), 8.25 (d, *J*=1.8 Hz, 1H), 8.16 (dd, *J*=8.8 Hz, *J*=1.8 Hz, 1H), 7.86 (d, *J*=8.4 Hz, 1H), 5.24 (m, *J*=6.6 Hz, 1H), 1.63 (d, *J*=7.0 Hz, 6H); ESI-MS (M+H)$^+$ *m/z* calcd 320.2, found 320.4.

Synthesis of 3-(3-amino-1H-indazol-6-yl)-1-isopropyl-1H-pyrazolo[3,4-d]pyrimidin-4-amine **(PP154)**

4-(4-amino-1-isopropyl-1H-pyrazolo[3,4-d]pyrimidin-3-yl)-2-fluorobenzonitrile (PP150, 20 mg, 0.07 mmol) was dissolved in *n*-BuOH (2 mL). Hydrazine monohydrate (0.400 mL) was added and the reaction was heated to 110°C under an argon atmosphere and left stirring over night. Reaction mixture was concentrated *in vacuo* and

purified by RP-HPLC (MeCN:H_2O:0.1% TFA) to yield PP154 (15 mg, 70 % yield). [1]H

NMR (CD$_3$OD) δ 8.43 (s, 1H), 8.07 (dd, *J*=8.4 Hz, *J*=0.7 Hz, 1H), 7.75 (m, 1H), 7.52 (dd,

J=8.4 Hz, *J*=1.5 Hz, 1H), 5.28 (m, *J*=6.6 Hz, 1H), 1.64 (d, *J*=6.6 Hz, 6H); ESI-MS (M+H)[+]

m/z calcd 309.2, found 309.4.

Synthesis of 4-(4-amino-1-isopropyl-1H-pyrazolo[3,4-d]pyrimidin-3-yl)-2-

hydroxybenzonitrile **(PP155)**

      4-(4-amino-1-isopropyl-1H-pyrazolo[3,4-d]pyrimidin-3-yl)-2-fluorobenzonitrile

(BA150, 25 mg, 0.1 mmol) was dissolved in DMF (1 mL). *t*-BuOK (24 mg, 0.21 mmol)

was added and the reaction was stirred at room temperature overnight. Reaction was

then heated to 150°C for 24 hours. The reaction was then concentrated *in vacuo* and

purified by RP-HPLC (MeCN:H_2O:0.1% TFA) to yield PP155 (21 mg, 89 % yield). [1]H

NMR (CD$_3$OD) δ 8.41 (s, 1H), 7.75 (m, 1H), 7.32 (d, *J*=1.5 Hz, 1H), 7.30 (dd, *J*=8.2 Hz,

J=1.5 Hz, 1H), 5.26 (m, *J*=7.0 Hz, 1H), 1.62 (d, *J*=7.0 Hz, 6H); ESI-MS (M+H)[+] *m/z* calcd

295.1, found 295.4.

Synthesis of 3-(3-aminobenzo[d]isoxazol-5-yl)-1-isopropyl-1H-pyrazolo[3,4-d]pyrimidin-

4-amine **(PP257)** & 5-(4-amino-1-isopropyl-1H-pyrazolo[3,4-d]pyrimidin-3-yl)-2-

hydroxybenzonitrile **(PP157)**

      5-(4-amino-1-isopropyl-1H-pyrazolo[3,4-d]pyrimidin-3-yl)-2-fluorobenzonitrile

(BA151, 20 mg, 0.07 mmol) was dissolved in DMF (1 mL). *t*-BuOK (24 mg, 0.21 mmol)

was added and the reaction was stirred at room temperature overnight. Reaction was

then heated to 150°C for 24 hours. The reaction was then concentrated *in vacuo* and

purified by RP-HPLC (MeCN:H_2O:0.1% TFA) to yield BA157_2 (7 mg), ^{1}H NMR

(CD$_3$OD) δ 8.36 (s, 1H), 7.88 (d, *J*=2.2 Hz, 1H), 7.83 (dd, *J*=8.4 Hz, *J*=2.2 Hz, 1H), 7.18

(d, J=8.1 Hz, 1H), 5.22 (m, J=7.0 Hz, 1H), 1.62 (d, J=6.6 Hz, 6H), ESI-MS (M+H)$^+$ m/z

calcd 295.1, found 295.4 and BA157_3 (8 mg), ^{1}H NMR (CDCl$_3$) δ 8.25 (s, 1H), 7.87 (s,

1H), 7.80 (dd, J=8.4 Hz, J=1.5 Hz, 1H), 7.62 (d, J=8.4 Hz, 1H), 5.23 (m, J=7.0 Hz, 1H),

1.64 (d, J=6.6 Hz, 6H); ESI-MS (M+H)$^+$ m/z calcd 310.1, found 310.4.

Synthesis of 3-(3-amino-1H-indazol-6-yl)-1-isopropyl-1H-pyrazolo[3,4-d]pyrimidin-4-

amine **(PP159)**

4-(4-amino-1-isopropyl-1H-pyrazolo[3,4-d]pyrimidin-3-yl)-2,6-

difluorobenzaldehyde (PP149, 20 mg, 0.063 mmol) was dissolved in n-BuOH (1 mL).

Hydrazine monohydrate (0.400 mL) was added and the reaction was heated to 100°C

under an argon atmosphere and left stirring for 2.5 hours. Reaction mixture was

concentrated *in vacuo* and purified by RP-HPLC (MeCN:H$_2$O:0.1% TFA) to yield PP159

(15 mg, 77 % yield). ^{1}H NMR (CD$_3$OD) δ 8.41 (s, 1H), 8.26 (d, J=1.1 Hz, 1H), 7.72 (s,

1H), 7.22 (dd, J=10.3 Hz, J=1.1 Hz, 1H), 5.27 (m, J=7.0 Hz, 1H), 1.64 (d, J=6.6 Hz, 6H);

ESI-MS (M+H)$^+$ m/z calcd 312.1, found 312.4.

Synthesis of 3-(3-amino-1H-indazol-5-yl)-1-isopropyl-1H-pyrazolo[3,4-d]pyrimidin-4-

amine (**PP160**)

4-(4-amino-1-isopropyl-1H-pyrazolo[3,4-d]pyrimidin-3-yl)-2-fluorobenzonitrile

(**PP151**, 17 mg, 0.06 mmol) was dissolved in n-BuOH (2 mL). Hydrazine monohydrate

(0.500 mL) was added and the reaction was heated to 110°C under an argon

atmosphere overnight. Reaction mixture was concentrated *in vacuo* and purified by RP-

HPLC (MeCN:H$_2$O:0.1% TFA) to yield PP160 (18 mg, 100% yield), ^{1}H NMR (CD$_3$OD) δ

8.42 (s, 1H), 8.23 (m, 1H), 7.88 (dd, J=8.8 Hz, 1.5 Hz, 1H), 7.62 (dd, J=8.8 Hz, J=0.7 Hz,

1H), 5.28 (m, J=7.0 Hz, 1H), 1.64 (d, J=7.0 Hz, 6H), ESI-MS (M+H)$^+$ *m/z* calcd 309.2, found 309.4.

Synthesis of 3-(2-fluoro-3-methoxyphenyl)-1H-pyrazolo[3,4-d]pyrimidin-4-amine (**BA76**)

2-fluoro-3-methoxybenzoic acid (2 g, 0.012 mol) was stirred in CH_2Cl_2 (20mL) at 0°C under an argon atmosphere. DMF (5 drops, catalytic) was added, followed by oxalyl chloride (5.09 mL, 0.059 mol). Reaction was warmed to room temperature then stirred under argon for one hour. Reaction was concentrated *in vacuo* to yield 2-fluoro-3-methoxybenzoyl chloride (**BA68**).

A solution of malononitrile (1.19 g, 0.018 mol) in dry THF (2 mL) was stirred at 0°C under an argon atmosphere. NaH in paraffin oil (1.92 g, 0.048 mol) was added piece-wise to solution. 2-fluoro-3-methoxybenzoyl chloride (**BA68**, 0.012 mol) was dissolved in 20 mL dry THF and added slowly to reaction. Reaction was warmed to room temperature and stirred under argon for 24 hours. 1N HCl (40 mL) was slowly added, then reaction mixture was extracted with EtOAc. Organic phases were combined, dried with magnesium sulfate, then concentrated *in vacuo* to yield 2-((2-fluoro-3-methoxyphenyl)(hydroxy)methylene)malononitrile (**BA70**).

2-((2-fluoro-3-methoxyphenyl)(hydroxy)methylene)malononitrile (**BA70**, 0.012 mol) and sodium bicarbonate (8.06 g, 96 mmol) were combined in a solution of 1,4-dioxane (32 mL) and water (5.3 mL). Dimethylsulphate (7.99 mL, 84 mmol) was slowly added and the reaction was heated to 80-90º C for 2 hours. The reaction was cooled to RT, water was added, and the aqueous phase extracted three times with diethyl ether (100 mL). The organic phases were combined, dried with $MgSO_4$, and filtered to give 2-((2-fluoro-3-methoxyphenyl)(methoxy)methylene)malononitrile (**BA72**), which appeared as an orange oil and was purified by silica gel chromatography (10% EtOAc/Hexanes slowly increasing to 40% EtOAc/Hexanes) to give a yellow oil.

2-((2-fluoro-3-methoxyphenyl)(methoxy)methylene)malononitrile (**BA72**, 0.012 mmol) was stirred in EtOH (20mL) at room temperature under an argon atmosphere. Hydrazine (0,58 mL, 12 mmol) was added and reaction was left stirring for 90 minutes. Reaction mixture was concentrated *in vacuo* and dried on vacuum pump overnight to yield intermediate 5-amino-3-(2-fluoro-3-methoxyphenyl)-1H-pyrazole-4-carbonitrile (**BA74)**, which appeared as an orange oil and was taken on without further characterization.

Formamide (20mL) was added to 5-amino-3-(2-fluoro-3-methoxyphenyl)-1H-pyrazole-4-carbonitrile (**BA74,** 0.012 mol) and the reaction was heated to 180°C under an argon atmosphere overnight. Reaction was cooled and dH_2O was added (40mL) forcing a white precipitate out of solution. Precipitate was collected and washed with dH_2O. Solid was dried and purified by silica gel column chromatography [MeOH— CH_2Cl_2, 10:90] to yield 3-(2-fluoro-3-methoxyphenyl)-1H-pyrazolo[3,4-d]pyrimidin-4-amine (**BA76**). ESI-MS $(M+H)^+$ *m/z* calcd 259.1, found 260.11.

Synthesis of 3-(4-amino-1-isopropyl-1H-pyrazolo[3,4-d]pyrimidin-3-yl)-2-fluorophenol (**PP77**)

3-(2-fluoro-3-methoxyphenyl)-1H-pyrazolo[3,4-d]pyrimidin-4-amine (**BA76**, 100 mg, 0.386 mmol) was dissolved in DMF (2 mL). K_2CO_3 (213 mg, 1.54 mmol) was added and reaction was stirred at room temperature under an argon atmosphere. 2-iodopropane (0.113 mL, 1.16 mmol) was added with a syringe and reaction was stirred for 2 hours. Solid K_2CO_3 was removed by filtration. Solvent was partially removed *in vacuo*. Water (50 mL) was added and reaction was extracted with CH_2Cl_2. Organic phases were dried with sodium sulfate, concentrated *in vacuo* yielding an oil. The oil was dissolved in 10 ml CH_2Cl_2 and placed under argon. BBr_3 (3.84 ml, excess) was added and reaction was stirred for 45 minutes at room temperature. The reaction was

quenched with saturated sodium bicarbonate (aqueous) and extracted three times with CH$_2$Cl$_2$ (20 ml). Organic phases were combined, concentrated *in vacuo* and the final product was purified using by RP-HPLC (MeCN:H$_2$O:0.1% TFA) to yield a white solid, PP77 (56 mg, 51% yield). ^{1}H NMR (CDCl$_3$) δ 8.24 (s, 1H), 7.20 (m, *J*=1.96 Hz, 1H), 7.18 (m, 1H), 7.07 (m, *J*=2.1 Hz, 1H), 6.32 (br), 5.21 (m, *J*=6.7 Hz, 1H), 1.62 (d, *J*=6.7 Hz, 6H); ESI-MS (M+H)$^+$ *m/z* calcd 287.1, found 288.11.

Synthesis of 3-(4-amino-1-cyclopentyl-1H-pyrazolo[3,4-d]pyrimidin-3-yl)-2-fluorophenol (**PP78**)

3-(2-fluoro-3-methoxyphenyl)-1H-pyrazolo[3,4-d]pyrimidin-4-amine (**BA76**, 100 mg, 0.386 mmol) was dissolved in DMF (2 mL). K$_2$CO$_3$ (250 mg) was added and reaction was stirred at room temperature under an argon atmosphere. Iodocyclopentane (0.066 mL, 1.5 mmol) was added with a syringe and reaction was stirred for 2 hours. Solid K$_2$CO$_3$ was removed by filtration. Solvent was partially removed *in vacuo*. Water (50 mL) was added and reaction was extracted with CH$_2$Cl$_2$. Organic phases were dried with sodium sulfate, concentrated *in vacuo* yielding an oil. The oil was dissolved in 10 ml CH$_2$Cl$_2$ and placed under argon. BBr$_3$ (3.84 ml, excess) was added and reaction was stirred for 45 minutes at room temperature. The reaction was quenched with saturated sodium bicarbonate (aqueous) and extracted three times with CH$_2$Cl$_2$ (20 ml). Organic phases were combined, concentrated *in vacuo* and the final product was purified using by RP-HPLC (MeCN:H$_2$O:0.1% TFA) to yield a white solid, PP78 (12 mg, 10% yield). ^{1}H NMR (CDCl$_3$) δ 8.26 (s, 1H), 7.91 (m, 1H), 7.21 (m, 1H), 7.07 m, 1H), 5.34 (m, *J*=7.7 Hz, 1H), 2.19 (m, 4H), 2.01 (m, 2H), 1.77 (m, 2H); ESI-MS (M+H)$^+$ *m/z* calcd 313.1 found 314.1.

Synthesis of 1-cyclopentyl-3-(3-fluoro-5-methoxyphenyl)-1H-pyrazolo[3,4-d]pyrimidin-4-amine (**BA79**)

3-fluoro-5-methoxybenzoic acid (5 g, 0.029 mol) was stirred in CH_2Cl_2 (50mL) at 0°C under an argon atmosphere. DMF (9 drops, catalytic) was added, followed by oxalyl chloride (12.7 mL, 0.147 mol). Reaction was warmed to room temperature then stirred under argon for one hour. Reaction was concentrated *in vacuo* to yield 3-fluoro-5-methoxybenzoyl chloride (**BA67**).

A solution of malononitrile (2.87 g, 0.044 mol) in dry THF (50 mL) was stirred at 0°C under an argon atmosphere. NaH in paraffin oil (4.64 g, 0.116 mol) was added piece-wise to solution. 3-fluoro-5-methoxybenzoyl chloride (**BA67**, 0.029 mol) was dissolved in 50 mL dry THF and added slowly to reaction. Reaction was warmed to room temperature and stirred under argon for 24 hours. 1N HCl (200 mL) was slowly added, then reaction mixture was extracted with EtOAc. Organic phases were combined, dried with magnesium sulfate, then concentrated *in vacuo* to yield 2-((3-fluoro-5-methoxyphenyl)(hydroxy)methylene)malononitrile (**BA69**).

2-((3-fluoro-5-methoxyphenyl)(hydroxy)methylene)malononitrile (**BA69**, 29 mmol)and sodium bicarbonate (19.5 g, 232 mmol) were combined in a solution of 1,4-dioxane (50 mL) and water (10 mL). Dimethylsulphate (19.3 mL, 203 mmol) was slowly added and the reaction was heated to 80-90° C for 2 hours. The reaction was cooled to RT, water was added, and the aqueous phase extracted three times with diethyl ether (200 mL). The organic phases were combined, dried with $MgSO_4$, and filtered to give 2-((3-fluoro-5-methoxyphenyl)(methoxy)methylene)malononitrile (**BA71**), which appeared as a brown oil and was purified using silica gel chromatography (10% EtOAc/Hexanes slowly increasing to 40% EtOAc/Hexanes) to give a yellow oil.

2-((3-fluoro-5-methoxyphenyl)(methoxy)methylene)malononitrile (**BA71**, 29mmol) was stirred in EtOH (20mL) at room temperature under an argon atmosphere.

Hydrazine (1.4 mL, 29 mmol) was added and reaction was left stirring for 90 minutes. Reaction mixture was concentrated *in vacuo* and dried on vacuum pump overnight to yield intermediate 5-amino-3-(3-fluoro-5-methoxyphenyl)-1H-pyrazole-4-carbonitrile (**BA73**). Formamide (20mL) was added and reaction was heated to 180°C under an argon atmosphere overnight. Reaction was cooled and dH_2O was added (40mL) forcing a white precipitate out of solution. Precipitate was collected and washed with dH_2O. Solid was dried and purified by silica gel column chromatography [MeOH—CH_2Cl_2, 10:90] to yield 3-(3-fluoro-5-methoxyphenyl)-1H-pyrazolo[3,4-d]pyrimidin-4-amine (**BA75**).

3-(3-fluoro-5-methoxyphenyl)-1H-pyrazolo[3,4-d]pyrimidin-4-amine (**BA75**, 100 mg, 0.386 mmol) was dissolved in DMF (10 mL). K_2CO_3 (250 mg, 1.54 mmol) was added and reaction was stirred at room temperature under an argon atmosphere. Iodocyclopentane (0.134 mL, 1.16 mmol) was added with a syringe and reaction was stirred for 2 hours. Solid K_2CO_3 was removed by filtration. Solvent was partially removed *in vacuo*. Sodium citrate (50 mL) was added and reaction was extracted with EtOAc. Organic phases concentrated *in vacuo* and purified using by RP-HPLC (MeCN:H_2O:0.1% TFA) to yield BA79.

Synthesis of 1-cyclopentyl-3-(3-fluoro-5-hydroxyphenyl)-1H-pyrazolo[3,4-d]pyrimidin-4-amine (**PP79**)

1-cyclopentyl-3-(3-fluoro-5-methoxyphenyl)-1H-pyrazolo[3,4-d]pyrimidin-4-amine (**BA79**, 0.386 mmol) was dissolved in CH_2Cl_2 (2 mL). BBr_3 (4 mL, 4 mol) was added slowly with a syringe, while stirring. The reaction was stirred at room temperature for 2 hours then concentrated *in vacuo* and purified using by RP-HPLC (MeCN:H_2O:0.1% TFA) to yield BA79 (69 mg, 57% yield). ^{1}H NMR (CDCl$_3$) δ 8.25 (s, 1H), 7.07 (s, 1H),

6.98 (d, *J*=8.1 Hz, 1H), 6.75 (dt, *J*=9.9 Hz, *J*=2.2 Hz, 1H), 5.32 (m, *J*=7.3 Hz, 1H), 2.18 (m, 4H), 2.02 (m, 2H), 1.78 (m, 2H).

2.9.2 *In vitro* kinase assays

p110α, p110β, p110δ, p110γ: Inhibitors were tested against recombinant PI3-Ks (Upstate (α, β, and γ isoforms) or Jena Biosciences (δ isoforms) at two-fold dilutions (concentration range: 50 μM - 0.003 μM) in an assay containing 25 mM HEPES, pH 7.5, 10 mM $MgCl_2$, 10 μM ATP (2.5 μCi of γ-32P-ATP), and 3 μg/mL BSA. Phosphatidylinositol, freshly sonicated for ~1 minute (Sigma; 1 mg/mL), was used as a substrate. Reactions were terminated by spotting onto nitrocellulose, which was washed with 1M NaCl/1% phosphoric acid (approximately 6 times, 5-10 min each). Sheets were dried and the transferred radioactivity quantitated by phosphorimaging. IC_{50} values were calculated by fitting the data to a sigmoidal dose-response curve using the Prism software package.

PI4-KIIIβ: Inhibitors were tested against recombinant PI4-KIIIβ at two-fold dilutions (concentration range: 50 μM - 0.003 μM) in an assay containing 50 mM Tris, pH 7.5, 20 mM $MgCl_2$, 0.4% Triton X-100, 10 μM ATP (2.5 μCi of γ-32P-ATP), and 3 μg/mL BSA. Freshly sonicated phosphatidylinositol (Sigma; 1 mg/mL) was used as a substrate. Reactions were terminated by spotting onto nitrocellulose, which was washed with 1M NaCl/1% phosphoric acid (approximately 6 times, 5-10 min each). Sheets were dried and the transferred radioactivity quantitated by phosphorimaging. IC_{50} values were calculated by fitting the data to a sigmoidal dose-response curve using the Prism software package.

DNA-PK: Inhibitors were tested against DNA-PK (Promega) at two-fold dilutions (concentration range: 50 µM - 0.003 µM) in an assay containing 50 mM HEPES, pH 7.5, 1mM EGTA, 10 mM MgCl$_2$, 10 µM ATP (2.5 µCi of γ-32P-ATP), and 3 µg/mL BSA. Dephosphorylated casein (Sigma; 10 mg/mL) was used as a substrate. Reactions were terminated by spotting onto nitrocellulose, which was washed with 1M NaCl/1% phosphoric acid (approximately 6 times, 5-10 min each). Sheets were dried and the transferred radioactivity quantitated by phosphorimaging. IC$_{50}$ values were calculated by fitting the data to a sigmoidal dose-response curve using the Prism software package.

mTOR (FRAP1): Inhibitors were tested against recombinant mTOR (Invitrogen) at two-fold dilutions (concentration range: 50 µM - 0.003 µM) in an assay containing 50 mM HEPES, pH 7.5, 1mM EGTA, 10 mM MgCl$_2$, 2.5 mM, 0.01% Tween, 10 µM ATP (2.5 µCi of γ-32P-ATP), and 3 µg/mL BSA. Rat recombinant PHAS-1/4EBP1 (Calbiochem; 2 mg/mL) was used as a substrate. Reactions were terminated by spotting onto nitrocellulose, which was washed with 1M NaCl/1% phosphoric acid (approximately 6 times, 5-10 min each). Sheets were dried and the transferred radioactivity quantitated by phosphorimaging. IC$_{50}$ values were calculated by fitting the data to a sigmoidal dose-response curve using the Prism software package.

c-Src, Src(T338I), and Hck: Inhibitors were tested at two-fold dilutions (concentration range: 50 µM - 0.003 µM) against recombinant kinase in an assay containing 25 mM HEPES, pH 7.4, 10 mM MgCl$_2$, 10 µM ATP (2.5 µCi of γ-32P-ATP), and 3 µg/mL BSA. The peptide substrate EIYGEFKKK was used as phosphoacceptor (200 µM) . Reactions were terminated by spotting onto phosphocellulose sheets, which

84

were washed with 0.5% phosphoric acid (approximately 6 times, 5-10 min each).

Sheets were dried and the transferred radioactivity quantitated by phosphorimaging.

IC_{50} values were calculated by fitting the data to a sigmoidal dose-response curve using

the Prism software package.

c-Abl: Inhibitors were tested at two-fold dilutions (concentration range: 50 µM -

0.003 µM) against recombinant c-Abl in an assay containing 25 mM HEPES, pH 7.4, 10

mM $MgCl_2$, 10 µM ATP (2.5 µCi of γ-32P-ATP), and 3 µg/mL BSA. The peptide substrate

EAIYAAPFAKKK was used as phosphoacceptor (200 µM) . Reactions were terminated

by spotting onto phosphocellulose sheets, which were washed with 0.5% phosphoric

acid (approximately 6 times, 5-10 min each). Sheets were dried and the transferred

radioactivity quantitated by phosphorimaging. IC_{50} values were calculated by fitting the

data to a sigmoidal dose-response curve using the Prism software package.

VEGFR2 (KDR): Inhibitors were tested at two-fold dilutions (concentration

range: 50 µM - 0.003 µM) against recombinant KDR receptor kinase domain (Invitrogen)

in an assay containing 25 mM HEPES, pH 7.4, 10 mM MgCl2, 0.1% BME, 10 µM ATP

(2.5 µCi of γ-32P-ATP), and 3 µg/mL BSA. Poly E-Y (Sigma; 2 mg/mL) was used as a

substrate. Reactions were terminated by spotting onto nitrocellulose, which was washed

with 1M NaCl/1% phosphoric acid (approximately 6 times, 5-10 min each). Sheets were

dried and the transferred radioactivity quantitated by phosphorimaging. IC_{50} values were

calculated by fitting the data to a sigmoidal dose-response curve using the Prism

software package.

EphB4 receptor: Inhibitors were tested at two-fold dilutions (concentration range: 50 µM - 0.003 µM) against recombinant Ephrin receptor B4 kinase domain (Invitrogen) in an assay containing 25 mM HEPES, pH 7.4, 10 mM MgCl2, 0.1% BME, 10 µM ATP (2.5 µCi of γ-32P-ATP), and 3 µg/mL BSA. Poly E-Y (Sigma; 2 mg/mL) was used as a substrate. Reactions were terminated by spotting onto nitrocellulose, which was washed with 1M NaCl/1% phosphoric acid (approximately 6 times, 5-10 min each). Sheets were dried and the transferred radioactivity quantitated by phosphorimaging. IC_{50} values were calculated by fitting the data to a sigmoidal dose-response curve using the Prism software package. IC_{50} values were calculated by fitting the data to a sigmoidal dose-response curve using the Prism software package.

EGF receptor: Inhibitors were tested at two-fold dilutions (concentration range: 50 µM - 0.003 µM) against recombinant EGF receptor kinase domain (Invitrogen) in an assay containing 25 mM HEPES, pH 7.4, 10 mM MgCl2, 0.1% BME, 10 µM ATP (2.5 µCi of γ-32P-ATP), and 3 µg/mL BSA. Poly E-Y (Sigma; 2 mg/mL) was used as a substrate. Reactions were terminated by spotting onto nitrocellulose, which was washed with 1M NaCl/1% phosphoric acid (approximately 6 times, 5-10 min each). Sheets were dried and the transferred radioactivity quantitated by phosphorimaging. IC_{50} values were calculated by fitting the data to a sigmoidal dose-response curve using the Prism software package.

c-KIT: Inhibitors were tested at two-fold dilutions (concentration range: 50 µM - 0.003 µM) against recombinant KIT kinase domain (Invitrogen) in an assay containing 25 mM HEPES, pH 7.4, 10 mM MgCl2, 1mM DTT, 10mM $MnCl_2$, 10 µM ATP (2.5 µCi of γ-32P-ATP), and 3 µg/mL BSA. Poly E-Y (Sigma; 2 mg/mL) was used as a substrate.

Reactions were terminated by spotting onto nitrocellulose, which was washed with 1M NaCl/1% phosphoric acid (approximately 6 times, 5-10 min each). Sheets were dried and the transferred radioactivity quantitated by phosphorimaging. IC_{50} values were calculated by fitting the data to a sigmoidal dose-response curve using the Prism software package.

RET: Inhibitors were tested at two-fold dilutions (concentration range: 50 μM - 0.003 μM) against recombinant RET kinase domain (Invitrogen) in an assay containing 25 mM HEPES, pH 7.4, 10 mM $MgCl_2$, 2.5mM DTT, 10 μM ATP (2.5 μCi of γ-32P-ATP), and 3 μg/mL BSA. The peptide substrate EAIYAAPFAKKK was used as phosphoacceptor (200 μM) . Reactions were terminated by spotting onto phosphocellulose sheets, which were washed with 0.5% phosphoric acid (approximately 6 times, 5-10 min each). Sheets were dried and the transferred radioactivity quantitated by phosphorimaging. IC_{50} values were calculated by fitting the data to a sigmoidal dose-response curve using the Prism software package.

PDGFRβ: Inhibitors were tested at two-fold dilutions (concentration range: 50 μM - 0.003 μM) against recombinant PDGF receptor β kinase domain (Invitrogen) in an assay containing 25 mM HEPES, pH 7.4, 10 mM $MgCl_2$, 2.5mM DTT,10 μM ATP (2.5 μCi of γ-32P-ATP), and 3 μg/mL BSA. The peptide substrate EAIYAAPFAKKK was used as phosphoacceptor (200 μM) . Reactions were terminated by spotting onto phosphocellulose sheets, which were washed with 0.5% phosphoric acid (approximately 6 times, 5-10 min each). Sheets were dried and the transferred radioactivity quantitated by phosphorimaging. IC_{50} values were calculated by fitting the data to a sigmoidal dose-response curve using the Prism software package.

FLT-3: Inhibitors were tested at two-fold dilutions (concentration range: 50 μM - 0.003 μM) against recombinant FLT-3 kinase domain (Invitrogen) in an assay containing 25 mM HEPES, pH 7.4, 10 mM $MgCl_2$, 2.5mM DTT,10 μM ATP (2.5 μCi of γ-32P-ATP), and 3 μg/mL BSA. The optimized Abl peptide substrate EAIYAAPFAKKK was used as phosphoacceptor (200 μM) . Reactions were terminated by spotting onto phosphocellulose sheets, which were washed with 0.5% phosphoric acid (approximately 6 times, 5-10 min each). Sheets were dried and the transferred radioactivity quantitated by phosphorimaging. IC_{50} values were calculated by fitting the data to a sigmoidal dose-response curve using the Prism software package.

TIE2: Inhibitors were tested at two-fold dilutions (concentration range: 50 μM - 0.003 μM) against recombinant TIE2 kinase domain (Invitrogen) in an assay containing 25 mM HEPES, pH 7.4, 10 mM MgCl2, 2mM DTT, 10mM $MnCl_2$, 10 μM ATP (2.5 μCi of γ-32P-ATP), and 3 μg/mL BSA. Poly E-Y (Sigma; 2 mg/mL) was used as a substrate. Reactions were terminated by spotting onto nitrocellulose, which was washed with 1M NaCl/1% phosphoric acid (approximately 6 times, 5-10 min each). Sheets were dried and the transferred radioactivity quantitated by phosphorimaging. IC_{50} values were calculated by fitting the data to a sigmoidal dose-response curve using the Prism software package.

2.9.3. SelectScreen profiling of kinase inhibitors

Compounds were assayed by Invitrogen at a final drug concentration of 1 μM and, typically, an ATP concentration of 10 μM. See Supplementary Table 3 for complete data, and http://www.invitrogen.com/downloads/PAC-SSBK.pdf for complete assay

details. Complete data for reference kinase inhibitors is available at

http://www.invitrogen.com/downloads/SelectScreen_Data_193.pdf.

2.9.4. Determination of p110γ crystal structures

This work was done by Beatriz Z. Gonzalez in the laboratory of Roger L. Williams at the MRC Laboratory of Molecular Biology in Cambridge, England. See Appendix 2.

2.9.5. Determination of c-Src crystal structures

This work was done by James Blair, a fellow graduate student in Kevan Shokat's laboratory at the University of California, San Francisco. See Appendix 2.

2.10   References

Alaimo, P. J., Z. A. Knight, et al. (2005). "Targeting the gatekeeper residue in phosphoinositide 3-kinases." Bioorg Med Chem 13(8): 2825-36.

Bishop, A. C., J. A. Ubersax, et al. (2000). "A chemical switch for inhibitor-sensitive alleles of any protein kinase." Nature 407(6802): 395-401.

Djordjevic, S. and P. C. Driscoll (2002). "Structural insight into substrate specificity and regulatory mechanisms of phosphoinositide 3-kinases." Trends Biochem Sci 27(8): 426-32.

Hanke, J. H., J. P. Gardner, et al. (1996). "Discovery of a novel, potent, and Src family-selective tyrosine kinase inhibitor. Study of Lck- and FynT-dependent T cell activation." J Biol Chem 271(2): 695-701.

Huse, M. and J. Kuriyan (2002). "The conformational plasticity of protein kinases." Cell 109(3): 275-82.

Knight, Z. A., G. G. Chiang, et al. (2004). "Isoform-specific phosphoinositide 3-kinase inhibitors from an arylmorpholine scaffold." Bioorg Med Chem 12(17): 4749-59.

Knight, Z. A., B. Gonzalez, et al. (2006). "A pharmacological map of the PI3-K family defines a role for p110alpha in insulin signaling." Cell 125(4): 733-47.

Knight, Z. A. and K. M. Shokat (2007). "Chemically targeting the PI3K family." Biochem Soc Trans 35(Pt 2): 245-9.

Liu, Y., A. Bishop, et al. (1999). "Structural basis for selective inhibition of Src family kinases by PP1." Chem Biol 6(9): 671-8.

Liu, Y. and N. S. Gray (2006). "Rational design of inhibitors that bind to inactive kinase conformations." Nat Chem Biol 2(7): 358-64.

Shah, N. P. and C. L. Sawyers (2003). "Mechanisms of resistance to STI571 in Philadelphia chromosome-associated leukemias." Oncogene 22(47): 7389-95.

Zhang, C., D. M. Kenski, et al. (2005). "A second-site suppressor strategy for chemical genetic analysis of diverse protein kinases." Nat Methods 2(6): 435-41.

Chapter 3: Dual-specificity inhibitors inhibit cellular targets and block oncogenic growth

3.1 Introduction

The biochemical activity of kinase inhibitors in *in vitro* kinase assays reflects cellular activity to a reasonable approximation (Knight and Shokat 2005). However, there are clear discrepancies between median inhibitory concentrations (IC_{50}s) measured *in vitro* and those measured in cells. These differences are partly due to cellular variations in kinase and substrate concentration, natural inhibitor abundance (such as the concentration of PTEN in an assay measuring PI3K activity), and bioavailability (Knight and Shokat 2005). Using cell-based experiments we characterized the activity of dual-specificity inhibitors in several cancer cell lines and explored the ability of these compounds to block processes such as angiogenesis that are critical to cancer cell survival.

3.2 Dual-specificity inhibitors block cellular targets in the PI3K/Akt pathway

To test the ability of dual-specificity inhibitors to block the PI3K/Akt pathway in cells, we treated several cancer cell lines with PP102 and PP121, two potent dual-specificity inhibitors and determined their effects on downstream targets using western blot analysis (Figure 3.1a). Both compounds potently blocked phosphorylation of Akt and S6 in LN229 (wt) and U87 (PTEN mutant) glioblastoma cells, and had no effect on ERK, an effector of the MAPK pathway. In comparison, the pure tyrosine kinase inhibitor Sorafenib (BAY 43-9006) had little effect on targets downstream of PI3K, but potently blocked ERK phosphorylation. Signficantly, PP121, which potently inhibits mTOR *in vitro* (IC_{50}(PP121)= 13 nM), blocks S6 phosphorlyation more completely than PP102, a less potent inhibitor of mTOR (IC_{50}(PP102)= 140 nM). PP121 and PP102 are slightly less potent in PTEN mutant cells (U87) than wild-type cells. This loss of potency
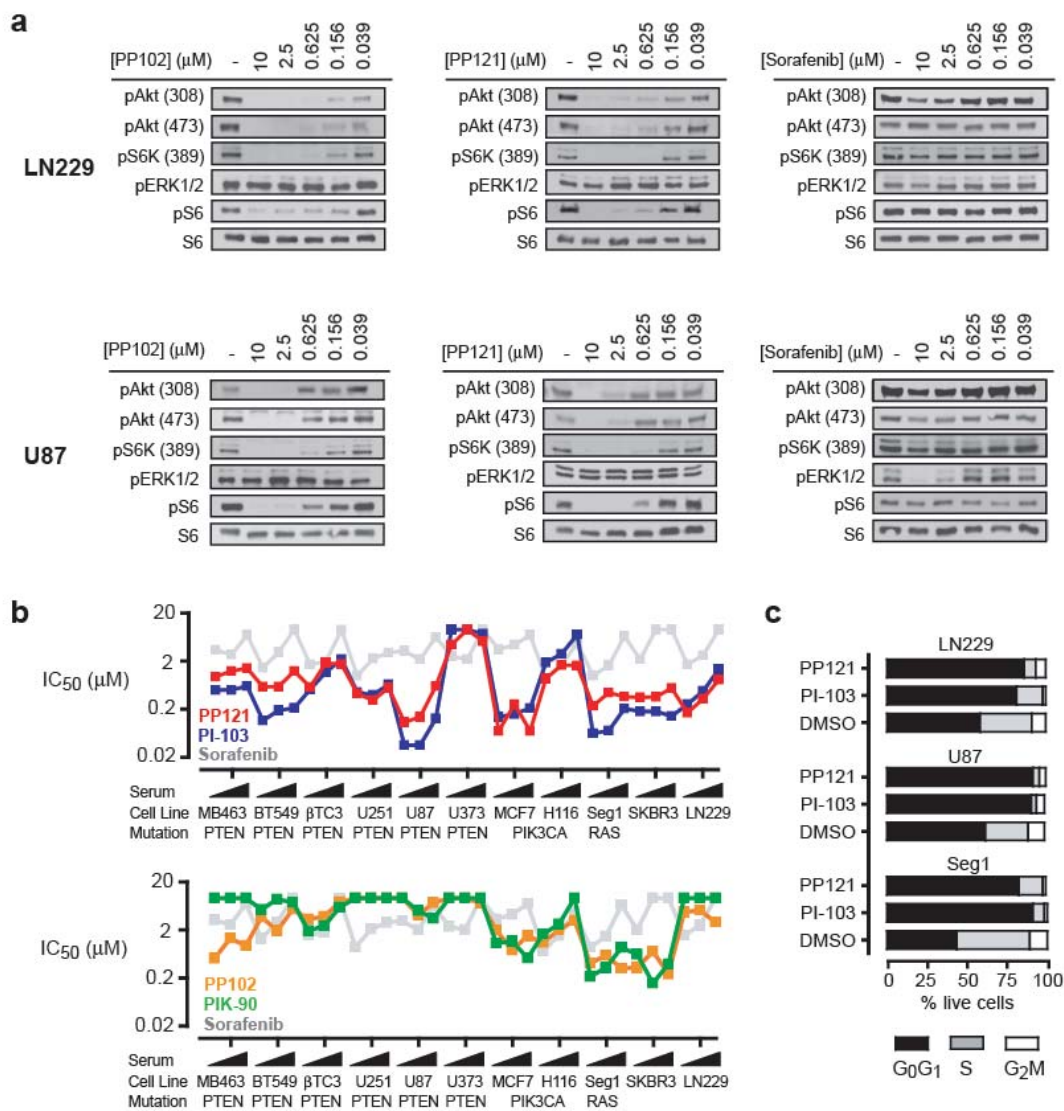
Figure 3.1 Dual-specificity inhibitors block activity of cellular targets. a) Western blots show that PP121 and PP102, unlike sorafenib, block phosphorylation of effectors in the PI3K pathway. b) Graphical analysis comparing IC_{50}s of PP121, PP102, PI-103, PIK-90 and sorafenib against PI3K-pathway mutant cells demonstrate PP121 has a potency profile to PI-103. c) Cell cycle analysis of cancer cell lines treated with compound and stained with propidium iodide show PP121, like PI-103, arrests cells in G_1G_0.

is expected as the PI3K pathway has lost its natural inhibitor in PTEN null cells and is consequently more difficult to block.

3.3 Dual-specificity inhibitors block PI3K pathway-dependent growth

We next assessed the ability of the dual-specificity inhibitors PP121 and PP102 to block the growth of cancer cell lines with well-characterized activating mutations in the PI3K/Akt pathway (Figure 2b). As benchmarks, several well-established inhibitors of the PI3K pathway were used in parallel assays. These inhibitors included: PI-103 (PI3K/mTOR inhibitor), PIK-90 (PI3K inhibitor) and sorafenib (clinical tyrosine kinase inhibitor) (Wilhelm, Carter et al. 2004; Knight, Gonzalez et al. 2006; Knight and Shokat 2007).   PP121 (tyrosine kinase/PI3K/mTOR inhibitor) potently blocked cancer cell growth in a pattern similar to PI-103, whereas PP102 (a more PI3K specific dual-specificity inhibitor) and PIK-90, were less potent and had unique potency profiles against the cell lines. The similar activity of PP121 and PI-103 established the importance of inhibiting mTOR in blocking PI3K-dependent cellular proliferation. Sorafenib was not able to inhibit growth of these PI3K pathway dependent cells (Figure 3.2b).

To better understand the effects of these compounds on PI3K-dependent cells we treated these cells with dual-specificity inhibitors and used FACS analysis to characterize the cell cycle stage at which these inhibitors achieved proliferative block (Figure 3.2c). We used PI-103, the dual PI3K/mTOR inhibitor as a bench mark, and observed that our inhibitors, like PI103, arrested cell growth in G_0G_1. Arrest of cells in G_0G_1 was expected, as it is the typical effect of inhibitors of the PI3K/AKT pathway in cells (Fan, Knight et al. 2006; Marques, Kumar et al. 2008).

94

3.4 Dual-specificity inhibitors block tyrosine kinase-dependent growth and combat drug resistance

To test the ability of our inhibitors to block a tyrosine kinase-dependent cellular phenotype, we treated Src-transformed NIH-3T3 cells with PP121 and compared the effects to treatment with PI-103 (PI3K/mTOR inhibitor) and PP1, the well-known inhibitor of Src family kinases (Hanke, Gardner et al. 1996; Fan, Knight et al. 2006). PP121, like PP1, was able to block Src-dependent transformation, as demonstrated by the high percentage of cells acquiring actin stress fibers (~85%) which is consistent with known effects of inhibiting Src in these cells and was similar to the effect of PP1 in the same assay (~85% actin stress fiber acquisition, Figure 3.2a) (Cohen, Zhang et al. 2005). In contrast, the stress fiber acquisition of Src-transformed NIH-3T3 cells treated with PI-103 was similar to those treated with DMSO, suggesting the molecular mechanism causing the phenotypic reversion by PP121 and PP1 is direct tyrosine kinase inhibition. This was confirmed by western blot analysis of tyrosine kinase phosphorylation, which showed PP121, but not PI-103, dose-dependently blocked tyrosine phosphorylation in these cells (Figure 3.2b).

We next assessed the ability of the dual-specificity inhibitors to block growth of hematological cells dependent on the Bcr-Abl tyrosine kinase. Bcr-Abl is a constitutively active tyrosine kinase that has been studied for over 50 years and has an established role in the development of CML (Nowell 2007). The tyrosine kinase inhibitor Imatinib, which is directed against this abnormal protein, has shown promising results in the treatment of patients with CML and is known to induce 100% apoptosis in CML cells treated in culture (Parada, Banerji et al. 2001; Okada, Adachi et al. 2004; Jacquel, Colosetti et al. 2007; Nowell 2007). We tested the ability of PP121 to stop the growth of Baf3 cells transfected with Bcr-Abl and Bcr-Abl-amplified K562 cells, and compared these results to Imatinib treatment. Both cell lines are dependent on Bcr-Abl activity for

growth and survival. PP121, but not PI-103, inhibited tyrosine phophorylation of both

cells lines with a potency similar to Imatinib (Figure 3.3a and Figure 3.4a). PP121, like

PI-103 and Imatinib, potently blocked cell proliferation in contrast to the more selective

PI3K inhibitors PP102 and PIK-90 which did not block proliferation of these cells (Figure

3.3b and Figure 3.3c). This result suggests inhibition of mTOR (PI-103 and PP121) or
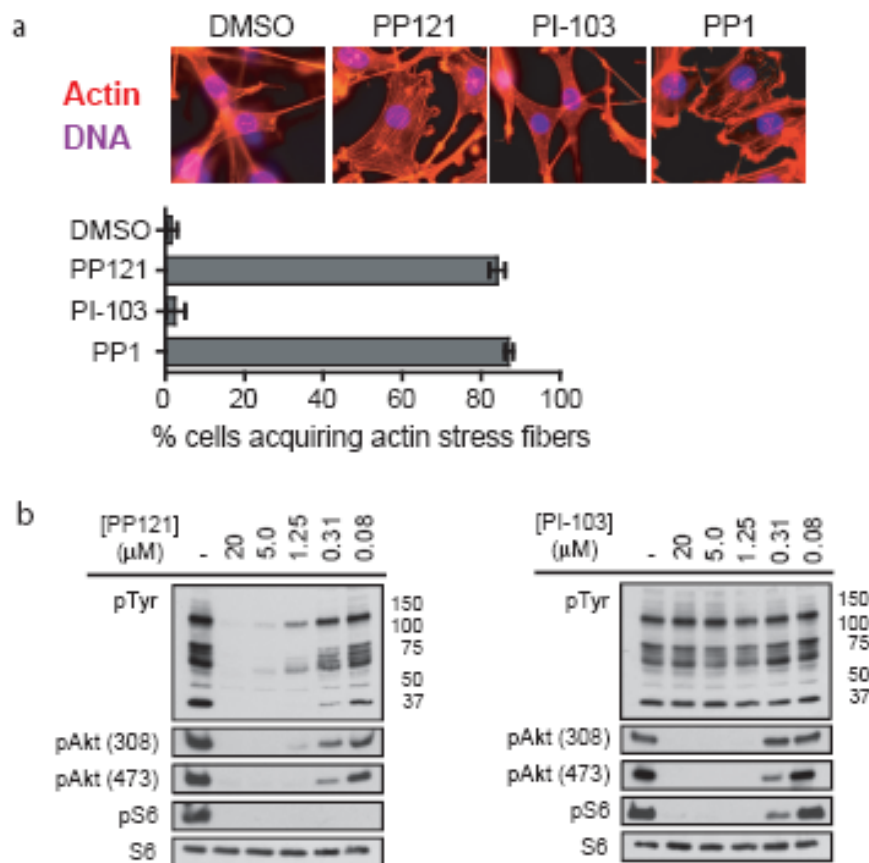

Figure 3.2 Dual-specificity inhibitors block tyrosine kinase activity in Src-transformed NIH-3T3 cells. a) Cells treated with PP121 and PP1 acquire actin stress fibers and reverse the morphology of Src-transformed NIH-3T3 cells; PI-103 does not inhibit Src and is unable to induce the morphological reversion. b) PP121, but not PI-103, blocks tyrosine phosphorylation in NIH-3T3 cells.

Bcr-Abl (Imatinib and PP121) are independently sufficient to block Bcr-Abl-dependent cell growth.

To elucidate the unique effects of PP121 as a dual phosphoinositide kinase/tyrosine kinase inhibitor and assess its ability to overcome drug resistance, we explored the effects of PP121 on a Baf3/Bcr-Abl cells with mutation in the gatekeeper residue (T315I) that renders the kinase resistant to inhibition by Imatinib (Shah and Sawyers 2003). We compared the effects of PP121 to the lipid kinase-selective inhibitors PI103, PIK-90 and PP102 as well as the selective tyrosine kinase inhibitor Imatinib. Similar to the wild-type cells, growth of the Baf3/Bcr-Abl(T315I) cells was not affected by treatment with PIK-90 or PP102, which are the PI3K family inhibitors lacking mTOR activity (Figure 4.4b). However, in contrast to wild-type cells, T315I mutant cells continued to proliferate when treated with Imatinib; this was the expected result, as it is well established that the Abl(T315I) mutation prevents Imatinib binding in the Abl active site (Shah and Sawyers 2003). Both PI103 and PP121 continued to inhibit proliferation of T315I mutant cells, further implicating mTOR kinase activitity as critical for maintaining the growth of these cells and suggesting the unique targets of PP121 are sufficient to overcome cellular resistance to singly targeted agents (Fig. 4b).

To better distinguish the effects of PP121 (dual mTOR/PTK inhibitor) and PI-103 (mTOR inhibitor) in the Baf3/Bcr-Abl cells and to uncover unique effects caused by PP121's dual-specificity inhibition, we did a FACS analysis to characterize the cell cycle stage at which the compounds cause proliferative block and assessed the fraction of cells that were induced to apoptose. In the clinic, apoptosis is the more desirable mechanism for drug-induced cell death, as it is expected to be a more natural process of cell death than necrosis and is believed to cause fewer unwanted side effects (Blagosklonny and Fojo 1999).
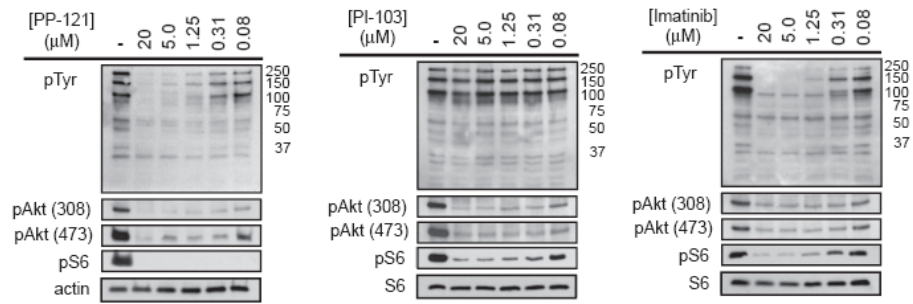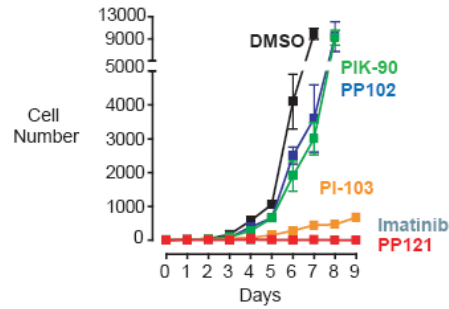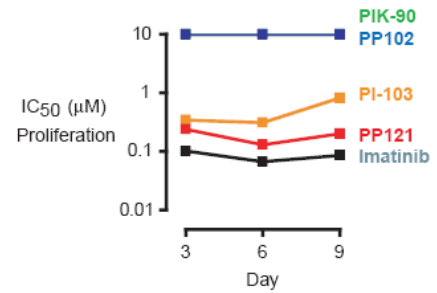
Figure 3.3 PP121 blocks Bcr-Abl-dependent CML cells. a) PP121 and Imatinib, but not PI-103, dose-dependently block tyrosine phosphorylation of K562 cells which over-express Bcr-Abl. b) PP121 blocks K562 cell proliferation with a potency similar to Imatinib and PI-103.
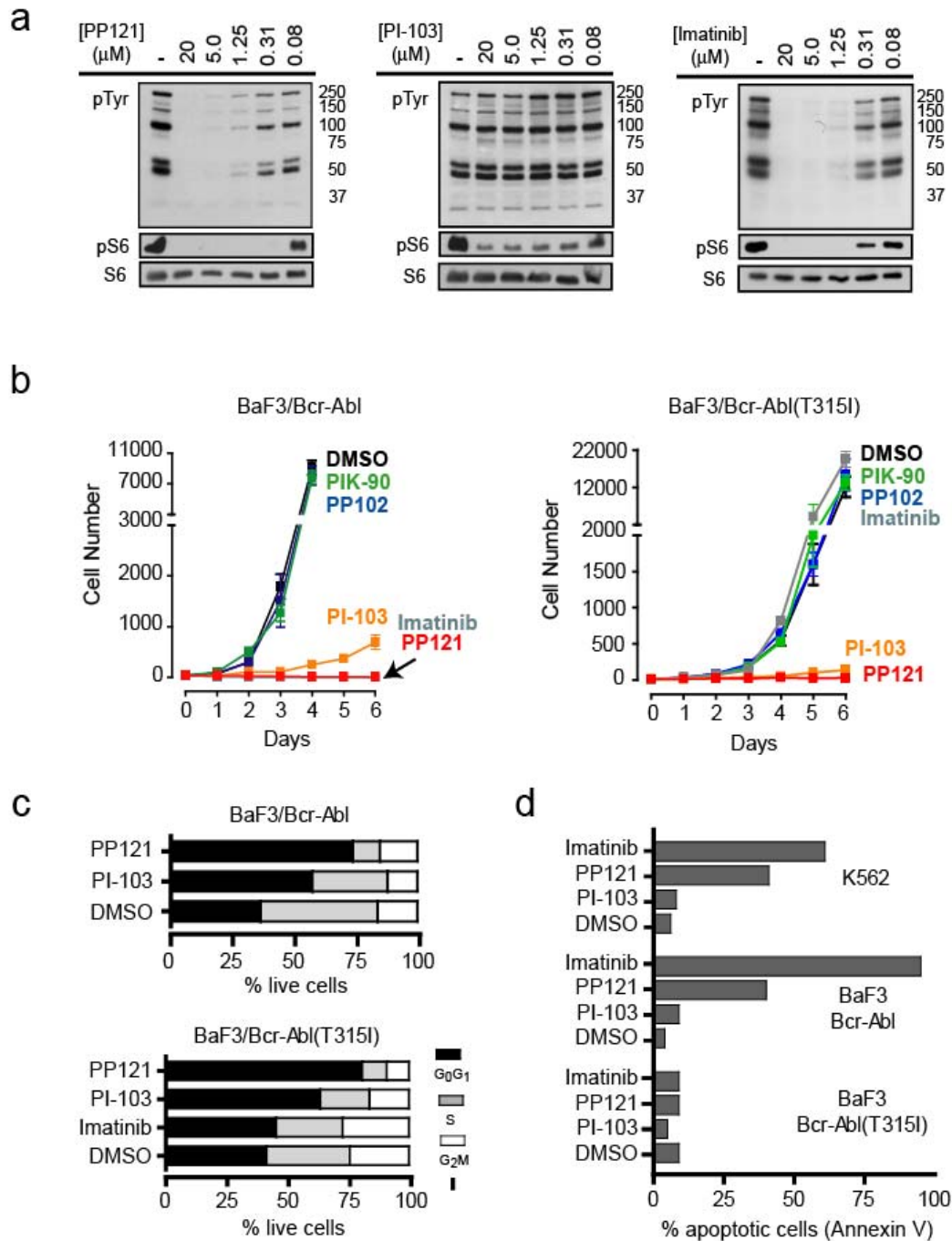
Figure 3.4 PP121 inhibits Bcr-Abl-dependent Baf3 cells and overcomes T315I resistance mutation. a) PP121 and Imatinib, but not PI-103, inhibit tyrosine phosphorylation in Baf3/Bcr-Abl cells. b) and c) PP121 inhibits proliferation of Baf3/Bcr-Abl cells resistant to Imatinib and arrests cells in G_0G_1, similar to PI-103. d) Imatinib and PP121, but not PI-103, induce apoptosis in cells dependent on wild-type Bcr-Abl.

99

Imatinib, which is known to cause 100% apoptosis in wild-type Bcr-Abl dependent cells, was used as a benchmark in these experiment. FACS analyses showed PP121 and PI103 arrested both wild-type and mutant Baf3/Bcr-Abl cells in G_0G_1, whereas Imatinib had no effect on the T315I mutant cells and caused all wild-type cells to die (Figure 4.4c). We stained compound-treated cells with AnnexinV-FITC, a well-established antibody that binds apoptotic cells and is conjugated to a florescent marker. The size of the apoptotic cell population was then determined using flow cytometry. In wild-type cells expressing Bcr-Abl, PP121 and Imatinib induced apoptosis, whereas PI-103 did not. In the Baf3/Bcr-Abl(T315I) cells, none of the compounds induced apoptosis, consistent with the idea that inhibition of Bcr-Abl is necessary for induction of apoptosis in these cells and showing that PP121 has the unique ability to both induce apoptosis by tyrosine kinase inhibition in cells addicted to tyrosine kinase activity and arrest cells in G_1G_0 by blocking mTOR and PI3K. These data suggest that our new class of inhibitors, which inhibit both tyrosine kinases and phosphoinositide kinases, may be more effective at blocking oncogenic growth and evading resistance through inhibition of over-activated signaling networks at multiple critical nodes.

3.5 Dual-specificity inhibitors block *in vitro* angiogenesis.

In addition to blocking oncogenic growth by direct inhibition of cancer cells, dual-specificity inhibitors have the potential to block angiogenesis by inhibiting the VEGF receptor tyrosine kinase. Angiogenesis is a critical process in cancer growth and inhibition of this process has been an effective way to treat cancer in the clinic (Folkman 2007; Strumberg, Clark et al. 2007). PP121 inhibits the VEGF receptor kinase with an *in vitro* IC_{50} of 12 nM and potently blocks phosphorylation of the VEGF receptor in HUVECs (Figure 4.5a). Given these data, we tested the ability of PP121 to block growth

of HUVECs in media containing no growth factors other than VEGF. PP121, unlike

PP102 which is not active against the VEGF receptor, potently
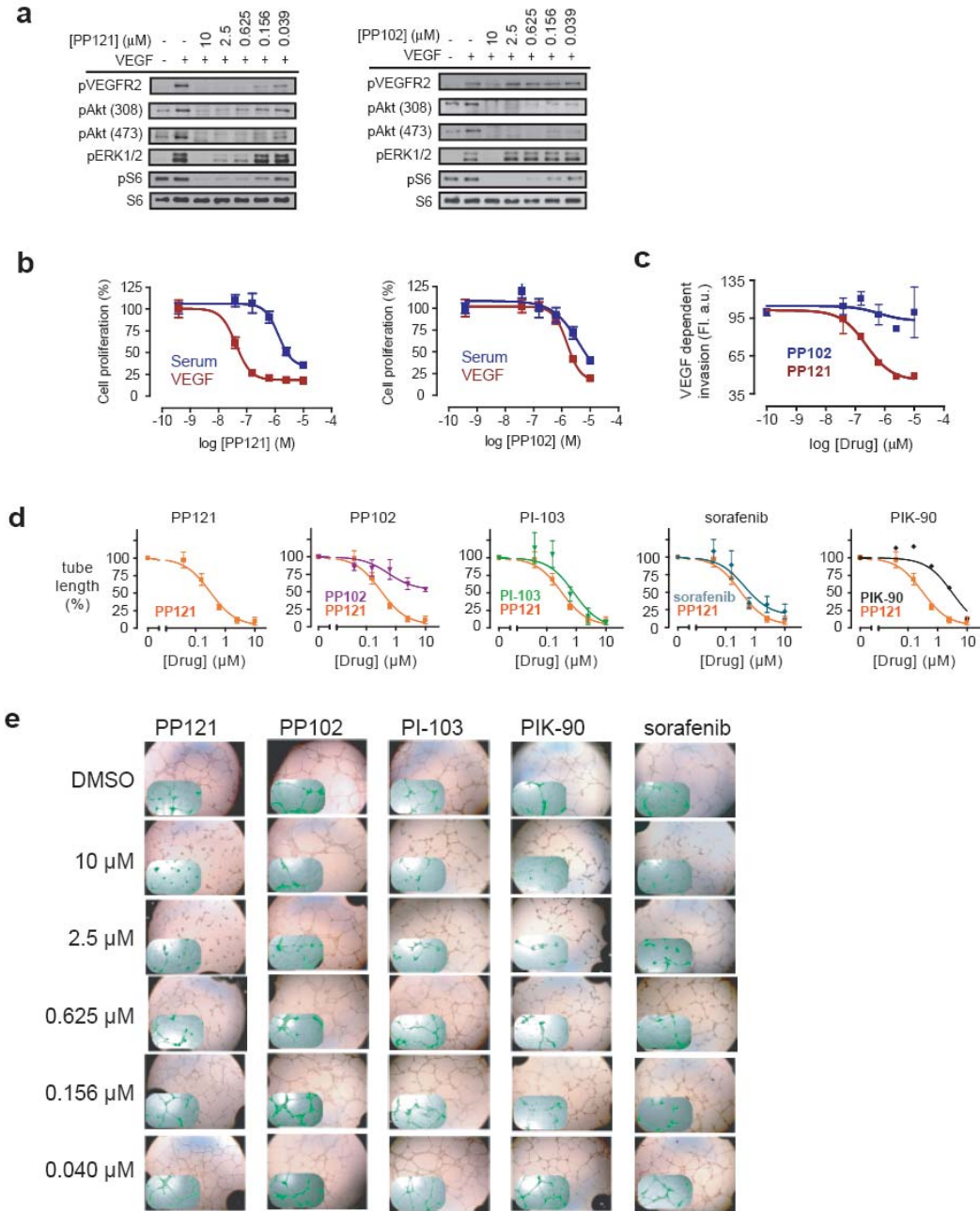
Figure 3.5 PP121 blocks *in vitro* angiogenesis. a) PP121, but not PP102, blocks VEGFR phosphorylation in HUVECS. b) PP121, but not PP102 blocks VEGF-dependent proliferation of HUVECs. c) PP121 blocks HUVEC invasion through a matrigel-covered porous membrane. d) and e) PP121 potently blocks endothelial cell tube formation.

inhibited VEGF-dependent HUVEC proliferation (Figure 4.5b). Futhermore, PP121 was able to block endothelial cell tube formation and endothelial cell migration in tissue culture (Figure 4.5c and Figure 4.5d). The ability for PP121 to inhibit the VEGF receptor and block angiogenesis in tissue culture suggests that dual-specificity inhibitors may have the ability to block blood vessel growth that is critical to cancer cell survival.

3.6 Conclusion

Small molecules hold a privileged position in basic science in that they are ultimately the agents used to treat human disease (Sawyers 2003; Wilhelm, Carter et al. 2004; Knight and Shokat 2005; Sams-Dodd 2005). Thus, it is important to understand both small-molecule inhibitors and the effects they have on biological systems. Through tissue culture based assays we probed the effects of our inhibitors on biological systems and observed that our dual-specificity inhibitors are able to elicit desirable anti-oncogenic phenotypes, including inhibition of cancer cell proliferation and survival, blockade of angiogenic growth and inhibition of cancer cells resistant to singly targeted agents.

3.7 Experimental procedures

Tumor cell western blotting: U87 and LN229 cells were grown in 12-well plates in DMEM containing 10% FBS and penicillin/streptomycin. Cells were treated for 1 h with either inhibitor at four-fold dilutions between 10 µM and 0.040 µM or vehicle (0.1% DMSO), then lysed in RIPA buffer containing protease and phosphatase inhibitors. Lysates were resolved by SDS-PAGE, transferred to nitrocellulose by electroblotting, and probed for the indicated proteins. All antibodies were from Cell Signaling Technology.

Tumor cell proliferation assays: All tumor cell lines were grown in media as recommended by the ATCC. Cells were plated in 96-well plates to approximately 30% confluence in serum with 0.5%, 2% or 10% FBS and left overnight to adhere. The following day cells were treated with inhibitor at four-fold dilutions in appropriate serum concentration so that the final inhibitor concentration was between 10 μM and 0.040 μM or vehicle (0.1% DMSO). After 72 hours of treatment 10μl of 440μM Resazurin sodium salt (Sigma) was added to each well. When a difference in color became detectable by eye (2-24 hours) florescence intensity in each well was measured using a top-reading florescence plate reader.

Cell cycle analysis by FACS: Cells were grown to 60% confluence in 6-well plates containing 10% fetal bovine serum (FBS). Media was removed, cells were washed with PBS and treated with 2.5 μM PI-103, PP121, or vehicle (0.1% DMSO) in media plus 10% FBS. After 24 h of incubation at 37ºC, cells were trypsinized, harvested and fixed with cold EtOH (70%). Cells were treated with RNase and stained with propidium iodide, then sorted using a FACS Calibur flow cytometer (Becton Dickinson). Results were analyzed and cell cycle stage of cells in samples were determined using Modifit-LT software (Verity Software).

HUVEC western blotting: HUVECs were grown in 12-well plates in complete media (Clonetics). Cells were then serum-starved for 8 h in basal media (Clonetics); pretreated with either inhibitor at four-fold dilutions between 10 μM and 0.040 μM or vehicle (0.1% DMSO) for 30 min; and then stimulated with VEGF (4 ng/mL) for 30 min. Cells were then lysed in RIPA buffer containing protease and phosphatase inhibitors. Lysates were resolved by SDS-PAGE, transferred to nitrocellulose by electroblotting,

and probed for the indicated proteins. All antibodies were from Cell Signaling

Technology.

Endothelial Cell Tube Formation Assays: *In vitro* angiogenesis was assayed

using the Endothelial Cell Tube Formation Assay (CellBiolabs) as described by the

manufacturer's protocol. Briefly, a 96-well plate was coated with ECM gel (50 µL/well).

ECM gel was solidified at 37º C and HUVECs (Clonetics) were plated on the matrix (1.4

x 10^4 cells/well) in complete media (Clonetics) with appropriate concentration of PP121,

PP102, PI-103, PIK-90 or sorafenib. After 24 h, cells were treated with Calcien AM and

four images/well were obtained using a fluorescent microscope. Tube length was

quantified using ImageJ software.

Endothelial Cell Invasion Assays: *In vitro* endothelial cell invasion was

measured using 24-well BD Biocoat fluoroblack assay kit (BD Biosciences) as described

by the manufacturer's protocol. Briefly, HUVECs were serum-starved in basal media for

8 h then added to the top chamber of the assay kit (5.0 x 10^4 cells/chamber) which

contained a Matrigel-coated 3 µM porous membrane. Cells were plated in basal media

(Clonetics) containing appropriate concentration of PP121 or PP102. Basal media with

4 ng/mL VEGF (Sigma) as a chemoattractant was added to the bottom chamber. After a

24 h incubation at 37º C, the insert plate containing the upper chambers was removed

and the bottom-side of the porous membrane was incubated in Calcein AM (4 µg/mL) for

90 min. Invaded cells were measured using a bottom-reading florescence plate reader.

3.8 References

Blagosklonny, M. V. and T. Fojo (1999). "Molecular effects of paclitaxel: myths and
        reality (a critical review)." Int J Cancer 83(2): 151-6.

Cohen, M. S., C. Zhang, et al. (2005). "Structural bioinformatics-based design of selective, irreversible kinase inhibitors." Science 308(5726): 1318-21.

Fan, Q. W., Z. A. Knight, et al. (2006). "A dual PI3 kinase/mTOR inhibitor reveals emergent efficacy in glioma." Cancer Cell 9(5): 341-9.

Folkman, J. (2007). "Is angiogenesis an organizing principle in biology and medicine?" J Pediatr Surg 42(1): 1-11.

Hanke, J. H., J. P. Gardner, et al. (1996). "Discovery of a novel, potent, and Src family-selective tyrosine kinase inhibitor. Study of Lck- and FynT-dependent T cell activation." J Biol Chem 271(2): 695-701.

Jacquel, A., P. Colosetti, et al. (2007). "Apoptosis and erythroid differentiation triggered by Bcr-Abl inhibitors in CML cell lines are fully distinguishable processes that exhibit different sensitivity to caspase inhibition." Oncogene 26(17): 2445-58.

Knight, Z. A., B. Gonzalez, et al. (2006). "A pharmacological map of the PI3-K family defines a role for p110alpha in insulin signaling." Cell 125(4): 733-47.

Knight, Z. A. and K. M. Shokat (2005). "Features of selective kinase inhibitors." Chem Biol 12(6): 621-37.

Knight, Z. A. and K. M. Shokat (2007). "Chemically targeting the PI3K family." Biochem Soc Trans 35(Pt 2): 245-9.

Marques, M., A. Kumar, et al. (2008). "Phosphoinositide 3-kinases p110alpha and p110beta regulate cell cycle entry, exhibiting distinct activation kinetics in G1 phase." Mol Cell Biol 28(8): 2803-14.

Nowell, P. C. (2007). "Discovery of the Philadelphia chromosome: a personal perspective." J Clin Invest 117(8): 2033-5.

Okada, M., S. Adachi, et al. (2004). "A novel mechanism for imatinib mesylate-induced cell death of BCR-ABL-positive human leukemic cells: caspase-independent, necrosis-like programmed cell death mediated by serine protease activity." Blood 103(6): 2299-307.

Parada, Y., L. Banerji, et al. (2001). "BCR-ABL and interleukin 3 promote haematopoietic cell proliferation and survival through modulation of cyclin D2 and p27Kip1 expression." J Biol Chem 276(26): 23572-80.

Sams-Dodd, F. (2005). "Target-based drug discovery: is something wrong?" Drug Discov Today 10(2): 139-47.

Sawyers, C. L. (2003). "Will mTOR inhibitors make it as cancer drugs?" Cancer Cell 4(5): 343-8.

Shah, N. P. and C. L. Sawyers (2003). "Mechanisms of resistance to STI571 in Philadelphia chromosome-associated leukemias." Oncogene 22(47): 7389-95.

Strumberg, D., J. W. Clark, et al. (2007). "Safety, pharmacokinetics, and preliminary antitumor activity of sorafenib: a review of four phase I trials in patients with advanced refractory solid tumors." Oncologist 12(4): 426-37.

Wilhelm, S. M., C. Carter, et al. (2004). "BAY 43-9006 exhibits broad spectrum oral antitumor activity and targets the RAF/MEK/ERK pathway and receptor tyrosine kinases involved in tumor progression and angiogenesis." Cancer Res 64(19): 7099-109.

Chapter 4: Conclusion
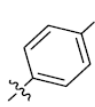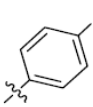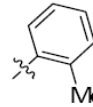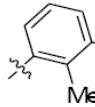
4.1 Summary
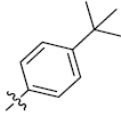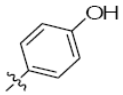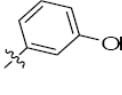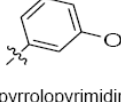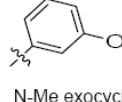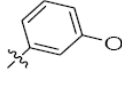
Genetic analysis shows that receptor tyrosine kinases and phosphoinositide-3-kinases play critical roles in growth and survival of human cancer cells. However, dual-specific, ATP-competitive inhibitors of PI3Ks and PTKs have never been reported and, before now, it has not been clear whether or not it is possible to design molecules that simultaneously target these two families of kinases. Through chemical synthesis and kinome profiling we were able to develop dual-specificity inhibitors that specifically and potently target protein tyrosine kinases and phosphoinositide-3-kinases. Through SAR analysis and crystallographic analysis we determined the chemical and structural features that control their selectivity and potency. We then used tissue culture-based assays to demonstrate the potential of dual-specificity inhibitors in stopping oncogenic growth and transformation. We showed that dual-specificity inhibitors block the activation of oncogenic protein tyrosine kinase/PI3K/mTOR pathways in cancer cells and inhibit growth of cancer cells that are driven by these aberrant pathways by sending the cells into apoptosis. Lastly, we demonstrated the functional potential of dual tyrosine kinase/phosphoinositide kinases inhibitors by showing their ability to inhibit proliferation of cells resistant to singly targeted molecular therapies and demonstrating their ability to block *in vitro* angiogenesis.

The rational design of dual protein tyrosine kinase/phosphoinositide kinase inhibitors represents a new paradigm for targeted drug discovery and may lead to the development of drug-like small molecules that inhibit oncogenic growth and oncogenic signaling cascades more potently and effectively than the current generation of kinase inhibitors.

Appendix 1: IC$_{50}$ Table

Table 1. IC$_{50}$ (μM) values of PP inhibitors against purified kinase domains

	PP200	PP201	PP2	PP204	PP205	PP206
R1	phenyl	4-Me-phenyl	4-Me-phenyl	3-Me-phenyl	2,?-Me-phenyl	2,3-diMe-phenyl
R2	H	H	(t-Bu)	H	H	H
p110α	8.6	8.5	20	4.2	15	9
p110β	100	50	100	23	100	50
p110δ	12.5	9.6	7.5	5.7	29	11
p110γ	10.9	7.7	100	2.4	25	15
mTOR	ND	ND	1.1	ND	ND	ND
DNAPK	1.6	1.3	1	1.1	7.1	3.7
PI4Kβ	ND	ND	ND	ND	ND	ND
Abl	ND	ND	0.158	ND	ND	ND
Hck	ND	ND	0.012	ND	ND	ND
Src	ND	ND	0.0064	ND	ND	ND
Src (T/I)	ND	ND	1.5	ND	ND	ND
VEGFR	ND	ND	0.103	ND	ND	ND
EGFR	ND	ND	0.15	ND	ND	ND
EphB4	ND	ND	0.171	ND	ND	ND

	PP125	PP56	PP207	PP208	PP209	S1
R1	4-tBu-phenyl	4-OH-phenyl	3-OH-phenyl	3-OH-phenyl (pyrrolopyrimidine)	3-OH-phenyl (N-Me exocyclic)	3-OH-phenyl
R2	H	(isopropyl)	H	(isopropyl)	(isopropyl)	(isopropyl)
p110α	19	0.51	4.1	3.8	ND	0.48
p110β	100	0.38	25	50	100	8.6
p110δ	18	0.084	3.1	2.9	100	0.25
p110γ	15	0.68	1.7	6.4	100	1.5
mTOR	ND	6	ND	ND	ND	2.1
DNAPK	5	0.62	0.44	0.25	ND	0.19
PI4Kβ	ND	1.6	ND	ND	ND	2.6
Abl	ND	1.7	ND	ND	ND	0.07
Hck	ND	0.047	ND	ND	ND	0.023
Src	ND	0.075	ND	ND	ND	0.015
Src (T/I)	ND	3.2	ND	ND	ND	3.1
VEGFR	ND	1.45	ND	ND	ND	0.213
EGFR	ND	0.922	ND	ND	ND	0.954
EphB4	ND	1.23	ND	ND	ND	0.316

	PP60	PP318	PP320	PP333	PP323	PP327
R1	(phenol, OH, Me)	(Me, OBn)	(Me, OH)	(Me, OH)	(Me, OH)	(Me, OH)
R2	(isopropyl)	H	H	Me	(isopropyl)	(sec-butyl)
p110α	1.35	14.7	1.5	0.64	0.28	0.75
p110β	4.23	100	5.87	3.13	1.72	5.29
p110δ	0.294	3.19	0.66	0.21	0.22	0.47
p110γ	1.31	3.34	0.852	0.55	0.435	0.772
mTOR	0.15	1.2	4	0.861	0.033	0.016
DNAPK	0.316	24.3	0.478	0.173	0.212	0.336
PI4Kβ	1.36	31	8.8	100	12	40
Abl	2.18	13	0.56	0.233	0.031	0.16
Hck	0.033	12.7	0.078	0.065	0.0051	0.019
Src	0.066	33	0.164	0.096	0.0043	0.016
Src (T/l)	0.821	20.3	10.6	9.97	0.67	1.56
VEGFR	9.63	100	0.237	0.151	0.01	0.043
EGFR	100	ND	12.4	19	0.663	1.67
EphB4	1.16	12.2	18.3	8.93	0.249	1.02

	PP77	PP78	PP22	PP79	PP85	PP87
R1	(OH, F)	(OH, F)	(F, OH)	(F, OH)	(Br, OMe)	(Br, OH)
R2	(isopropyl)	(cyclopentyl)	(isopropyl)	(cyclopentyl)	(isopropyl)	(isopropyl)
p110α	2.01	1.27	0.175	0.266	6.31	0.802
p110β	5.81	5.61	0.35	0.343	50.3	0.255
p110δ	0.677	0.249	0.046	0.072	2.97	0.13
p110γ	1.47	1.21	0.34	0.64	4.25	0.27
mTOR	0.192	0.692	14	10	10	30
DNAPK	0.251	0.185	0.735	0.919	0.826	0.309
PI4Kβ	2.78	4.02	3.7	7.39	100	4.09
Abl	0.075	0.063	0.052	0.024	1.5	0.026
Hck	0.076	0.028	0.047	0.0044	0.436	0.01
Src	0.025	0.01	0.033	0.005	0.286	0.031
Src (T/l)	4.81	4.01	2.1	1.65	12.6	0.729
VEGFR	1.66	0.901	0.093	0.048	1.02	0.044
EGFR	3.72	1.77	0.576	0.751	11	0.249
EphB4	0.566	1.02	0.251	0.096	3.3	0.017

111

	PP502	PP489	PP487	PP491	PP493	PP262
R1						
R2	(isopropyl)	Me	(isopropyl)	(cyclobutyl)	(cyclopentyl)	(isopropyl)
p110α	1.7	0.07	0.046	0.076	0.142	0.187
p110β	4.6	0.173	0.24	0.235	0.32	0.613
p110δ	0.206	0.023	0.027	0.041	0.112	0.065
p110γ	7.9	0.039	0.104	0.044	0.054	0.209
mTOR	1.1	0.548	0.045	0.127	0.156	0.037
DNAPK	0.218	0.012	0.017	0.019	0.03	0.088
PI4Kβ	ND	ND	ND	ND	ND	2.5
Abl	0.319	0.109	0.021	0.023	0.045	0.014
Hck	0.034	0.024	0.0041	0.0089	0.012	0.0092
Src	0.072	0.061	0.01	0.0095	0.011	0.0069
Src (T/I)	7.44	100	1.9	1.9	1.69	0.865
VEGFR	2.02	3	0.055	0.04	0.055	0.068
EGFR	4.32	100	0.55	0.324	0.236	1.4
EphB4	100	5.8	0.215	0.322	0.347	0.166

	PP450	PP454	PP469	PP471	PP461	PP413
R1						
R2	(NH₂)	(NH₂)	(CN)	(CN)	(cyclobutyl)	(NH)
p110α	6.52	4.87	0.693	0.394	0.482	1.63
p110β	6.47	16.3	0.481	0.169	1.58	0.364
p110δ	3.03	4.35	1.37	0.716	0.777	0.213
p110γ	0.808	0.606	0.502	0.448	1.07	0.633
mTOR	11	2.9	2.2	0.833	1.5	30
DNAPK	1.61	0.5	0.194	0.149	0.336	0.242
PI4Kβ	31.9	12.4	ND	ND	ND	24
Abl	0.199	0.726	0.963	0.433	0.055	0.293
Hck	0.161	1.4	0.258	0.071	0.011	0.042
Src	0.101	0.405	0.09	0.018	0.024	0.017
Src (T/I)	100	100	100	100	100	100
VEGFR	1.9	2.8	2.13	2.9	0.517	1.15
EGFR	100	26	18	11	2.9	2.9
EphB4	1	100	13	100	2	ND

	PP379	PP421	PP403	PP405	PP432	PP434
R1						
R2						
p110α	0.525	0.347	5.76	9.15	0.65	0.66
p110β	1.02	1.24	0.432	1.42	1.86	0.715
p110δ	0.142	0.058	0.193	0.514	0.015	0.049
p110γ	0.257	0.283	0.78	1.19	0.554	0.342
mTOR	1.8	0.815	6.5	5	9.2	1
DNAPK	0.11	0.107	0.543	0.61	0.151	0.277
PI4Kβ	11.5	4.06	100	100	9.02	2.86
Abl	0.0043	0.0064	0.072	0.483	0.021	0.021
Hck	0.0045	0.0057	0.025	0.086	0.021	0.051
Src	0.00055	0.001	0.015	0.046	0.014	0.031
Src (T/l)	2.03	0.63	10.8	9.2	9.9	11
VEGFR	0.106	0.077	0.369	1.75	0.401	0.555
EGFR	0.318	0.366	8.7	15.6	4.8	2.6
EphB4	0.064	0.054	0.492	100	0.882	0.611

	PP465	PP377	PP399	PP401	PP62	PP358
R1						
R2						
p110α	0.244	5.25	1.099	100	0.543	0.135
p110β	100	5.69	2.82	100	3.21	0.66
p110δ	0.074	1.985	0.172	1.07	0.281	0.012
p110γ	0.808	16.4	1.07	100	0.551	0.14
mTOR	1.1	100	50	100	8.2	0.13
DNAPK	0.37	2.74	0.049	3.69	0.824	0.017
PI4Kβ	ND	100	100	100	13	4.6
Abl	0.067	5.842	0.393	0.565	0.558	0.0055
Hck	0.03	1.53	0.596	0.714	0.037	0.002
Src	0.014	0.747	0.082	0.042	0.098	0.004
Src (T/l)	100	100	100	100	100	1.5
VEGFR	0.178	11.8	100	100	100	0.02
EGFR	0.775	100	100	100	3.86	0.158
EphB4	0.254	100	18.7	100	0.244	0.106

	PP452	PP456	PP463	PP371	PP409	PP428
R1						
R2						
p110α	1.62	0.784	0.176	0.225	0.863	0.113
p110β	3.62	3.53	1.35	0.941	0.864	0.55
p110δ	1.62	1	0.15	0.103	0.203	0.02
p110γ	0.637	0.08	0.293	0.147	0.366	0.058
mTOR	2	0.88	0.23	0.439	2.4	0.377
DNAPK	0.18	0.064	0.043	0.013	0.077	0.028
PI4Kβ	14.6	12.9	ND	10	41.2	8.8
Abl	0.13	0.695	0.032	0.0012	0.505	0.021
Hck	0.033	0.194	0.0058	0.00018	0.02	0.0088
Src	0.073	0.284	0.011	0.00012	0.03	0.002
Src (T/I)	9.5	100	9.8	1.5	27	3.83
VEGFR	0.554	1.14	0.062	0.0043	0.174	0.066
EGFR	4.8	9.14	1.15	0.067	12.4	1.58
EphB4	1	10	1.5	0.018	0.468	0.256

	PP430	PP387	PP389	PP369	PP385	PP391
R1						
R2						
p110α	0.293	6.29	3.85	100	2.66	3.68
p110β	0.809	6.98	0.962	100	2.7	2.64
p110δ	0.012	5.47	0.207	6.05	0.199	0.156
p110γ	0.043	1.82	1.39	12.5	1.53	2.41
mTOR	0.45	15	4.8	3.2	3	3.6
DNAPK	0.035	0.367	0.169	1.93	0.408	0.179
PI4Kβ	100	100	100	100	100	100
Abl	0.017	1.044	0.082	7.93	4.5	1.28
Hck	0.008	0.328	0.067	1.13	0.862	0.244
Src	0.007	0.096	0.025	0.132	0.202	0.144
Src (T/I)	5.5	86.4	18.6	100	100	100
VEGFR	0.103	3.12	0.435	7.16	3.78	1.28
EGFR	1.4	9.38	2.01	2.72	100	20.5
EphB4	0.519	8.05	0.352	100	7.27	3.71

	PP155	PP157	PP59	PP63	PP93	PP49
R1	(structure: CN, OH)	(structure: OH, CN)	(structure: OH, F)	(structure: OMe, F, F)	(structure: OH, F, F)	(structure: OMe)
R2	(isopropyl)	(isopropyl)	(isopropyl)	(isopropyl)	(isopropyl)	(isopropyl)
p110α	0.357	0.086	0.092	ND	0.296	3.2
p110β	0.744	0.742	1.45	1.28	2.53	100
p110δ	0.187	0.088	0.161	ND	0.09	0.73
p110γ	0.6	0.028	0.187	0.821	0.118	1.1
mTOR	0.752	0.596	0.003	0.404	1.13	8
DNAPK	0.022	0.009	0.036	0.873	0.048	1.26
PI4Kβ	ND	ND	0.21	3.5	0.47	8.2
Abl	1.1	7.7	0.664	2.5	1.9	1.7
Hck	0.708	7.2	0.026	0.113	0.076	0.18
Src	0.408	2.9	0.043	0.476	0.054	0.16
Src (T/I)	33	4.3	0.424	17.2	2.1	13
VEGFR	2.1	1.4	1.53	3.12	8.1	100
EGFR	2.6	8.1	1.04	10.2	6.9	1.4
EphB4	5	15	0.628	1.76	2.7	0.628

	PP15	PP321	PP337	PP347	PP325	PP349
R1	(structure: OH, OMe)	(structure: OMe, OH)	(structure: OMe, OH)	(structure: OMe, OH)	(structure: OMe, OH)	(structure: OMe, OH)
R2	(isopropyl)	H	Me	(structure)	(isopropyl)	(cyclopentyl)
p110α	0.26	0.705	0.403	0.276	0.164	0.068
p110β	2.1	1.36	0.216	0.809	0.697	0.261
p110δ	0.061	0.198	0.076	0.047	0.074	0.01
p110γ	0.19	0.523	0.2	0.355	0.34	0.12
mTOR	1.2	0.71	0.098	0.02	0.003	0.04
DNAPK	0.46	0.576	0.15	0.214	0.212	0.111
PI4Kβ	0.87	3.4	100	100	3.9	100
Abl	1.5	0.784	0.53	0.177	0.09	0.056
Hck	0.1	0.624	0.794	0.115	0.018	0.018
Src	0.12	0.489	0.51	0.067	0.017	0.0063
Src (T/I)	3.6	12.7	ND	7.11	1.77	0.431
VEGFR	100	1.06	ND	0.279	0.119	0.259
EGFR	0.908	100	100	6.45	2.19	0.437
EphB4	1.37	38.1	7.28	2.52	0.737	0.258

	PP423	PP411	PP407	PP98	PP23	PP485
R1	OMe / OH	OMe / OH	OMe / OH	OEt / OH	OMe / OMe	OMe / OMe
R2	(structure)	(structure, NH)	(structure, NH)	(structure)	(structure)	(structure)
p110α	0.192	2.22	2.26	0.813	0.08	0.464
p110β	0.949	2.67	2.27	3.18	0.23	0.525
p110δ	0.013	0.215	0.68	0.255	0.048	0.197
p110γ	0.113	0.46	1.27	0.381	0.2	1.08
mTOR	0.17	5.1	3.9	0.11	3.1	100
DNAPK	0.155	0.683	1.31	0.383	0.439	1.3
PI4Kβ	7.8	15	18	5	5.9	ND
Abl	0.068	4	2.05	0.608	4.1	4.4
Hck	0.01	1.2	0.311	0.082	1.1	0.44
Src	0.004	0.241	0.131	0.135	0.53	0.293
Src (T/I)	0.633	100	100	4.96	15.2	100
VEGFR	0.055	1.15	0.872	0.109	100	100
EGFR	0.27	17	12.6	0.768	3.02	6.34
EphB4	0.166	3.6	100	1.25	3.5	1.18

	PP495	PP496	PP494	PP90	PP341	PP343
R1	OMe / OMe	OMe / OMe	OMe / OMe	OMe / OMe	OEt / OMe	OEt / OMe
R2	(structure, OH)	(structure, OH)	(structure)	(structure)	H	(structure)
p110α	0.57	1.5	0.036	0.289	3.5	0.62
p110β	5.4	3.8	0.27	0.232	4.82	1.67
p110δ	0.12	0.067	0.008	0.057	0.473	0.042
p110γ	1.9	2.3	0.15	0.087	0.909	5.16
mTOR	1.7	1.2	1.7	2.5	100	3.3
DNAPK	0.709	0.66	0.099	0.463	2.02	0.847
PI4Kβ	9	ND	ND	5.1	5.6	5.5
Abl	12	6.4	0.7	1	6.15	2.1
Hck	0.92	2	0.27	0.117	6	0.551
Src	3.9	3.2	0.36	0.18	100	0.361
Src (T/I)	5.9	16	6.3	2.6	100	100
VEGFR	100	10	14.7	1.69	100	13.4
EGFR	12	18	4.8	3.3	100	5.95
EphB4	17	19	2.9	1.5	100	4.45

	PP361	PP359	PP362	PP64	PP65	PP305
R1	(phenyl, OEt/OMe)	(phenyl, OEt/OMe)	(phenyl, OEt/OMe)	(phenyl, MeO/OMe/OMe)	(phenyl, OMe/OMe/OMe)	(phenyl, OMe/OEt)
R2	(allyl/butenyl)	(cyclopentyl)	(cyclohexyl)	(isopropyl)	(isopropyl)	(isopropyl)
p110α	1.9	0.135	0.615	100	100	0.433
p110β	2.45	0.294	9.86	100	100	0.492
p110δ	0.276	0.017	0.177	1.9	37	0.103
p110γ	0.311	0.116	0.353	100	100	0.723
mTOR	4.8	6.5	0.616	100	5.5	2.4
DNAPK	0.556	0.242	2.5	3.41	2.27	0.63
PI4Kβ	12	1.5	100	3	3.6	4
Abl	14.6	0.85	6.05	0.83	11.2	6
Hck	3.4	0.285	0.861	0.096	0.733	1.2
Src	15.2	0.142	0.175	0.076	0.499	2
Src (T/I)	100	9.16	100	9.41	6.01	12.6
VEGFR	100	2.07	100	100	5.29	100
EGFR	5.08	1.4	1.16	5.14	3.66	54.2
EphB4	100	0.456	100	0.76	1.1	14.7

	PP306	PP66	PP48	PP133	PP203	PP202
R1	(phenyl, OMe/OEt)	(pyrimidine, OMe/OMe)	(phenyl, OMe)	(phenyl, OH)	(phenyl, NH₂/OH)	(phenyl, NH₂/OMe)
R2	(propanol)	(isopropyl)	(isopropyl)	H	(isopropyl)	(isopropyl)
p110α	1.37	1.91	1.25	100	3.74	1.5
p110β	100	1.61	1.5	100	14.2	3.5
p110δ	2.4	0.686	0.125	100	1.26	0.28
p110γ	2.01	8.02	1.4	50	1.45	0.7
mTOR	100	0.635	4.3	ND	3.6	100
DNAPK	3.84	0.789	0.331	12	0.717	0.64
PI4Kβ	25	4.9	7.4	ND	4.72	9.3
Abl	65	1.19	3.6	ND	0.208	0.26
Hck	10.5	1.6	0.38	ND	0.046	0.037
Src	9.8	1.43	0.38	ND	0.04	0.023
Src (T/I)	15.8	100	16	ND	7.81	2.9
VEGFR	12.6	ND	4.36	ND	2.16	2.6
EGFR	8.01	100	4.3	ND	2.12	3.85
EphB4	100	1.09	2.98	ND	27.2	2.63

	PP20	PP99	PP281	PP81	PP211	PP212
R1	NHBoc OMe	H N OH OMe	NH$_2$ OH	NH$_2$ OMe	NH$_2$	NH$_2$
R2	(isopropyl)	(isopropyl)	(cyclopentyl)	(cyclopentyl)	**H**	**H**
p110α	10.4	3.4	0.65	0.52	14	17
p110β	ND	100	5.23	2.88	100	100
p110δ	10.2	1.2	0.252	0.144	11	82
p110γ	1.8	100	0.735	0.271	11	9.6
mTOR	100	18	0.911	1.9	ND	ND
DNAPK	6.37	5.8	100	0.509	0.4	2.4
PI4Kβ	29	ND	2.34	0.53	ND	ND
Abl	0.0005	8.7	0.113	0.026	ND	ND
Hck	0.0005	0.567	0.013	0.002	ND	ND
Src	0.0005	0.341	0.011	0.0022	ND	ND
Src (T/I)	0.025	28	2.03	1.32	ND	ND
VEGFR	2.23	0.194	0.566	0.752	ND	ND
EGFR	0.168	5.32	0.033	0.084	ND	ND
EphB4	100	11	0.764	0.045	ND	ND

	PP213	PP128	PP26	PP46	PP45	PP39
R1	NO$_2$	NO$_2$	OH	CN	CN	CN
R2	**H**	**H**	(isopropyl)	(isopropyl)	(isopropyl)	(isopropyl)
p110α	100	12	3.1	2.9	10	4.6
p110β	100	100	6.1	7.2	100	
p110δ	100	2.3	0.67	0.9	1.2	0.64
p110γ	100	3	0.89	1.3	10	2.4
mTOR	ND	ND	5.4	12	3.5	40
DNAPK	100	5	1.35	0.883	2.68	1.23
PI4Kβ	ND	ND	5.1	4.4	3.5	7.2
Abl	ND	ND	1.8	50	7.9	17
Hck	ND	ND	2.4	5	0.51	50
Src	ND	ND	0.53	3	0.89	5.9
Src (T/I)	ND	ND	12	100	12	50
VEGFR	ND	ND	100	4.8	11	43
EGFR	ND	ND	100	17	13	100
EphB4	ND	ND	100	13	100	10

	PP150	PP151	PP21	PP52	PP53	PP31
R1	(structure)	(structure)	(structure)	(structure)	(structure)	(structure)
R2	(structure)	(structure)	(structure)	(structure)	(structure)	(structure)
p110α	47	3	12.9	7.6	50	1.4
p110β	100	100	6.1	50	100	3.3
p110δ	6.3	1.4	6.9	1.9	100	0.41
p110γ	3.5	6.2	ND	2.3	100	0.86
mTOR	100	100	5.8	5.5	50	100
DNAPK	6	2.6	4.28	2.75	10.1	1.96
PI4Kβ	ND	ND	24	14	100	3.4
Abl	3.4	5	50	32	50	2
Hck	1	4.3	13	9.2	13	1.4
Src	1.5	4.4	12	8.7	50	2.1
Src (T/I)	100	100	100	100	100	100
VEGFR	4.3	100	100	100	100	100
EGFR	100	8.9	100	100	100	12
EphB4	12	14	100	100	100	100

	PP152	PP149	PP32	PP55	PP35	PP34
R1	(structure)	(structure)	(structure)	(structure)	(structure)	(structure)
R2	(structure)	(structure)	(structure)	(structure)	(structure)	(structure)
p110α	1.4	2.7	2.6	3.4	1.6	1.1
p110β	5.9	7.2	7	8	ND	80
p110δ	0.213	3.9	0.49	0.8	0.69	0.14
p110γ	2.4	4.2	ND	1.2	0.94	1.4
mTOR	2.4	30	10	16	0.766	0.934
DNAPK	0.216	100	0.565	1.17	0.737	0.184
PI4Kβ	ND	ND	5.5	9.1	2.8	1.7
Abl	0.688	1.3	50	16	4.5	2.6
Hck	0.855	0.516	7.9	2.3	4.4	7.9
Src	0.49	0.764	15	3.4	5.2	1.5
Src (T/I)	59	2.4	100	100	2.9	7
VEGFR	1.2	1.4	100	100	1.02	1.05
EGFR	9	10	100	2.8	5.96	9.9
EphB4	15	7.1	3.1	3.8	17	23

119

	PP38	PP40	PP41	PP14	PP12	PP30
R1					I	
R2						
p110α	1.6	13.7	1	2.5	1.25	3
p110β			2.1	5.2	1.9	5.8
p110δ	0.65	1.4	0.21	0.24	0.25	0.68
p110γ	0.68	7.2	0.9	4	2	0.99
mTOR	5	3.8	4.3	5	6.5	0.08
DNAPK	0.365	0.979	0.713	0.894	1.14	0.339
PI4Kβ	4.9	2	4.9	2.7	6.4	5.7
Abl	13	11	11	58	25	3.2
Hck	3.6	2.3	5.3	1.5	2.2	2.4
Src	7.2	2.3	5	11	11	3.2
Src (T/l)	10	6.4	1.6	50	5.1	3.3
VEGFR	100	5.89	4.6	98.8	4.98	1.68
EGFR	100	12.8	100	100	17.8	0.579
EphB4	100	100	18	15	15.9	2.91

	PP149	PP126	PP215	PP216	PP217	PP218
R1						
R2	H	H	H	Me	H	H
p110α	100	12	100	10	17	100
p110β	25	100	100	100	100	100
p110δ	15	23	100	100	6.3	100
p110γ	25	50	100	100	20	100
mTOR	ND	ND	ND	ND	ND	ND
DNAPK	100	5	100	10	0.67	100
PI4Kβ	ND	ND	ND	ND	ND	ND
Abl	ND	ND	ND	ND	ND	ND
Hck	ND	ND	ND	ND	ND	ND
Src	ND	ND	ND	ND	ND	ND
Src (T/l)	ND	ND	ND	ND	ND	ND
VEGFR	ND	ND	ND	ND	ND	ND
EGFR	ND	ND	ND	ND	ND	ND
EphB4	ND	ND	ND	ND	ND	ND

	PP219	PP220	PP221	PP222	S2	PP223
R1						
R2	Me	H	H	H	Me	Me
p110α	100	100	100	3	1.1	100
p110β	100	100	100	100	16	100
p110δ	100	100	100	0.81	0.8	100
p110γ	100	100	50	0.97	0.57	100
mTOR	ND	ND	ND	ND	100	ND
DNAPK	0.86	100	4.4	0.15	0.029	0.42
PI4Kβ	ND	ND	ND	ND	ND	ND
Abl	ND	ND	ND	ND	1.2	ND
Hck	ND	ND	ND	ND	0.26	ND
Src	ND	ND	ND	ND	1.1	ND
Src (T/I)	ND	ND	ND	ND	7.2	ND
VEGFR	ND	ND	ND	ND	1.1	ND
EGFR	ND	ND	ND	ND	0.388	ND
EphB4	ND	ND	ND	ND	4.3	ND
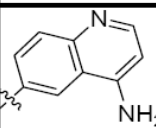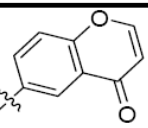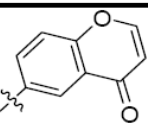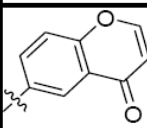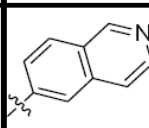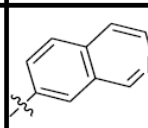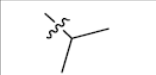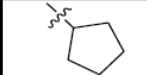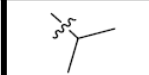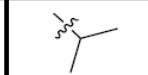
	PP224	PP225	PP226	PP227	PP228	PP229
R1						
R2						
p110α	ND	5.6	4.8	100	12	100
p110β	ND	50	32	100	50	50
p110δ	0.75	2.9	1.2	100	6.7	28
p110γ	ND	3.6	4.5	100	6.8	17
mTOR	ND	ND	ND	ND	ND	ND
DNAPK	0.21	0.35	0.2	0.42	0.78	2.1
PI4Kβ	ND	ND	ND	ND	ND	ND
Abl	ND	ND	ND	ND	ND	ND
Hck	ND	ND	ND	ND	ND	ND
Src	ND	ND	ND	ND	ND	ND
Src (T/I)	ND	ND	ND	ND	ND	ND
VEGFR	ND	ND	ND	ND	ND	ND
EGFR	ND	ND	ND	ND	ND	ND
EphB4	ND	ND	ND	ND	ND	ND
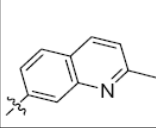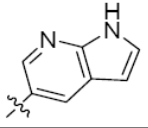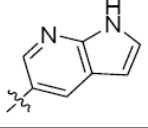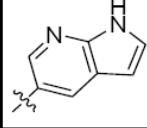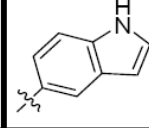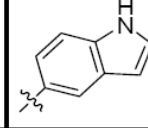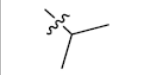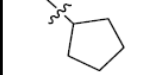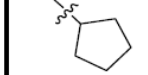
	PP230	PP231	PP165	PP232	PP167	PP168
R1	naphthalene	naphthalene	naphthalene	naphthalene	naphthalene	naphthalene
R2	phenethyl	acetamide	cyclopropylmethyl	isopentyl	cinnamyl	butynyl
p110α	33	9.3	5	29	ND	ND
p110β	50	100	100	100	ND	ND
p110δ	21	3	1.8	12	3.6	3
p110γ	6.3	5.1	4	16	ND	ND
mTOR	ND	ND	ND	ND	ND	ND
DNAPK	0.34	0.63	0.4	1.1	1.1	0.28
PI4Kβ	ND	ND	ND	ND	ND	ND
Abl	ND	ND	ND	ND	ND	ND
Hck	ND	ND	ND	ND	ND	ND
Src	ND	ND	ND	ND	ND	ND
Src (T/I)	ND	ND	ND	ND	ND	ND
VEGFR	ND	ND	ND	ND	ND	ND
EGFR	ND	ND	ND	ND	ND	ND
EphB4	ND	ND	ND	ND	ND	ND

	PP116	PP17	PP134	PP105	PP122	PP111
R1	naphthalene-OEt	naphthalene-OH	2-Cl-quinoline	quinoline	quinoline	quinoline
R2	Me	isopropyl	isopropyl	isopropyl	cyclopentyl	Me
p110α	100	1.3	15	2.8	1.8	0.035
p110β	5.3	3.2	100	16	2.7	1.4
p110δ	3.7	0.059	1.8	0.4	0.453	0.09
p110γ	2.7	0.587	100	2.7	1.3	0.22
mTOR	100	0.109	2.2	1.9	0.243	3
DNAPK	0.26	0.1	1.1	0.317	0.214	0.036
PI4Kβ	ND	7.4	ND	ND	ND	ND
Abl	15	0.057	2	1	0.759	100
Hck	0.54	0.02	1.6	0.422	0.326	100
Src	2.4	0.055	2.1	1.53	0.716	12
Src (T/I)	ND	0.055	3.4	5.8	17	3
VEGFR	0.55	0.01	100	5.6	1.6	12
EGFR	21	0.088	100	1	0.54	34
EphB4	1.1	0.095	2.5	1.7	0.66	10

	PP102	PP112	PP118	PP130	PP132	PP139
R1	(structure)	(structure)	(structure)	(structure)	(structure)	(structure)
R2	(structure)	(structure)	(structure)	(structure)	(structure)	(structure)
p110α	0.0175	0.07	0.462	0.8	0.206	1.7
p110β	0.244	2.7	1.6	5.5	0.975	6.5
p110δ	0.006	0.089	0.056	0.123	0.049	0.409
p110γ	0.043	0.59	0.461	0.184	0.095	100
mTOR	0.14	0.55	0.565	0.113	0.632	6.8
DNAPK	0.008	0.047	0.102	0.08	0.126	8.1
PI4Kβ	0.049	ND	ND	ND	ND	ND
Abl	0.134	1.5	5.1	3.8	2.2	2
Hck	0.088	0.54	2.2	0.878	0.946	12
Src	0.235	0.81	100	2.7	1	30
Src (T/I)	3.6	7.4	9.6	5.7	100	100
VEGFR	0.31	4.4	1.1	0.96	13	12
EGFR	0.61	2.1	100	100	18	70
EphB4	0.23	2.7	2.7	3.2	32	100
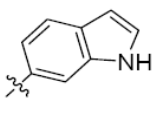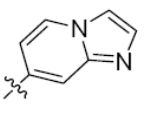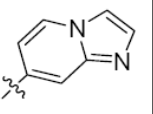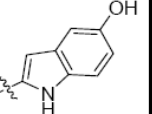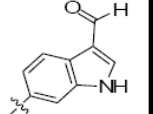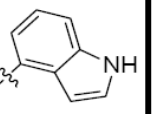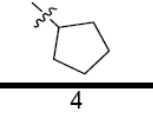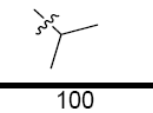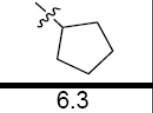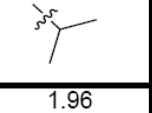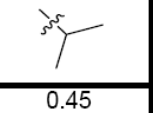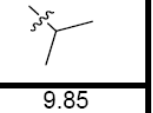
	PP158	PP140	PP141	PP146	PP142	PP145
R1	(structure)	(structure)	(structure)	(structure)	(structure)	(structure)
R2	(structure)	(structure)	(structure)	(structure)	(structure)	(structure)
p110α	0.08	100	100	0.245	0.467	2.8
p110β	0.467	15	100	0.5	4.6	8.9
p110δ	0.066	100	100	0.375	1	1.5
p110γ	0.089	100	100	0.242	0.586	7.3
mTOR	0.02	8.7	100	0.033	0.783	3.2
DNAPK	0.0005	18	100	0.014	0.314	1.9
PI4Kβ	ND	ND	ND	ND	ND	ND
Abl	0.328	35	100	2	3	65
Hck	0.248	2.7	1.1	17	4.3	17
Src	0.131	7.2	100	7.6	0.8	12
Src (T/I)	3.8	9.4	100	100	100	100
VEGFR	8.1	100	100	5.1	50	100
EGFR	7.4	6.7	1.4	12	7	100
EphB4	14	12	100	18	87	17
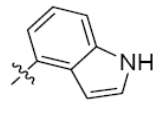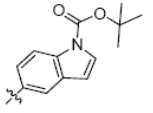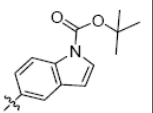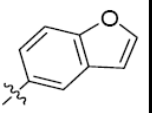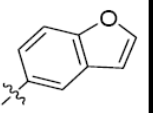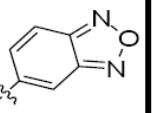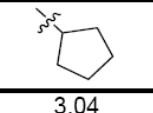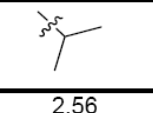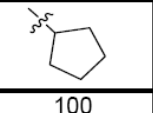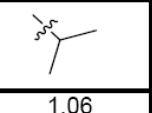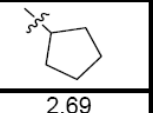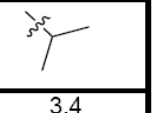
	PP147	PP148	PP143	PP144	PP129	PP131
R1						
R2		Me				
p110α	5.1	6.8	2.4	0.344	32	0.443
p110β	12	8.1	25	1.1	100	1.3
p110δ	5.2	3.9	1.7	0.12	3.4	0.085
p110γ	6.9	3	3	0.06	100	0.167
mTOR	10	100	1.3	0.426	2.2	1.5
DNAPK	2	0.283	0.26	0.046	2.7	0.049
PI4Kβ	ND	ND	ND	ND	ND	ND
Abl	6.4	100	2.2	2	12	2.1
Hck	3.4	17	2.5	1.1	100	1.8
Src	2.7	15	1.6	0.525	0.8	11
Src (T/l)	100	100	8.7	100	100	100
VEGFR	7	100	100	14	49	19
EGFR	100	10	29	100	25	100
EphB4	14	100	8.6	18	12	12

	PP133	PP120	PP108	PP121	PP89	PP94
R1						
R2		Me				
p110α	0.752	0.091	0.12	0.052	0.652	0.531
p110β	0.476	1.6	1	1.4	3.22	4.1
p110δ	0.11	0.14	0.077	0.15	0.173	0.228
p110γ	0.228	0.64	1.3	1.1	0.123	0.435
mTOR	1.1	0.412	0.06	0.013	0.364	0.407
DNAPK	0.359	0.12	0.071	0.06	0.09	0.08
PI4Kβ	ND	ND	ND	ND	4.1	9.8
Abl	4.3	0.31	0.022	0.018	0.295	0.234
Hck	16	0.42	0.01	0.008	0.015	0.0054
Src	0.55	0.44	0.02	0.014	0.039	0.008
Src (T/l)	100	6.8	0.48	0.22	0.103	0.206
VEGFR	100	0.94	0.019	0.012	0.076	0.009
EGFR	18	15	0.38	0.26	0.176	0.734
EphB4	3.8	2.9	0.34	0.19	0.23	0.105

	PP135	PP136	PP137	PP138	PP160	PP1573
R1	(structure)	(structure)	(structure)	(structure)	(structure)	(structure)
R2	(structure)	(structure)	(structure)	(structure)	(structure)	(structure)
p110α	0.642	0.831	0.145	0.209	1.6	0.25
p110β	0.854	1.1	0.55	1.5	16	1.9
p110δ	0.037	0.443	0.1	0.142	0.276	0.303
p110γ	0.627	31	0.113	0.09	0.451	0.141
mTOR	0.457	0.205	0.657	1.1	1.8	0.019
DNAPK	0.349	0.244	0.105	0.085	0.023	0.016
PI4Kβ	ND	ND	ND	ND	ND	ND
Abl	0.69	0.816	0.498	0.469	0.327	1.5
Hck	0.153	0.148	0.053	0.033	0.035	0.23
Src	0.157	0.211	0.073	0.049	0.058	0.321
Src (T/I)	2.4	1.3	0.393	0.261	2.2	10
VEGFR	0.715	0.172	0.295	0.411	6.3	100
EGFR	0.955	0.539	1.1	0.571	0.207	3.8
EphB4	100	2.2	2.3	2	1.3	7

	PP154	PP110	PP115	PP159	PP119	PP107
R1	(structure)	(structure)	(structure)	(structure)	(structure)	(structure)
R2	(structure)	(structure)	(structure)	(structure)	Me	(structure)
p110α	0.193	0.069	0.082	0.144	1.8	2.6
p110β	0.658	1	1.9	0.548	2.9	5
p110δ	0.068	0.12	0.19	0.162	0.66	0.34
p110γ	0.101	0.33	0.83	0.625	1.8	2
mTOR	1.64	1.2	0.596	7	8.3	0.467
DNAPK	0.01	0.077	0.11	3.4	0.15	0.088
PI4Kβ	ND	ND	ND	ND	ND	ND
Abl	0.52	0.11	0.14	0.087	1.5	0.2
Hck	0.4	0.03	0.037	0.076	0.22	0.018
Src	0.088	0.069	0.042	0.103	0.25	0.042
Src (T/I)	22	4.9	0.93	2.3	11	1.2
VEGFR	6.7	0.42	0.33	0.215	11	0.47
EGFR	9.6	2.5	0.76	1.2	2.9	0.22
EphB4	21	1.6	1.4	4.5	5	0.29

	PP124	PP161	PP162	PP242	PP43	PP91
R1						
R2						
p110α	4	100	6.3	1.96	0.45	9.85
p110β	7	52	15	2.2	ND	4.75
p110δ	0.966	72	2.3	0.102	0.125	2.02
p110γ	1.5	100	2.4	1.27	0.14	1.022
mTOR	0.493	7.6	4.8	0.008	0.22	8
DNAPK	0.054	0.222	0.053	0.408	0.019	0.953
PI4Kβ	ND	ND	ND	22	4.2	2.6
Abl	0.165	14	13	3.6	12	2.6
Hck	0.005	100	8.9	1.18	0.27	1.2
Src	0.017	23	11	1.4	1.2	0.037
Src (T/I)	0.25	100	100	5.14	11.7	1
VEGFR	0.134	100	100	1.54	2.2	6.9
EGFR	0.085	45	12	4.38	0.638	4.6
EphB4	0.17	100	21	3.46	2.05	2.9

	PP92	PP86	PP88	PP96	PP97	PP44
R1						
R2						
p110α	3.04	2.56	100	1.06	2.69	3.4
p110β	10.6	45	100	67.2	28.7	0.44
p110δ	0.446	2.48	1.03	0.436	0.429	3.7
p110γ	1.14	0.799	0.873	0.347	0.239	5.9
mTOR	5.4	0.3	0.576	3.4	1.6	100
DNAPK	0.929	0.43	0.916	0.303	0.22	1.2
PI4Kβ	3.5	13	100	5.7	8	14
Abl	2.2	0.527	0.92	0.538	0.893	13
Hck	0.057	0.009	0.048	0.091	0.056	1.3
Src	0.057	0.046	0.194	0.238	0.14	3
Src (T/I)	1.3	0.116	0.44	12	15	50
VEGFR	4.13	0.153	0.84	2.9	1.22	100
EGFR	1.4	0.179	0.391	0.964	0.575	8.3
EphB4	1.6	0.353	0.871	0.675	0.38	100

	PP156	PP95	P233	PP54	PP234	PP42
R1						
R2			H		Me	
p110α	2.2	1.95	4.9	2.2	1.3	3.4
p110β	9.2	46.8	30	1.4	15	50
p110δ	2	0.643	7.4	1.3	1.2	1.9
p110γ	22	0.43	4	1.1	1.6	2.4
mTOR	3.6	4.5	ND	1.9	ND	4.5
DNAPK	0.186	0.546	0.88	0.489	0.085	0.288
PI4Kβ	ND	5	ND	9.1	ND	12
Abl	8.4	5.2	ND	1.3	ND	50
Hck	4.8	0.889	ND	1	ND	12
Src	3.5	1.03	ND	0.93	ND	12
Src (T/I)	52	100	ND	6.9	ND	50
VEGFR	13	100	ND	21	ND	1.64
EGFR	0.937	5	ND	15	ND	100
EphB4	17	3	ND	6.76	ND	22

127

Appendix 2: Additional Experimental Methods

A2.1 Determination of p110γ crystal structures

This work was done by Beatriz Z. Gonzalez in the laboratory of Roger L. Williams at the MRC Laboratory of Molecular Biology in Cambridge, England. Protein expression and purification: Recombinant human p110γ (residues 144-1102, with a His$_6$ tag directly fused to the C-terminus) was purified from baculovirus-infected Sf9 cells. Cells were sonicated in buffer A (0.1M NaCl, 0.005M potassium phosphate pH 8 (4° C), 10 mM Tris-Hcl pH 8 4°C) and 1 mM MgCl$_2$) and the supernatant from a 1 hr ultracentrifugation was fractionated by heparin affinity, metal chelate affinity and gel filtration. The purified protein in gel filtration buffer (20 mM Tris pH 7.2 (4°C), 0.5 mM ammonium sulfate, 1% ethylene glycol, 0.02% CHAPS and 5 mM DTT) was concentrated to approximately 6 mg/ml.

Crystallisation of p110γ and soaking with inhibitors: Crystals were grown at 17 ºC using sitting-drop vapour-diffusion by mixing 1 μl p110γ sample (4 mg/mL in a buffer containing 0.5 mM (NH$_4$)$_2$SO$_4$, 20 mM Tris pH 7.2, 1% ethylene glycol, 0.02% Chaps and 5 mM DTT) and 1 μL of a reservoir solution (16-17% PEG 4000, 250 mM (NH$_4$)$_2$SO$_4$ and 100mM Tris pH 7.5). Crystal seeds were introduced in the drops by hair seeding with a cat whisker. The crystals grow over 1-2 weeks reaching a maximum size of 0.2 mm x 0.1 mm x 0.1 mm.

Inhibitor stocks were diluted in cryoprotectant solution (23% PEG 4000, 250 mM (NH$_4$)$_2$SO$_4$, 100mM Tris pH 7.5 and 14% glycerol) to final concentrations of 0.01 mM, 0.1 mM and 1 mM. Aliquots of increasing inhibitor concentration in cryoprotectant solution were added to the drops in which the crystals were grown. The additions were

of 0.5 μL and drops were incubated for 30-60 min between additions. Finally, 1 μL was taken out of the drop and 1 μL of 1 mM inhibitor in cryoprotectant solution was added, and the crystals were soaked in this solution for three hours. After soaking, the crystals were transferred to a fresh drop containing 1mM inhibitor in cryoprotectant solution then immediately frozen by dunking the crystals in liquid nitrogen.

Diffraction data collection and structure refinement: Diffraction data were collected at ESRF ID14-4. Data were integrated with MOSFLM and scaled using SCALA. Human p110γ was used as an initial model for molecular replacement using AMORE. The model was refined using REFMAC, starting with rigid-body refinement then using restrained maximum-likelihood refinement with individual isotropic B factors alternated with restrained refinement using TLS parameters. Cycles of REFMAC refinement were alternated with manual rebuilding. The data collection and refinement statistics are summarised in Supplementary Table 4.

A2.2. Determination of c-Src crystal structures: This work was done by James Blair, a fellow graduate student in Kevan Shokat's laboratory at the University of California, San Francisco. Protein expression, purification, and crystallisation: The chicken c-Src kinase domain (residues 251–533) was expressed, purified and crystallized as described. M. A. Seeliger and J. Kuriyan provided the chicken c-Src gene cloned into pSKB-3 and a plasmid containing tyrosine phosphatase YopH. G. Montelione provided a plasmid containing GroEL/Trigger Factor (cloned into pACYADuet-1, Novagen). Inhibitor stock solutions were prepared by dissolving each inhibitor in DMSO to 5 mM (S1) or 20 mM (PP102, PP121 and PP494). Each inhibitor was added in a 1.5-molar excess to aliquots of concentrated c-Src protein solutions (14–26 mg mL^{-1} c-Src, 50 mM Tris (pH 8.0), 100 mM NaCl, 5% (v/v) glycerol, 1 mM DTT). After incubation at room temperature for 30 min, these mixtures were centrifuged for 10 min at 15,000 $\times$ g, and

the clear supernatants were used for crystallization. Cocrystals were grown using

hanging-drop vapor diffusion with a 1:1 ratio mixture of protein and 18–22% (w/v)

ethylene glycol precipitant solutions. Crystals of space group P1 grew within one week

as thin plates. For each co-crystal structure, the following conditions were used:

c-Src complex	[Protein] (mg mL^{-1})	[Precipitant] % ethylene glycol (w/v)	Hanging drop volume (μL)
PP121	14	20	2
PP102	14	20	2
S1	16	18	3
PP494	26	22	2

The c-Src cocrystals were cryo-protected using 20% glycerol before flash-

freezing the crystals in liquid nitrogen. Diffraction data were collected at the Advanced

Light Source (Berkeley, California, United States) beamlines 8.2.1 and 8.2.2 under a

nitrogen gas stream at 100 K, using a wavelength of 1.0000 nm. The data were

processed with DENZO and SCALEPACK using the HKL2000 program suite.

Chicken c-Src co-crystal structures were solved by molecular replacement with

Phaser. Starting coordinates were taken from the catalytic domain of human c-Src (PDB

entry 1yoj). Topology and parameter files for the inhibitors were generated using the

Dundee PRODRG2 Server (http://davapc1.bioch.dundee.ac.uk/programs/prodrg/).

Refinement of the structures was carried out through multiple cycles of manual fitting

using Coot and crystallographic refinement using REFMAC5. Crystallographic

refinement involved TLS refinement followed by restrained refinement with the maximum

likelihood method. During the initial rounds of manual fitting and refinement, optimal

TLS groups were determined with the TLSMD web server

(http://skuld.bmsc.washington.edu/~tlsmd/). For the later rounds of fitting and

refinement, two TLS groups were used – one for the N-lobe (residues 248–342) and one

for the C-lobe (residues 343–533). Ramachandran outliers were calculated with

RAMPAGE. Detailed data and refinement statistics are available in Supplementary

Table 4. Ramachandran statistics for each complex are as follows:

c-Src complex	PP121	PP102	S1	PP494
Number of residues in favored region	506 (97.9%)	446 (97.2%)	452 (97.4%)	477 (97.9%)
Number of residues in allowed region	11 (2.1%)	13 (2.8%)	11 (2.4%)	10 (2.1%)
Number of residues in outlier region	0 (0.0%)	0 (0.0%)	1 (0.1%)	0 (0.0%)

A2.3 Alignment and analysis of PI3K-γ and c-Src structures:
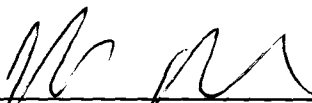
The kinase structures were structurally aligned in UCSF Chimera using Scheeff

and Bourne's manual structural alignment of 31 kinases

(http://www.sdsc.edu/pb/kinases/). Since the structure of VEGFR-2 (1vr2) was not

included in Scheef and Bourne's alignment, we created our own alignment of the

"universal" core of 1vr2 to 2src (c-Src) and 1e8x (p110γ) using the reported method. To

allow the best direct comparison between the protein kinases and p110γ, 1vr2 and the

structures reported here were aligned against 1e8x (p110γ) using the residues for the

"universal" core as defined by Scheeff and Bourne. Likewise, the root mean square

deviation (RMSD) of the aligned Cα backbone of 1vr2, the c-Src/PP121 complex and

1e8x was calculated using the residues for the "universal" core except the activation loop

residues in all three structures and the kinase insert domain residues of 1vr2. These

residues are often disordered or missing in kinase crystal structures, thereby contributing

to an unusually high RMSD. The crystallographic figures were produced using PyMOL.

To compare the relative binding orientations of pyrazolopyrimidine-containing

inhibitors in p110γ versus c-Src, the p110γ and c-Src inhibitor complexes were

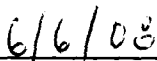structurally aligned based on the adenine ring of ATP. The adenine ring atoms of ATP in

1e8x and ANP in 2src were aligned using the PyMOL pair-fitting tool. Using the UCSF Chimera MatchMaker tool, the p110γ/S2 and p110γ/S1 complexes were aligned against the adenine-aligned 1e8x structure. Similarly, we aligned the c-Src/PP121, c-Src/PP102, c-Src/S1 and c-Src/PP494 complexes against the adenine-aligned 2src structure.

It is the policy of the University to encourage the distribution of all theses and dissertations. Copies of all UCSF theses and dissertations will be routed to the library via the Graduate Division. The library will make all theses and dissertations accessible to the public and will preserve these to the best of their abilities, in perpetuity.

I hereby grant permission to the Graduate Division of the University of California, San Francisco to release copies of my thesis or dissertation to the Campus Library to provide access and preservation, in whole or in part, in perpetuity.

_____   _____
Author Signature   Date